ABSTRACT

Title of dissertation: LEPTOGENESIS AND PHASE TRANSITION IN A WARPED EXTRA DIMENSION

Peizhi Du
Doctor of Philosophy, 2019

Dissertation directed by: Professor Kaustubh Agashe
Department of Physics

Despite the success of the standard model (SM) of particle physics, a few unsolved problems call for new physics beyond the SM. In this thesis, we focus on one theoretical problem of the SM—Planck-electroweak (EW) hierarchy problem, as well as two experimental facts—non-zero neutrino mass and observed baryon asymmetry, which can not be explained by the SM. One plausible solution to the Planck-EW hierarchy problem is Randall-Sundrum (RS) models with a warped extra dimension, or their AdS/CFT dual composite Higgs (CH) theories. Moreover, it is well-known that type I seesaw mechanism can naturally generate tiny but non-zero SM neutrino mass. The same seesaw mechanism can also explain the baryon asymmetry of the universe via leptogenesis. Therefore, in order to address these three problems in a single model, we study a warped/composite seesaw model, a natural embedding of the high scale type I seesaw mechanism in RS/CH framework. In contrast to the usual high scale type I seesaw mechanism in four dimensions (4D), 5D warped seesaw model becomes a TeV scale "inverse" seesaw like model

after Kaluza-Klein decomposition into 4D theories. In order to study leptogenesis in warped/composite seesaw, we first develop a simplified version of this model, as part of a general framework called hybrid seesaw. We then demonstrate that hybrid seesaw can achieve successful leptogenesis and feature an interesting interplay of high scale generation of the asymmetry and TeV scale washouts, which has a larger viable parameter space and richer phenomenology than usual type I seesaw models. To make this mechanism realistic in the full warped seesaw model, we also study the phase transition from the high temperature black hole phase to low temperature phase with two branes in 5D theories. According to AdS/CFT duality, this phase transition is dual to the deconfined and confined phase transition in strongly coupled nearly conformal 4D theories. It was previously believed that this phase transition rate is too slow at the critical temperature, resulting in a large amount of supercooling and low scale inflation. All primordial abundance in this case would be significantly diluted. We analyze a new mechanism to achieve fast phase transition around the critical temperature and thus the asymmetry generated from high scale leptogenesis can survive until today.

LEPTOGENESIS AND PHASE TRANSITION IN A WARPED EXTRA DIMENSION

by

Peizhi Du

Dissertation submitted to the Faculty of the Graduate School of the
University of Maryland, College Park in partial fulfillment
of the requirements for the degree of
Doctor of Philosophy
2019

Advisory Committee:
Professor Kaustubh Agashe, Chair/Advisor
Professor Zackaria Chacko
Professor Theodore Jacobson
Professor Raman Sundrum
Professor Richard Wentworth

Preface

Some chapters of this thesis are based on my work in collaboration with other people. Chapter 3 is mostly *JHEP 1904 (2019) 029* co-authored with Kaustubh Agashe, Majid Ekhterachian, Chee Sheng Fong, Sungwoo Hong and Luca Vecchi. Chapter 4 is based on the ongoing project in collaboration with Kaustubh Agashe, Majid Ekhterachian, Soubhik Kumar and Raman Sundrum.

Acknowledgments

I owe a debt of gratitude to all the people who have made this thesis possible and my graduate school experience unforgettable.

First and foremost I'd like to express my deepest gratitude to my advisor, professor Kaustubh Agashe for offering me a chance to learn from and work with him. He always guided me through the projects and encouraged me to express my own opinions and ideas, which is very inspiring and I benefit a lot from it. I truly appreciate his patience in answering my questions and helping me understand a general class of theories. Other than research projects, he is also concerned about my current life as a graduate student and the future plan of my research career. It was he who made my PhD study smooth and fruitful.

I would also like to thank professor Zackaria Chacko for extensive discussion and collaboration. I'm always amazed by my his critical insights of the current status of our field and the promising future directions. It was he who broadened my knowledge to cosmology and neutrino experiments. I owe him a debt of gratitude for his help on improving various aspects of my abilities in scientific research.

I would like to thank professor Raman Sundrum for wonderful collaboration and valuable guidance. His global view and deep understanding of our research field sets the highest level of goals that I have been pursuing. I truly admire his way of decomposing complicated ideas into simple examples and basic principles, which sharpens my way of thinking and conducting research. I greatly appreciate the chance to work with him.

Many thanks go to my other committee members—professor Theodore Jacobson and professor Richard Wentworth for serving on my dissertation committee and providing valuable comments on my thesis.

Interaction with faculty members at Maryland Center for Fundamental Physics (MCFP) is enjoyable and rewarding. I would like to thank professor Paulo Bedaque, professor Alessandra Buonanno, professor Thomas Cohen, professor Anson Hook, professor Bei-Lok Hu, professor Xiangdong Ji and professor Rabindra Mohapatra.

The experience with my collaborators have enriched my knowledge and they deserve a special mention. They are Jack Collins, Csaba Csaki, Abhish Dev, Majid Ekhterachian, Chee Sheng Fong, Michael Geller, Sungwoo Hong, Doojin Kim, Soubhik Kumar, Rashmish Mishra, Vivian Poulin, Ofri Telem, Yuhsin Tsai, Luca Vecchi. Especially I would like to thank professor Csaba Csaki for his advice and help on my current and future research career.

I also enjoyed chatting physics and many other things with other postdocs and students in particle physics group of MCFP. They are Arushi Bodas, Yanou Cui, David Curtin, Saurav Das, Kaustubh Deshpande, Anton de la Fuente, Changhun Lee, Zhen Liu, Prashant Saraswat, Gustavo Marques Tavares, Christopher Verhaaren and Guanwen Yan.

I am especially grateful to my family - my mother and father who have always stood by me and guided me through my career. Words cannot express my gratitude to them.

It is impossible to remember all, and I apologize to those I've inadvertently

left out. Thank you all.

Table of Contents

Preface ii

Acknowledgements iii

Table of Contents vi

List of Tables ix

List of Figures x

List of Abbreviations xii

1 Introduction 1
- 1.1 Composite Higgs and Randall-Sundrum models . . . 3
- 1.2 Seesaw mechanism . . . 6
- 1.3 Leptogenesis . . . 8
- 1.4 Outline of the thesis . . . 10

2 Warped/composite seesaw and hybrid seesaw 12
- 2.1 Warped/composite seesaw: 4D view . . . 12
- 2.2 Warped/composite seesaw: 5D view . . . 16

3 Leptogenesis in the hybrid seesaw 20
- 3.1 Introduction . . . 21
- 3.2 Scenarios with small $U(1)_{B-L}$ breaking . . . 30
- 3.3 Leptogenesis with small $U(1)_{B-L}$ breaking . . . 35
  - 3.3.1 Leptogenesis in TeV scale inverse and linear seesaw . . . 36
    - 3.3.1.1 CP asymmetry . . . 38
    - 3.3.1.2 Washout and baryon asymmetry . . . 42
  - 3.3.2 Nanopoulos-Weinberg theorem . . . 46
  - 3.3.3 Possible variations to achieve successful leptogenesis . . . 48
    - 3.3.3.1 Inverse seesaw with degeneracy among different generations . . . 48
    - 3.3.3.2 Inverse seesaw + linear seesaw . . . 51
    - 3.3.3.3 Other mechanisms . . . 54

3.4 General idea of the hybrid seesaw . . . 56
3.4.1 Natural μ term and successful leptogenesis . . . 57
3.5 Formalism for the hybrid genesis . . . 62
3.5.1 Generalities . . . 63
3.5.2 Hybrid genesis: qualitative description . . . 66
3.5.2.1 Symmetries of the hybrid model . . . 68
3.5.2.2 High scale leptogenesis ($T \sim M_N$) . . . 71
3.5.2.3 Survival of the asymmetry at $T \lesssim M_N$ . . . 73
3.5.2.4 Low scale washout ($T \sim m_\Psi$) . . . 77
3.5.2.5 Initial conditions and assumptions . . . 81
3.5.3 Hybrid genesis: quantitative description . . . 83
3.5.3.1 CP violation . . . 83
3.5.3.2 Thermal averaged reaction densities . . . 85
3.5.3.3 Boltzmann equations . . . 87
3.6 Results . . . 93
3.6.1 General parameter space . . . 95
3.6.1.1 TeV scale module . . . 97
3.6.1.2 High scale module . . . 98
3.6.1.3 Combining high scale and TeV scale modules . . . 100
3.6.2 Selected benchmark points . . . 105
3.6.2.1 Super-heavy singlet: $\gtrsim 10^{15}$ GeV . . . 105
3.6.2.2 Going below Davidson-Ibarra bound of $\sim 10^9$ GeV . . . 107
3.6.2.3 Intermediate scales: $\sim 10^9 - 10^{15}$ GeV . . . 111

4 Fast phase transition in Randall-Sundrum models 113
4.1 Introduction . . . 113
4.2 4D Equilibrium description of the two phases . . . 118
4.3 5D geometry and the structure of the bounce . . . 121
4.3.1 Phase transition in thin-wall regime . . . 125
4.4 A non-trivial RG flow between a UV and an IR fixed point . . . 128
4.5 Phase transition in thick wall regime . . . 131
4.6 Phenomenology . . . 132

5 Conclusions 134

A Leptogenesis in TeV scale linear seesaw 137

B Boltzmann equations and analytical approximate solutions 141
B.1 Generalities . . . 142
B.2 Analytical approximate solutions . . . 145
B.2.1 Weak washout regime ($cK \ll 1$) with $Y_X(z_i) = 0$ . . . 150
B.2.2 Strong washout regime ($cK \gg 1$) . . . 153
B.2.3 Regimes with thermal initial abundance of X . . . 153

B.2.4 For all regimes 154

C Spectator effects 155

D Comments on Boltzmann equations for ISS and LSS 158

E Gauge model 164

Bibliography 167

List of Tables

3.1 Our comparison of various UV completions of eq. (3.1): see explanation in text. 24

3.2 Summary of the parametric dependence of CP asymmetry, washout, baryon asymmetry in inverse [see eq. (3.12)] and linear seesaw [see eq. (3.13)]. The parameters $\varepsilon, \varepsilon'$ are defined in eq. (3.14), wheres δ below eq. (3.31). 46

3.3 Charge assignments of $\ell_\alpha, \Psi_a, \Psi^c_a, \Phi_\kappa, \Phi_\lambda$ under the two global symmetries of the **fully-symmetric model**. The former coincides with the baryon minus lepton number of the SM particles. Besides the lepton doublet ℓ_α, we do not show the charges of the rest of SM particles. In the gauge model presented in Appendix E, $U(1)_{B-L}$ is a gauge symmetry while $U(1)_{\lambda-B}$ remains an accidental global symmetry. Under $U(1)_{\lambda-B}$, the rest of SM particles carry the charges same as $U(1)_{L-B}$. On the other hand, the two symmetries are absent in the **non-symmetric model** originated from warped extra dimension since $\Phi_{\kappa,\lambda}$, which are identified with the dilaton, are real. 70

3.4 Summary of formulae for hybrid-leptogenesis with $r \equiv \lambda_1/\lambda_2$. High scale and TeV scale modules are defined in eq. (3.92). Generally we assume that $M_N \sim M_{N_1} \sim M_{N_2}$ and $r \leq 1$ 94

3.5 Three different benchmark points consistent with neutrino mass data and leptogenesis, organized by Majorana singlet mass scale. 107

C.1 We list the values of c_Ψ, c_{Φ_λ} and $c_{W1} = \frac{1}{3}c_\Psi + \frac{1}{2}c_{\Phi_\lambda}$ in different temperature regimes in the **fully-symmetric model**, as well as the values of $c_{W1} = \frac{1}{3}c_\Psi$ in the **non-symmetric model.** For simplicity, in our numerical estimations, we will fix $c_{W1} = 0.7(0.1)$ for all temperature regimes in the **fully-symmetric (non-symmetric) model** 157

E.1 Beyond the SM fields and their charges under new gauge symmetries $U(1)_{B-L} \times U(1)_X$. Here α is some arbitrary real number. 165

List of Figures

3.1 Schematic representation of physics (seesaw and genesis) of the hybrid model. 27

3.2 The baryon asymmetry $Y_{\Delta B}$ as a function of y in the case where $\delta \sim \varepsilon'$ in ISS+LSS models. Here m_Ψ is fixed to be 1 TeV. The blue dashed line shows result with initial thermal abundance of $\tilde{\Psi}_i$ while the solid brown line shows the results with no initial $\tilde{\Psi}_i$ abundance. The vertical dotted lines indicate the border between the strong and weak washout regions. The orange line shows where the observed baryon asymmetry is obtained. Here we only plot the region where $y > y'$, meaning $y > \sqrt{yy'} \sim \sqrt{m_\nu m_\Psi / v^2} \approx 10^{-6}$. When $y < y'$, the results can be simply obtained by the exchange the role of y and y'. 54

3.3 Contours of needed UV asymmetry (solid black lines) and μ (dashed brown lines) in the (m_Ψ, y) plane to obtain the observed baryon asymmetry $Y_{\Delta B} \sim 10^{-10}$ and $m_\nu = 0.05$ eV. In the green shaded region, washout at the TeV scale is negligible so that the UV asymmetry needs to be the observed baryon asymmetry $\sim 10^{-10}$. On the other hand, for smaller values of y, due to exponential sensitivity in y and m_Ψ, UV asymmetry lines get closer to each other. In the gray shaded region, TeV scale washout becomes so large that even saturating maximal allowed $Y_\Delta(z_{UV,f}) \sim 10^{-3}$ results in too small final asymmetry to explain the observation. 97

3.4 Contours of UV asymmetry and μ generated in the high scale module in the (M_N, λ_2) plane for $\langle \Phi_\lambda \rangle = 10$ TeV and $r = 0.1$. Solid curves are contours of UV asymmetry assuming zero initial abundance of N and dot-dashed curves are contours of UV asymmetry with the assumption of thermal initial abundance for N. The brown dashed lines are contours of constant μ. The blue dotted line sets the boundary between strong washout regime (to the left of the line) and weak washout regime (to the right of the line) for the high scale module. . 99

3.5 Interplay of high-scale washout and asymmetry generation with TeV scale washout. Solid (dot-dashed) curves are contours on which observed baryon asymmetry and SM neutrino masses are produced for fixed r and $\langle\Phi_\lambda\rangle$ and different choices of M_N, assuming zero (thermal) initial abundance for N . The dashed green line sets the boundary between the weak washout and strong washout regimes in the IR (around the TeV scale), and the dashed black line is the boundary of weak and strong washout regimes in UV. The gray shaded region is constrained by $\mu \to e\gamma$. 101

3.6 Solid (dot-dashed) curves are contours in (m_Ψ, y) plane on which the observed neutrino mass and baryon asymmetry is produced assuming zero (thermal) initial abundance for N, similar to figure 3.5. In the left panel, we vary r and keep M_N and $\langle\Phi_\lambda\rangle$ fixed, while the right panel shows the results with varying $\langle\Phi_\lambda\rangle$ while keeping M_N and r fixed. The gray shaded region is constrained by $\mu \to e\gamma$. 105

4.1 The ansatz of the bubble configuration in 5D. The bulk geometry is AdS-S everywhere and the black solid (dashed) line indicates the position of the UV brane scale $\rho_{\rm UV}$ (horizon ρ_h). The deconfined phase is outside of the bubble, where it is purely AdS-S. Inside the bubble (the confined phase), $\phi(r)$ cuts off the spacetime and smoothly connects to ρ_h at the end of the bubble. 117

4.2 The contour plot for $\Gamma = H^4$ in N and T/T_c plane with fixed $\bar{\lambda} = 0.5$ and different ϵ' 130

List of Abbreviations

AdS	Anti-de Sitter
AdS-S	Anti-de Sitter-Schwarzschild
ARS	Akhmedov-Rubakov-Smirnov
BE	Boltzmann equation
BSM	Beyond the standard model
CFT	Conformal field theory
CP	Charge conjugation-parity (symmetry)
CKM	Cabibbo-Kobayashi-Maskawa
EFT	Effective field theory
eV, keV, MeV, GeV, TeV	Electro-volt, kilo-, mega-, giga-,tera- electron-volt
EW	Electroweak
FP	Fixed point
GW	Goldberger-Wise
IR	Infrared
ISS	Inverse seesaw
KK	Kaluza-Klein
LHC	Large Hadron Collider
LISA	Laser Interferometer Space Antenna
LSS	Linear seesaw
pNGB	Pseudo-Nambu-Goldstone boson
PT	Phase transition
QCD	Quantum Chromodynamics
RG	Renormalization group
RGE	Renormalization group equation
RS	Randall-Sundrum
SM	Standard model (of particle physics)
UV	Ultraviolet
VEV	Vacuum expectation value
4(5)D	Four(five) dimensional

Chapter 1: Introduction

After the discovery of the Higgs boson in 2012 by the Large Hadron Collider (LHC) [1, 2], the last building block of the standard model (SM) (for a review, see e.g. [3]) of particle physics is finally observed. Till now, the SM has achieved a great success in experimental tests. It is truly amazing that almost all particle phenomena we have seen so far can be described by the 17 elementary particles (and their anti-particles) as well as their interactions in the SM. Also, all properties of the elementary particles, including the interactions among them, can be deduced from 26 input parameters of the SM. The great success of a physical model is predicting various phenomena using minimal amount of free parameters. In this regard, the SM is the best model of particle physics so far.

However, the SM is not perfect both from theoretic and also experimental point of view. Even if we completely neglect gravity, just studying the SM as a theoretic model in the flat spacetime using quantum field theory (QFT), it is still incomplete due to, for instance, the existence of Landau pole of the $U(1)_Y$ gauge field, the ultimate ultraviolet (UV) scale where the theory breaks down. Of course, the SM can not explain gravity and the theory must break down around or below the Planck scale $M_{\rm Pl} = 1.2 \times 10^{19}$ GeV. Therefore, the SM can only be viewed as an

effective field theory (EFT) below some UV scale Λ, where new physical degrees of freedom and new interactions beyond standard model (BSM) must be considered.

All physical quantities in an interacting QFT with a UV new physics scale, also called UV cutoff of the theory, will get quantum corrections depending on the cutoff Λ, unless being protected by some symmetries. For example, being protected by the gauge symmetry, the gauge boson corresponding to an unbroken gauge symmetry is exactly massless even considering quantum corrections. The quantum correction of fermion mass is proportional to the mass and only logarithmically depends on Λ. Such effect is due to chiral symmetry of fermions, a global symmetry under which the left-handed and right-handed fermions have the opposite charge. However, there is no symmetry for elementary scalars masses. In fact, the SM Higgs mass squared gets a quantum correction with the order of Λ^2. Then the physical Higgs mass squared would naturally be the order of Λ^2. Assuming no new physics up to the Planck scale, one would expect $m_H^2 \sim M_{\rm Pl}^2$. Nevertheless, the observed mass is $m_H^2 \approx (125\text{GeV})^2$. This indicates the new physics contribution to the m_H^2 should cancel each other to a great precision, one part in 10^{34}. Such extremely fine tuning of the fundamental parameters to get the observed Higgs mass is often called Planck-electroweak (EW) hierarchy problem, a theoretic imperfection of the SM.

Moreover, many concrete experimental results can not be explained within the SM. Neutrino oscillation experiments [4–6], for instance, indicate that neutrinos, weakly interacting neutral particles of the SM, have extremely small but non-zero mass. The SM does not allow the mass term for neutrinos at renormalizable level (operators with mass dimension ≤ 4). Higher dimensional operators suppressed

by the UV cutoff Λ may generate neutrino mass if the UV physics break lepton number global symmetry. However, if we put $\Lambda \sim M_{\rm Pl}$ and the coupling to be order unity, the neutrino mass is too small compared to the observed neutrino mass $m_\nu = O(0.1)\,\text{eV}$ [7], hence in tension with experimental facts. Also, the observed asymmetry between the abundance of baryons and anti-baryons can not be generated within the SM and standard cosmology. Moreover, the SM can not predict the observed abundance of dark matter and dark energy. All of these experimental results call for theories beyond the SM.

In this thesis, we will focus on three of the above problems of the SM: Planck-EW hierarchy (section 1.1), neutrino mass (section 1.2) and baryon anti-baryon asymmetry (section 1.3), and introduce plausible solutions.

1.1 Composite Higgs and Randall-Sundrum models

We first study the Planck-EW hierarchy problem. Actually, the idea of a possible solution might already exist in the strongly coupled quantum chromodynamics (QCD) of the SM. There are light scalars predicted by QCD, for example pions π with mass $m_\pi \sim 100\,\text{MeV} \ll M_{\rm Pl}$. We don't consider the mass of pion has a hierarchy problem mainly because pions are composite states (made of quarks and gluons) after QCD confinement, and thus they should not be viewed as elementary particles all the way up to $M_{\rm Pl}$. Pions may be described as "elementary" particles in an EFT called chiral perturbation theory, which has a cutoff at $\Lambda_{\rm QCD} \sim 1\,\text{GeV}$ instead of $M_{\rm Pl}$ (reviewed in [8]). The cutoff of chiral perturbation theory is associated

with the confinement scale of QCD, which can naturally be much smaller than $M_{\rm Pl}$ because QCD is asymptotically free and the associated gauge coupling undergoes a large amount of renormalization group (RG) running to become large enough in the IR to trigger confinement. Furthermore, the minor gap between m_π and $\Lambda_{\rm QCD}$ is also nicely explained since pions are pseudo Nambu Goldstone bosons (pNGB) from chiral symmetry breaking. Because of these two pieces of magic, light pion mass is natural.

We could try to apply the same mechanism to the SM Higgs. One can imagine the SM Higgs as composite Goldstone bosons from a new strongly coupled sector which confines at around TeV scale. Such class of models are named *composite Higgs* (CH) models [9–13]. Other than being asymptotically free like QCD, the strongly coupled sector of CH models may involve an approximate conformal symmetry near a strongly coupled fixed point (for a review, see [14]). The confinement scale is originated from the spontaneous breaking of the conformal symmetry of the strongly coupled sector. The large hierarchy between the UV cutoff $\Lambda_{\rm UV}$ and confinement scale $\Lambda_{\rm confine}$ is controlled by the small perturbation to the conformal symmetry. One way to achieve this is Goldberger-Wise stabilization (GW) mechanism [15]:[1] adding a slightly relevant scalar operator $\mathcal{O}_{\rm GW}$ whose scaling dimension is $4-\epsilon$ with $\epsilon \ll 1$. In this mechanism,

$$\frac{\Lambda_{\rm confine}}{\Lambda_{\rm UV}} \propto e^{-\frac{1}{\epsilon}}. \tag{1.1}$$

[1] This mechanism was first proposed in 5D and we will discuss it in the next paragraph. Here we present its 4D dual picture.

Therefore $\Lambda_{\text{confine}} \sim 1$ TeV can be naturally achieved if $\epsilon \sim 1/30$ for $\Lambda_{\text{UV}} \sim M_{\text{Pl}}$. The remaining hierarchy between m_H and Λ_{confine} is due to Higgs being pNGBs.

CH models are theoretically attractive but it is difficult to calculate physical observables quantitatively in these models, due to the lack of perturbative control in such strongly coupled system. Luckily, thanks to AdS/CFT duality [16–18], the strongly coupled conformal field theory (CFT) in four spacetime dimensions (4D) can be mapped to a weakly coupled theory in five dimensional (5D) Anti-de sitter (AdS) spacetime including gravity. The AdS/CFT dual of CH is the Randall-Sundrum (RS) model [19, 20]. RS models contains a finite interval of a Poincare patch of 5D AdS bounded by two branes. In RS models, different fields have characteristic wave functions along the extra dimension. Elementary graviton is localized on the UV brane, thus also often called Planck brane. The SM Higgs field is localized on the IR brane, which corresponds to TeV scale. Therefore, Planck-EW hierarchy problem is solved due to the strong gravitational warping along the fifth dimension between UV and IR branes. The position of IR brane can be stabilized by GW mechanism: adding a bulk scalar with small 5D mass and appropriate boundary conditions on two branes. In the dual 4D picture [21, 22], the distance along the five dimension can be thought at the RG scale. The UV brane corresponds to the UV cutoff of the 4D theory while the IR brane indicates the confinement scale. SM Higgs localized on the IR brane indicates it is a composite field. The 5D GW scalar is dual to the scalar operator $\mathcal{O}_{\text{GW}}$ in previous paragraph. The small 5D mass corresponds to the small anomalous dimension of $\mathcal{O}_{\text{GW}}$, denoted as ϵ.

Assuming the cutoff of 5D RS models are much higher than the curvature

scale, the perturbative calculation in RS models are under theoretic control. To get the interaction strength among different fields, one needs to calculate the overlap of the wave functions among different fields. All observables can be calculated using fundamental 5D parameters. It has been robustly shown that the Higgs mass is naturally a loop factor below the IR brane scale [12, 13]. Moreover, accurate predictions of signals of heavy excitations of SM particles can be achieved in RS models, making the phenomenological study of RS/CH models more attractive (for a recent summary, see, for example, [23]).

1.2 Seesaw mechanism

Now we consider the neutrino mass problem. The first trial is adding right-handed neutrinos (N) to the SM with Yukawa interactions, $yNH\ell$, among SM lepton doublet (ℓ) and Higgs doublet field (H). Just like other SM charged leptons, neutrinos obtain mass after Higgs get a vacuum expectation value (VEV). The neutrino mass is then given by the product of Yukawa coupling y and Higgs VEV $v \approx 174\,\text{GeV}$. The neutrino mass scale from neutrino oscillation data is around 0.1 eV, meaning $y \sim 10^{-12}$. Though the smallness of y is stable under quantum corrections, having such extremely small number in the fundamental theory still seems unnatural.

One way to naturally address tiny neutrino mass, or equivalently this tiny Yukawa coupling constant, is so called seesaw mechanism [24–28]. There are various types of seesaw mechanism and we will classify it more carefully in section 3.1.

Here we only study the original high scale type I seesaw to illustrate the main idea. Apart from the Yukawa coupling $yNH\ell$ mentioned earlier, right-handed neutrinos are also allowed to have a Majorana mass term $M_N NN$ since they are singlets of SM gauge symmetries in type I seesaw. The scale for M_N is roughly the UV cutoff of the theory. Below the scale of M_N, right-handed neutrinos N can be integrated out. A mass dimension five operator $y^2 \frac{\ell H \ell H}{M_N}$, first pointed out by Weinberg [29], is generated. After Higgs gets a VEV, SM neutrinos acquire mass

$$m_\nu \sim \frac{y^2 v^2}{M_N}. \tag{1.2}$$

The heavier the right-handed neutrinos are, the lighter SM neutrinos are, hence the term seesaw. Putting numerical values in, for $y = O(0.1 - 1)$ and $m_\nu = O(0.1)\,\text{eV}$, the scale for M_N is $10^{12} - 10^{14}$ GeV. Such scale can be dynamically generated from extra gauge symmetry breaking (see e.g. [25, 26, 28, 30, 31]). In conclusion, seesaw mechanism provides an elegant way of generating tiny neutrino mass using order unity couplings and a UV scale.

Furthermore, seesaw mechanism has more interesting implications. Since the heavy singlet right-handed neutrinos have a Majorana mass, the SM neutrinos are also Majorana and the lepton number L (or more correctly baryon number minus lepton number $B - L$) global symmetry is broken. Such lepton number violation can be tested in experiments like neutrinoless double beta decay (for a review, see e.g. [32]). The idea of such experiments is that nucleus with proton number Z and total nucleon number A can decay into nucleus with the same nucleon number A

but $Z+2$ protons, associated with two electrons (e^-). For normal double beta decay mode, two anti-neutrinos ($\bar{\nu}_e$) will also be produced. However, if neutrinos are Majorana, meaning they are the anti-particle of themselves, it is possible to have a double beta decay mode without any neutrino emission. Therefore, such a decay mode is called $0\nu\beta\beta$.

$$\begin{aligned} (A,Z) &\rightarrow (A,Z+2)+2e^-+2\bar{\nu}_e \quad \text{(double beta decay)} \\ (A,Z) &\rightarrow (A,Z+2)+2e^- \qquad\quad \text{(neutrinoless double beta decay)} \end{aligned} \tag{1.3}$$

Non-observation of this $0\nu\beta\beta$ decay mode sets a bound on the Majorana mass of neutrinos, or the amount of lepton number violation in the SM.

1.3 Leptogenesis

The last problem we try to address is the baryon anti-baryon asymmetry of the universe. We are made of baryons, so are the stars and planets in the universe we have observed so far. This baryon overabundance can not directly come from initial conditions of the universe, since all primordial asymmetries will be exponentially diluted after the inflation. Therefore, the observed baryon asymmetry ($\eta_B^{\text{obs}} \equiv \frac{n_B - n_{\bar{B}}}{n_\gamma} \sim 10^{-10}$, where $n_{B,\bar{B},\gamma}$ denotes the number density of baryon, anti-baryon and photon respectively) must be dynamically generated in the early universe. The scenario to achieve the observed baryon asymmetry is often called *baryogenesis*. All theories of baryogenesis need to satisfy the following three conditions, also called Sakharov conditions [33]:

- Baryon number (B) or lepton number (L) violation: this is needed to dynamically generate a non-zero asymmetry at the first place.

- Charge conjugation (C) and Charge conjugation-Parity (CP) violation: if C or CP were conserved, the process involving baryons would have the same rate as C or CP conjugated process involving anti-baryons. Which means even if baryon number is violated and some baryon asymmetry is generated from one process, the inverse process has the same rate, resulting in zero net baryon asymmetry.

- Out of equilibrium dynamics: equilibrium requires the net asymmetry of a non-conserved quantum number (like B according to the first condition) to be zero. Thus the process responsible for the generation of the asymmetry must be out of equilibrium.

Actually the SM almost satisfies these three conditions: (i) $B + L$ in the SM is violated via non-perturbative quantum anomalies, the EW sphaleron process. (ii) The weak interaction violates CP, and the CP phase in the CKM matrix is order unity. (iii) The out of equilibrium condition is fulfilled if the EW phase transition is first order [34, 35]. Unfortunately, the observed Higgs mass ($m_H \approx 125$GeV) indicates the EW phase transition within the SM is not first order [36,37]. Therefore, the SM can not predict the observed baryon asymmetry of the universe and some BSM physics are necessary to achieve successful baryogenesis.

The seesaw mechanism discussed in the previous section allows a candidate mechanism for baryogenesis, often named *leptogenesis* [38] (see also reviews [39,40]).

High scale type I seesaw, for instance, satisfies Sakharov three conditions: (i) lepton number is violated due to the Majorana mass of right-handed neutrinos. (ii) The CP phase in the Yukawa coupling y could lead to CP violation. Also, (iii) the heavy right-handed neutrinos can decay out of equilibrium. The idea of leptogenesis is the following. The out-of-equilibrium decay of heavy right-handed neutrinos generate non-zero L asymmetry. As long as the decay happens before sphaleron process goes out of equilibrium ($T \sim 100$ GeV), asymmetry in L is transferred to B asymmetry because EW sphaleron process violates $B + L$ but preserves $B - L$. In addition to B asymmetry, leptogenesis predicts also L asymmetry of the similar size. Current bounds on L asymmetry in the cosmic neutrinos are rather weak: $\lesssim O(0.1)$ asymmetry is still allowed [41]. Therefore, seesaw mechanism, together with leptogenesis, provides plausible solutions to two problems of the SM: neutrino mass and baryon asymmetry.

1.4 Outline of the thesis

As we discussed in previous sections, RS/CH models can solve Planck-EW hierarchy problem and seesaw mechanism addresses the neutrino mass and baryon asymmetry problems. To unify the solutions in one framework, we study a natural embedding of high scale type I seesaw mechanism in the RS/CH models, namely warped/composite seesaw in chapter 2. Since it is technically difficult to study leptogenesis in warped/composite seesaw, we propose a simplified 4D version, hybrid seesaw, and analyze leptogenesis in hybrid seesaw in chapter 3. In order to make

leptogenesis in the full warped seesaw realistic, we need to understand its full cosmological history. Therefore, we also study the phase transition in RS models in chapter 4. Then we conclude in chapter 5.

Chapter 2: Warped/composite seesaw and hybrid seesaw

In this chapter, we shall study the warped/composite seesaw model which can address both Planck-EW hierarchy and neutrino mass problems. We first discuss the qualitative feature of warped/composite seesaw in 4D strongly coupled CFT point of view in section 2.1 and then discuss its 5D dual in RS framework in section 2.2.

2.1 Warped/composite seesaw: 4D view

As mentioned in chapter 1, CH models may contain a strongly coupled sector with approximate conformal symmetry, called *CFT sector*, of which SM Higgs originates as the composite state. The detailed underlying gauge group structure and field contents of the composite sector are not relevant for the qualitative discussion in this section. Therefore we will simply denote the physics of the composite sector as $\mathcal{L}_{\rm CFT}$. To get the observed properties of the SM (e.g. the hierarchical charged lepton masses), CH models also need a weakly coupled *elementary sector* external to the CFT sector. The natural scale for the elementary sector is the UV cut-off of the CH models, say $M_{\rm Pl}$. Fields in the elementary sector can mix with the states in the CFT sector with the same quantum numbers. The resulting SM particles are massless states after CFT sector confines, which are generally a mixture of elementary

and composite degrees of freedom. This scenario is called *partial compositeness* [42].

Now we study warped/composite seesaw—an implementation of high scale type I seesaw mechanism in the CH framework, which can be represented by the following Lagrangian:

$$\mathcal{L} = \mathcal{L}_{\rm CFT} + \lambda \overline{N_R} \mathcal{O}_N + \frac{1}{2} M_N^{\rm bare} N_R^2 \tag{2.1}$$

where N_R is an elementary (external to CFT) right-handed fermion and $\mathcal{O}_N$ is a CFT operator that mixes with N_R with coupling λ[1] and hence interpolates left-handed composite fermionic states. We take the bare Majorana mass of N_R to be its natural size $M_N^{\rm bare} \lesssim M_{\rm Pl}$. We assume that CFT sector preserves lepton number, and the only source of lepton-number violation is the Majorana mass term $M_N^{\rm bare}$ present in the elementary sector. It turns out that the observed neutrino mass can be reproduced when the operator $\overline{N_R}\mathcal{O}_N$ is relevant, i.e. the scaling dimension of $\mathcal{O}_N$ is $[\mathcal{O}_N] < 5/2$. In this case, the theory flows to a new IR fixed point where the operator $\overline{N_R}\mathcal{O}_N$ becomes marginal so that $\left[N_R^2\right] > 3$. For the case of $M_N^{\rm bare} < M_{\rm Pl}$, renormalization group (RG) flow then drives the N_R mass term to a significantly smaller value until the singlet fermion N_R gets integrated out at its physical mass,[2] which can be estimated to be

$$M_N^{\rm phy} \sim M_N^{\rm bare} \left(\frac{M_N^{\rm bare}}{M_{\rm Pl}} \right)^{\frac{1}{2[\mathcal{O}_N]-4}-1} . \tag{2.2}$$

[1] in analogy with similar effect for the SM charged fermions and gauge bosons.

[2] Of course, the singlet field N_R will mix with composite fermion states and hence it is not quite mass eigenstate. Still, the composite state that mixes with N_R will have a mass of $\sim M_N^{\rm phy}$. The resulting mass eigenstate, therefore, will have a mass $\sim M_N^{\rm phy}$.

Integrating out N_R at this $M_N^{\rm phy}$ scale generates

$$\Delta\mathcal{L}_{\rm CFT}^{\rm UV} = \lambda\overline{N_R}\mathcal{O}_N + \frac{1}{2}M_N^{\rm phy}N_R^2 \;\;\rightarrow\;\; \frac{\lambda^2}{M_N^{\rm phy}}\mathcal{O}_N^2. \tag{2.3}$$

As is clear from the appearance of lepton-number breaking spurion $M_N^{\rm phy}$, the CFT operator $\mathcal{O}_N^2$ is a lepton-number violating perturbation to the CFT sector. Integrating out N_R, therefore, effectively transfers lepton-number breaking into the CFT sector. One notices that this is like generating Weinberg operator in type I seesaw and a rather precise match may be seen when $\mathcal{O}$ is (roughly) identified with $H\ell$.

RG running the theory further down to the TeV scale where strongly coupled sector confines we get

$$\Delta\mathcal{L}_{\rm CFT}^{\rm IR} \sim \frac{\lambda^2}{M_N^{\rm phy}}\left(\frac{\rm TeV}{M_N^{\rm phy}}\right)^{2[\mathcal{O}_N]-5}\mathcal{O}_N^2 \sim \frac{\lambda^2}{M_N^{\rm bare}}\left(\frac{\rm TeV}{M_{\rm Pl}}\right)^{2[\mathcal{O}_N]-5}\mathcal{O}_N^2, \tag{2.4}$$

where $[\mathcal{O}_N]$ denotes the scaling dimension of $\mathcal{O}_N$ and we used (hence assumed accordingly) the large-N approximation for the scaling dimension of $\mathcal{O}_N^2$.

Now we study the physics after confinement using "hadron" picture instead of "quark-gluons" as physical degrees of freedom. When the CFT sector confines at TeV scale, each operator $\mathcal{O}_N$, when acted on the vacuum, creates a tower of left-handed composite fermions, with the lightest mode denoted as Ψ. They combine with the right-chirality states (with the lightest mode being Ψ^c) generated by another CFT operator to form composite Dirac fermions, with mass starting at

TeV and with TeV mass gap between adjacent states, i.e, we have $m_\Psi \sim$ TeV. The "Weinberg"-type operator in eq. (2.4) then can be viewed as generating a small Majorana mass terms for left-handed fermion (called μ), i.e.,

$$\mu \sim \frac{\lambda^2\ \mathrm{TeV}^2}{M_N^{\mathrm{bare}}} \left(\frac{\mathrm{TeV}}{M_{\mathrm{Pl}}}\right)^{2[\mathcal{O}_N]-5} \tag{2.5}$$

Together with the $\sim$ TeV Dirac mass, this makes these composite fermions pseudo-Dirac. Finally, the composite singlet has a coupling to SM Higgs and composites with quantum numbers of SM lepton (interpolated by $\mathcal{O}_L$). We then obtain a coupling between composite singlet (Ψ^c), SM Higgs and lepton via mixing of elementary lepton with latter composites (including a different RG factor, i.e., determined by scaling dimension of $\mathcal{O}_L$)[3]:

$$y \sim \lambda_L \left(\frac{\mathrm{TeV}}{M_{\mathrm{Pl}}}\right)^{[\mathcal{O}_L]-5/2}. \tag{2.6}$$

Putting eqs. (2.5) and (2.6) together, the Lagrangian involving Ψ, Ψ^c takes the form

$$\mathcal{L}_{\Psi,\Psi^c} \sim y\Psi^c H\ell + m_\Psi \Psi\Psi^c + \mu\Psi\Psi. \tag{2.7}$$

This Lagrangian is similar to a TeV scale seesaw mechanism called *inverse seesaw* [43, 44]. Just like inverse seesaw, the SM neutrino mass is generated via exchange

[3]For the case of $[\mathcal{O}_L] > 5/2$ assumed here, the corresponding mixing is *ir*relevant. Note also that a similar factor was used in the spurion/dimensional analysis estimate in eq. (2.8) above.

of pseudo-Dirac TeV scale composite singlets (Ψ, Ψ^c), rendering

$$m_\nu \sim \frac{y^2 v^2}{m_\Psi^2}\mu \sim \frac{\lambda_L^2 \lambda^2 v^2}{M_N^{\rm bare}} \left(\frac{\rm TeV}{M_{\rm Pl}}\right)^{2([\mathcal{O}_N]+[\mathcal{O}_L]-5)}, \tag{2.8}$$

where we assume the couplings among composite states are $O(1)$. Remarkably, although the composite seesaw at UV scale has the feature of high scale type I seesaw, the dynamics that generates SM neutrino mass after confinement is actually TeV scale inverse seesaw. Moreover, notice [as per eq. (2.5)] that in this composite seesaw framework, the required small Majorana mass terms for Ψ is generated dynamically via type I seesaw mechanism.

2.2 Warped/composite seesaw: 5D view

In this section, we provide a brief discussion of warped seesaw model in 5D RS framework. RS models are formulated in a Poincare patch of $\rm AdS_5$ bounded by two branes. The metric of the $\rm AdS_5$ spacetime is

$$ds^2 = \frac{1}{(kz)^2}\left(\eta_{\mu\nu}dx^\mu dx^\nu - dz^2\right), \tag{2.9}$$

where z is the coordinate of the fifth spatial dimension and k is the AdS curvature. The UV (IR) boundary of the spacetime is at $z = z_h(z_v)$. We consider all SM fermions and gauge bosons propagating the bulk of $\rm AdS_5$. For concreteness, we assume SM Higgs to be localized on the IR brane. The 5D SM gauge singlet field, N, which is the analog of the right-handed neutrinos of the usual, 4D seesaw models,

propagates the bulk. Like all 5D fermion fields, N can be decomposed into *both* left (L) and right (R) chiralities (denoted by $N_{L,R}$, respectively) from the 4D viewpoint. N_R couples to SM $SU(2)_{\rm L}$ lepton doublet, in particular left-handed neutrinos, and the Higgs on the IR brane with 5D Yukawa coupling $y_{\rm 5D}$. We impose that lepton-number is *un*broken in the bulk/IR brane,[4] but is broken on the UV brane. Hence, a Majorana mass term for N_R is forbidden in the bulk/IR brane, whereas it is allowed on the UV brane. Furthermore, we assume that the order parameter for breaking of lepton-number on the UV brane is not tuned, i.e., it is (roughly) the mass scale corresponding to its location in the extra dimension. It is then natural to include a Planck (or AdS curvature) scale-size Majorana mass term for N_R on the UV brane. These aspects can be summarized in the following 5D Lagrangian

$$-\mathcal{L}_{\rm 5D} \ni y_{\rm 5D} N_R H \ell + c_N k \bar{N}_L N_R + \delta(z - z_h) \frac{1}{2} \frac{m_N}{k} N_R^T C N_R + \text{h.c.}, \tag{2.10}$$

where N is a 5D fermion field with $N_{L/R}$ being left(right)-chirality of N. In addition, $c_N k$ is 5D mass parameter for N, m_N is Majorana mass of N_R[5] and C denotes charge conjugation operation.

The above model was studied in [45] using so-called KK-basis where KK decomposition was done without taking into account the large Majorana mass term from the beginning. The effects of the Majorana mass was added as a posteriori process and this leads to large Majorana masses for zero- and KK-modes and large mixing among all modes. Hence, although analysis using KK-basis produces correct neutrino mass

[4] This symmetry should be gauged in the 5D model.

[5] As indicated above, $m_N \sim O(k)$ naturally.

formula, using a basis that is vastly different from the *mass* basis obscures the physical picture. In particular, the results from KK-basis *naively* suggest (or give the misleading impression) that the above 5D warped seesaw model is indeed of Type I in the sense that the SM neutrino mass is generated by the *dynamical* exchange of a super-heavy singlet mode, i.e., at the (effective) seesaw scale (for more discussion of this point, see [46]).

However, as shown in [46], analysis based on the mass basis, including the Majorana mass term from the beginning, reveals very *different* dynamical picture. The mass eigenstates of 4D effective theory (after KK-decomposition) of eq. (2.10) is a tower of pseudo-Dirac singlet fermions with tiny Majorana splitting. For the choice of $c_N \sim -0.3$ that renders correct SM neutrino mass, dominant contributions to the SM neutrino masses come from the exchange of a few low lying mass eigenstates (cf. super-heavy modes in the KK basis). Namely, the SM neutrino mass is generated not by an exchange of super-heavy Majorana singlet mode, but by exchanges of O(TeV) pseudo-Dirac singlet modes. Therefore, the dynamical nature of the warped seesaw is inverse seesaw, not Type I. Moreover, it is indeed very *natural* realization of it, because the SM neutrino mass is obtained with all dimensionful parameters taken to be near the cut-off scale and all dimensionless parameters to be $O(1)$. This new finding, then, *re*-focuses attention on LHC signals from the O(TeV) scale singlet pseudo-Dirac fermions that arise in this model. We demonstrate in refs. [47,48] that various kinds of interesting signals can be probed at the LHC.

According to AdS/CFT duality, the fields on the UV brane corresponds to the elementary sector external to the CFT sector. Therefore, UV value of 5D N_R field

is dual to N_R in the composite seesaw (see eq. (2.1)). Also, the lightest KK modes of 5D fields $N_{L/R}$ are dual to Ψ, Ψ^c in eq. (2.7). The exact 5D calculation justifies the qualitative argument of composite seesaw in section 2.1.

Chapter 3: Leptogenesis in the hybrid seesaw

In this chapter, we will move on the study leptogenesis in warped/composite seesaw. To avoid the technical difficulty in full warped seesaw obscuring underline physics in leptogenesis, we propose a simplified weakly coupled 4D model, *hybrid seesaw*, which captures most of attracting features of warped/composite seesaw. The detailed analysis of leptogenesis will be presented in this chapter based on hybrid seesaw. We believe this result can illustrate the qualitative features of leptogenesis in full warped/composite seesaw.

Apart from a simplified version of warped/composite seesaw, hybrid seesaw can be generalized to a class of models which can address some issue of inverse seesaw models. To see this point, we will introduce hybrid seesaw as a UV completion of standard inverse seesaw models in this chapter. Before diving into the details of leptogenesis, we first review some existing seesaw models, including our warped/composite and hybrid seesaw, in theoretic as well as phenomenological point of view in section 3.1. Despite a bit of repetition of previous chapters, we feel it is necessary to clarify some physical points in a collective manner. The detailed outline of this chapter will be present at the end of section 3.1.

3.1 Introduction

Viewing the Standard Model (SM) as an effective field theory, Majorana neutrino masses m_ν dominantly arise from the unique dimension-five Weinberg operator:

$$C\frac{y^2}{m_{\rm NP}}\ell H\ell H \qquad \to \qquad m_\nu = C\frac{y^2v^2}{m_{\rm NP}}, \tag{3.1}$$

where ℓ and H are respectively the SM lepton and Higgs doublets with vacuum expectation value (VEV) v. Within our conventions, the new degrees of freedom responsible for generating the operator in eq. (3.1) are assumed to be characterized by a mass scale $m_{\rm NP}$ and a leading coupling y to the SM lepton (and the Higgs) (couplings among new states are measured by other couplings in general). We next elaborate on the "C" parameter.

The operator in eq. (3.1) violates $U(1)_{B-L}$ by two units. Such a violation may be induced directly from $y^2/m_{\rm NP}$, as in ordinary type I seesaw scenarios [24–28]. In all those cases we conventionally say $U(1)_{B-L}$ breaking is *maximal* and set $C \equiv 1$ to mean that no further parameter is necessary to generate neutrino masses. On the other hand, in all UV completions in which $y^2/m_{\rm NP}$ does not have spurious $U(1)_{B-L}$ charge 2, eq. (3.1) will have to be proportional to some additional $U(1)_{B-L}$-breaking parameter C. In particular, when $m_{\rm NP} \ll 10^{14}$ GeV and $y = \mathcal{O}(1)$ such $U(1)_{B-L}$-breaking parameter is forced to be very small, i.e. $C \ll 1$. Note that while in the former case, setting $C = 1$ merely means effectively we did not need the C parameter, in the latter case $C \ll 1$ encodes the required $U(1)_{B-L}$ breaking. The new parameter

$C \ll 1$ in the second scenario could be a ratio of mass scales or couplings within the new sector, or simply be controlled by a new $U(1)_{B-L}$-breaking interaction to the SM. We will refer to these models as scenarios with *small* $U(1)_{B-L}$ breaking.

UV completions of the Weinberg operator have other important physical implications. The necessary source of $U(1)_{B-L}$ breaking indicates for example that the UV dynamics responsible for generating eq. (3.1) may also have the possibility to realize baryogenesis through leptogenesis [38]. Furthermore, the parameters $m_{\rm NP}, y$ control the possible collider signatures of the new particles involved, suggesting that models with $m_{\rm NP} \sim$ TeV and $y \sim 1$ certainly represent the most promising ones experimentally.

Combining these considerations, we find that small neutrino masses may be obtained in three qualitatively different ways, depending on whether TeV/$m_{\rm NP}$ or y or C is the small parameter suppressing m_ν:

(I) high-scale scenarios TeV/$m_{\rm NP} \ll 1$ in which C, y are not necessarily small, such as the popular high scale seesaw model [24–28];

(II) scenarios with small couplings $y \ll 1$ and unsuppressed C and TeV/$m_{\rm NP}$, like in low scale seasaw models;

(III) scenarios with *small* $U(1)_{B-L}$ breaking, $C \ll 1$, where y and TeV/$m_{\rm NP}$ may be unsuppressed. The inverse seesaw [43, 44] or linear seesaw [53] belong to this latter class.

In table 3.1, we summarize how the most common realizations of the above three classes of UV completions of eq. (3.1) compare with respect to the generation

of small neutrino masses, the realization of successful leptogenesis, and the possibility of featuring interesting signatures at colliders. Needless to say, this table reflects our own perspective on the topic, as well as our biases as model-builders. For example, in the table and the remainder of the chapter we will often use the term *natural*. To help the reader appreciate this terminology we hereby attempt to provide an operative definition of this concept, which we may call *Dirac naturalness*: dimensionless couplings (like y or the new physics and SM self-couplings) are of natural size if they are not too far from one, say of $O(10^{-2}) - O(1)$; mass scales ($m_{\rm NP}$) are of natural size if they are either generated via dimensional transmutation of natural couplings or are related to a more fundamental dynamical scale (for e.g. the TeV, the GUT or the Planck scales) by factors of order unity; in the absence of a symmetry reason, the differences among masses and among couplings should be of the same order as the respective masses and couplings themselves (i.e. *anarchic* masses and couplings). Our naturalness criteria is more restrictive than t' Hooft's technical naturalness, which only calls for stability under quantum corrections.

We can now proceed to explain table 3.1. In **High scale type-I seesaw** models the new physics is in the form of heavy Majorana right-handed neutrinos N with coupling $y \sim 10^{-2} - 1$ to the SM leptons. Once both a mass $m_{\rm NP} \equiv M_N$ for N and the coupling y are turned on, $U(1)_{B-L}$ is broken collectively by y^2/M_N and hence the model belongs to class (I). In these cases leptogenesis is realized naturally [38, 40]. Unfortunately, with a high scale $M_N \sim 10^{10} - 10^{14}$ GeV there are no detectable LHC or low-energy experimental signals. Small neutrino masses can be obtained quite elegantly. However, the required mass $m_{\rm NP}$ must be a few orders

UV seesaw model	Natural m_ν?	Signals?	Leptogenesis?
High scale type I	Almost	No	Yes
TeV scale type I	Not really	Possible	Possible
TeV scale inverse/linear	Not really	Yes	Possible
Hybrid	Possible	Yes	Yes

Table 3.1: Our comparison of various UV completions of eq. (3.1): see explanation in text.

of magnitude smaller than the known fundamental scales (say the Planck or GUT scale of $\sim 10^{18}$ or 10^{16} GeV, respectively), at an intermediate value that is not fully understood. In view of our definitions above, we may view such a scale as *almost* natural.

In **TeV scale type-I seesaw** the $U(1)_{B-L}$ symmetry is again maximally broken ($C \equiv 1$). However, here the small neutrino masses ($m_\nu = O(0.1)$ eV) are obtained for $m_{\rm NP} \equiv M_N \sim$ TeV with tiny couplings to the SM, $y \sim 10^{-6}$.[1] This model thus belongs to our class (II). The smallness of y is considered a tuning and hence neutrino mass is not natural according to our definition. The small y also makes the direct production of the exotic N unlikely. To make this scenario more visible one may consider extensions with additional gauge symmetries ($B-L$ or LR models) so that N may be produced via the associated *gauge* couplings, which can be sizable, giving collider signals with *same*-sign dileptons due to Majorana nature of N (see references in [57]). Overall, this model scores a "possible" in the experimental signals entry. Finally, leptogenesis is not natural unless one imposes quasi-degeneracy among singlets of different generations to resonantly enhance the CP violation [58]. This cannot be achieved without additional ingredients for example in the form of

[1] Unless we invoke some special textures [56], which we do not consider here.

flavor symmetry. Hence, leptogenesis scores a "possible" here as well.

TeV scale inverse seesaw (ISS) and linear seesaw (LSS) have, besides the right-handed neutrinos (here denoted by Ψ) which couple to the SM lepton and Higgs with Yukawa y, additional fermion singlets with left-handed chirality Ψ^c. The latter are introduced such that the singlets can form a Dirac mass term $m_{\rm NP} \equiv m_\Psi \sim$ TeV preserving $U(1)_{B-L}$. Such a symmetry is broken by a small Majorana mass term for the singlets μ in the ISS, or by a small lepton number breaking Yukawa coupling y' of Ψ^c to the SM in the LSS. In the language introduced in eq. (3.1) this means

$$C \sim \frac{\mu}{m_\Psi} \ll 1 \qquad\qquad C \sim \frac{y'}{y} \ll 1 \tag{3.2}$$

respectively, and these models belong to class (III). Since $\mu \ll$ TeV is not set by any fundamental scale, and similarly the coupling y' must be very small, the observed neutrino mass is not obtained naturally according to our criteria. Yet, an attractive feature here is that experimental signals from singlets Ψ, Ψ^c can arise from sizable Yukawa coupling y — including a contribution to the rare process $\mu \to e\gamma$ as well as direct production of singlets themselves (see for example [59] and references therein). The model therefore scores a clear "yes" in the signal column.[2]

Unfortunately, as we have shown recently in ref. [54] (focusing on the case of strong washout and anarchic couplings/masses of singlets) leptogenesis is not

[2]Even though we get accessibility to the singlets, it is true that it is difficult to directly probe the very small μ-term, i.e. lepton-number breaking.

achieved naturally in the ISS (i.e. $\mu \neq 0$ and $y' = 0$),[3] according to our naturalness criteria. We will elaborate more on this in section 3.3. We then include the effects of quasi-degenerate mass among different generation singlets: while such possibility provides a sizable improvement of the final asymmetry, it can barely accommodate the observed value. We also discuss the case of weak washout and demonstrate various subtleties, which have not been discussed in the previous literature—though it does not change qualitatively our earlier conclusions. We further extend our conclusions to LSS (i.e. $\mu = 0$ and $y' \neq 0$) and show that leptogenesis is not natural there either. Another result of the present work is that even turning on both μ, y' still requires very small couplings $y' \ll y \ll \mathcal{O}(10^{-2})$ to achieve a successful leptogenesis (see also for example refs. [62, 63]). Our conclusion is that in this scenario leptogenesis scores a "possible".

Finally, table 3.1 includes the **Hybrid seesaw** [54,55] (see detailed discussion in section 3.4). This was designed to overcome *simultaneously* the two limitations of the ISS: unnaturally small μ term and difficulty in leptogenesis [54]. The essential idea of hybrid seesaw is to introduce, on top of the ISS module, i.e. a Dirac pair Ψ, Ψ^c of fermions with $m_{\rm NP} \equiv m_\Psi \sim$ TeV and unsuppressed coupling to leptons $y \sim 1$, a high scale type I seesaw module, namely heavy ($M_N \gg$ TeV) *Majorana* singlets N, see figure 3.1. The theory has no bare μ-term, but the two modules suitably mix via a IR-scale mass term $m_{\rm IR}$ arising from a scalar vacuum expectation value. In this manner, integrating out the heavy Majorana singlet generates an

[3]Some of these results have been obtained by others (for example, in refs. [60, 61] and more recently, in ref. [62]).

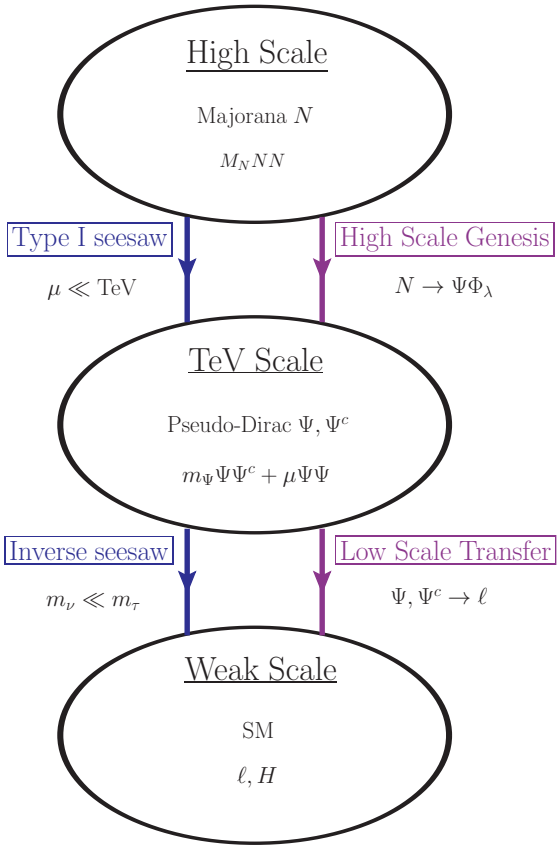

Figure 3.1: Schematic representation of physics (seesaw and genesis) of the hybrid model.

effective $\mu \ll$ TeV for Ψ[4]

$$\mu \sim \frac{m_{\rm IR}^2}{M_N}. \tag{3.3}$$

Taking now $m_{\rm IR} \sim$ TeV we can explain why $\mu/m_\Psi \ll 1$, and therefore the smallness of neutrino masses: see left-hand side (LHS) of figure 3.1.

The structure of hybrid seesaw, and in particular the characteristic mixing between the low and high scales modules, arises elegantly from warped extra-

[4]The basic idea of this model is along the lines of ref. [64], but those authors considered $M_N \sim$ TeV instead. For this reason Leptogenesis is not as successful as in our picture, and μ is not naturally small according to our criteria.

dimensions (dual to composite Higgs models) [45,49–52] as shown in ref. [46]. In this sense, the hybrid seesaw could be taken as a "toy" version of the warped/composite one. Alternatively, the peculiar coupling structure in figure 3.1 can be enforced in weakly-coupled 4D models via a gauge symmetry as we will see in appendix E. Because in the 5D completions $m_\Psi \sim m_{\rm IR}$ are both related to the same fundamental scale (the TeV), that arises dynamically, and simultaneously M_N can be effectively reduced dynamically compared to the Planck scale [46], then it is clear that neutrino masses can be fully natural in the hybrid picture *once UV-completed* (i.e., strictly speaking, going beyond the hybrid model on which we will focus here). This explains the score "possible" in the appropriate entry in the table (i.e., why it's not quite an actual "yes").

How about leptogenesis in the hybrid seesaw model? We have just seen that neutrino masses are suppressed by $C \ll 1$, suggesting that this is a scenario with small $U(1)_{B-L}$-breaking (class (III) above). However, this is not the complete story. As we will see in detail below (see also [54]), the high scale module violates *maximally* a global $U(1)$ carried by Ψ. Because $U(1)$ number violation is large at scales $\sim M_N \gg m_\Psi$, leptogenesis can *naturally* proceed through the decay of N to Ψ (analogously to type I seesaw in class (I)), followed by the asymmetry in Ψ being transferred to the SM leptons: see right-hand side (RHS) of figure 3.1. Hence, the hybrid model also turn out to score a "yes" in natural leptogenesis.

In particular, in ref. [54] we emphasized that high scale leptogenesis with anarchic couplings can be realized for $M_N \sim 10^{11} - 10^{16}$ GeV. In this work, we will study this scenario in more detail and also explore the lower scale $M_N \gtrsim 10^6$ GeV

where leptogenesis can be realized albeit with hierarchical Yukawa couplings (among different generations of N). Such a relaxation of the lower bound on the heavy singlet mass, compared to the ordinary type I seesaw, might be especially relevant for resolving the SUSY gravitino problem. Overall, due to the hybrid structure, the allowed mass window gets enlarged compared to the usual case, $10^9 - 10^{15}$ GeV.

Regarding possible experimental signals in the hybrid seesaw, besides signals associated with TeV scale fermions as in the conventional ISS (as mentioned above), the model generally predicts new TeV scale scalars potentially within the reach of present and future colliders as we have shown in ref. [54]. Certain realizations, like the gauge model presented in appendix E, also contain light states that may contribute to $\Delta N_{\rm eff}$ and might thus be probed by CMB-Stage-IV [65]. Hence, we put a "yes" in the experimental signals. Remarkably, this model has the ability to realize the most attractive features of the high and low scale modules simultaneously.

This chapter is organized as follows. We begin in the next section with an overview of scenario with small lepton-number breaking ($C \ll 1$), i.e. the ISS and LSS models, and discuss the constraint from the non-observation of $\mu \to e\gamma$. A thorough analysis of leptogenesis in these models is given in section 3.3 (see also appendices A and D). Section 3.4 outlines our hybrid seesaw solution of the problems of the original ISS model. Explicit UV completions of the scenario are presented in appendix E (gauge model) and chapter 2 (warped/composite model). This is followed by a detailed discussion of leptogenesis in the hybrid model. In section 3.5 (and appendices B and C) we will provide a *systematic* derivation of the necessary analytic formalism, which we believe clarifies many of underlying physics. This

formalism is then used in section 3.6 to identify what parameter choices give the right baryon asymmetry, including some interesting benchmark points.

3.2 Scenarios with small $U(1)_{B-L}$ breaking

We begin with a review of what we will refer to as *small $U(1)_{B-L}$ breaking models*, that according to our earlier definition have $C \ll 1$ [see eq. (3.1)]. These are characterized by an effective theory with exotic particles not far from the TeV scale and unsuppressed couplings to the SM, say of order $0.1 - 1$. This guarantees that these scenarios have testable consequences at colliders. Because all new degrees of freedom are heavy, the SM neutrinos are Majorana particles. To ensure that small neutrino masses are generated, these scenarios must possess an approximate lepton number broken by a small dimensionless parameter. The most minimal incarnations of this scenario has been called inverse seesaw and linear seesaw. We will focus on these mostly for simplicity sake.

Let us add to the SM two Weyl fermions Ψ and Ψ^c, singlet under the SM, carrying lepton number $L(\Psi) = +1$, $L(\Psi^c) = -1$ respectively. In principle we can combine the pair of Weyl fermions into a Dirac fermion with Ψ (or $i\sigma^2\Psi^{c*}$) playing the role of the left (right) chiralities, but we will not do it here for later convenience. The only $U(1)_{B-L}$ invariant couplings, besides the kinetic terms, are:

$$\mathcal{L}_{B-L} \supset m_\Psi \Psi\Psi^c + y\Psi^c H\ell + O(1/\Lambda) + \text{h.c.}, \tag{3.4}$$

with ℓ, H the SM lepton and Higgs doublets, respectively. Gauge contractions are

understood, and the flavor indices for ℓ (possibly carried by Ψ, Ψ^c as well) are not displayed here for brevity. We will include the flavor indices in later parts whenever they are relevant. We will take $m_\Psi = O(\text{TeV})$ as a reference value. Possible higher dimensional operators (denoted by $O(1/\Lambda)$ in eq. (3.4)) are assumed to be negligible because they are suppressed by a large scale Λ. We will assume Λ is of the order of the Planck scale for definiteness.

In the theory eq. (3.4) the active neutrinos remain exactly massless. In order to obtain a realistic theory with tiny neutrino masses without adding additional light degrees of freedom, we introduce small sources of $U(1)_{B-L}$ breaking. At the renormalizable level there exist only three $(B-L)$-breaking couplings:[5]

$$\mathcal{L}_{\not{B}-\not{L}} = \frac{\mu}{2}\Psi\Psi + \frac{\mu'}{2}\Psi^c\Psi^c + y'\Psi H\ell + O(1/\Lambda) + \text{h.c.}. \tag{3.5}$$

The assumption that the $U(1)_{B-L}$ breaking terms are small reads $|\mu|, |\mu'| \ll |m_\Psi|$, $|y'| \ll |y|$. The terms μ, μ' correspond to small Majorana masses for the fields Ψ, Ψ^c. Conventionally, the ISS model is defined by $y' = 0$ while the LSS model by $\mu = 0$. Generally, in both of these models, μ' is taken to be zero as well.

The new couplings appearing in eq. (3.5) can all be assigned a spurionic lepton number, namely $L(\mu) = L(y') = -2$ and $L(\mu') = +2$. Because the accidental charges of μ, μ'^*, y' are the same, in generic UV completions the new couplings in eq. (3.5) may in fact arise from a unique fundamental coupling with $L = -2$. In that case, a natural consequence of naive dimensional analysis is that, at the order of magnitude

[5] One may also add $Z\Psi^\dagger i\bar{\sigma}^\mu\partial_\mu\Psi^c + \text{hc}$. However, after a field redefinition one realizes this is equivalent to a correction to the couplings we show.

level,

$$\frac{y'}{y} \sim \frac{\mu}{m_\Psi} \sim \frac{\mu'^*}{m_\Psi}. \tag{3.6}$$

Of course it is possible to build a UV dynamics in such a way that this relation is violated. Yet, the scaling in eq. (3.6) is what one expects to emerge from truly generic UV theories. More generally, setting one of the couplings in eq. (3.5) to zero is not always a radiatively stable assumption. For example, inspecting 1-loop diagrams we find that starting with a non-vanishing y' one generates (from log-divergent piece)

$$y' \neq 0 \quad \Longrightarrow \quad \delta\mu \sim m_\Psi \frac{y^* y'^t}{16\pi^2}, \quad \delta\mu' \sim m_\Psi^t \frac{y'^* y^t}{16\pi^2}. \tag{3.7}$$

On the other hand, no renormalization effects are induced by μ, μ' because these correspond to a soft-breaking of $U(1)_{B-L}$. That is, μ and μ' only self-renormalize and do not radiatively generate other terms.

Majorana masses m_ν for the active neutrinos, that have $L(m_\nu) = -2$, must be linear in the couplings of eq. (3.5) to leading order in the small $(B-L)$-breaking. This can be readily verified by integrating out Ψ, Ψ^c at tree-level to obtain, in the leading approximation:

$$\mathcal{L}_{\rm EFT} \;=\; \frac{1}{2}(H\ell)^t \frac{m_\nu}{v^2}(H\ell) + \text{h.c.} + O(1/\Lambda). \tag{3.8}$$

where $v = 174$ GeV and

$$m_\nu \;=\; v^2 \left[y^t \frac{1}{m_\Psi} \mu \frac{1}{m_\Psi^t} y - \left(y'^t \frac{1}{m_\Psi^t} y + y^t \frac{1}{m_\Psi} y' \right) \right] . \tag{3.9}$$

Note that μ' does not enter because its $U(1)_{B-L}$ charge forces it to appear in front of $(H\ell)^t(H\ell)$ as complex conjugate, which is not possible at tree-level. With the relation eq. (3.6) the two contributions in eq. (3.8) are naturally of the same order. The parameter introduced in eq. (3.1) may now be identified as

$$C \equiv \max\left(\frac{y'}{y}, \frac{\mu}{m_\Psi} \right) . \tag{3.10}$$

Lacking a UV description of $U(1)_{B-L}$ breaking, it is fair to say that the smallness of μ, y' is merely an assumption in our effective field theory eqs. (3.4) and (3.5). While this model does not truly explain the size of the SM neutrino masses, it provides an interesting laboratory to investigate the phenomenology of scenarios with small $U(1)_{B-L}$ breaking. A distinctive feature of these models is the presence of signatures in colliders (see for example [59] and references therein). For $m_\Psi \lesssim 1$ TeV and sizable y it is in fact possible to produce the pseudo-Dirac fermions at the LHC via mixing with SM neutrinos and observe its subsequent resonant decay. Unfortunately, we will not be able to measure the tiny couplings $\propto \mu, \mu', y'$ and hence unambiguously connect the exotic particles to a mechanism for neutrino mass generation. The reason is that in the typical benchmark models from eq. (3.8) one derives from eq. (3.9) that $\mu/m_\Psi, y'/y \sim 10^{-10}$, that is certainly out of reach of

current and future colliders.

Besides direct production of Ψ^c, there can be indirect signatures in rare processes, like $\mu \to e\gamma$ and the electron EDM. At leading order in $(yv)^2/m_\Psi^2$, the branching ratio can be written as [66]

$$\mathrm{BR}_{\mathrm{ISS}}(\mu \to e\gamma) \simeq \frac{3\alpha_{\mathrm{em}}}{8\pi} \left| \left(y^t \frac{v^2}{m_\Psi^\dagger m_\Psi} y^* \right)_{\mu e} \right|^2 , \tag{3.11}$$

where $\alpha_{\mathrm{em}} \approx 1/137$ is the fine structure constant, $v \approx 174$ GeV the SM Higgs VEV, and we have neglected corrections of order m_W^2/m_Ψ^2. The current experimental bound is $\mathrm{BR}(\mu \to e\gamma) < 4 \times 10^{-13}$ [67]. For anarchic couplings and masses this translates into $y/m_\Psi \lesssim 2.7 \times 10^{-2}/\mathrm{TeV}$. However, the bound can be significantly relaxed by using flavor symmetries. One very efficient way to achieve this is to assume that the Lagrangian eq. (3.4) has a global $U(1)_e \times U(1)_\mu \times U(1)_\tau$ symmetry under which the three generations of ℓ, e, Ψ, Ψ^c transform [68].[6] This assumption forces y, m_Ψ, as well as the SM lepton Yukawa coupling, to be diagonal in flavor space and therefore $\mu \to e\gamma$ to vanish. The symmetry $U(1)_e \times U(1)_\mu \times U(1)_\tau$ is then weakly broken by the $(B-L)$-violating couplings in eq. (3.5) to ensure large mixing angles in the PMNS matrix. As a result, we find a huge suppression $O(C^4)$ with respect to the result eq. (3.11), i.e. $\mathrm{BR}(\mu \to e\gamma) \sim \mathrm{BR}_{\mathrm{ISS}}(\mu \to e\gamma)\, C^4$. Similarly, one can verify that all CP-odd phases can be removed from y, m_Ψ, and the first new physics contribution to the EDMs is suppressed by at least C^4. We thus see that the non-observation of rare processes does not represent a robust constraint on this

[6] One may use gauge symmetries to enforce this possibility.

scenario. The most model-independent constraints on y, m_Ψ come from ElectroWeak (EW) precision tests and are of order $y/m_\Psi \lesssim 0.1/$ TeV (see for example [59] and references therein).

3.3 Leptogenesis with small $U(1)_{B-L}$ breaking

In this section we present *analytic* estimations of the baryon asymmetry from thermal leptogenesis in TeV scale models with small $U(1)_{B-L}$ breaking. We show the results for two specific models: the inverse seesaw and linear seesaw models, as well as combinations of the two. Our qualitative conclusions are however more general and may extend to a broader class of models with small lepton number violation. In section 3.3.1 we determine the size of the CP parameter, the washout factor and the final baryon asymmetry. Our results will demonstrate that TeV scale models with anarchic (i.e., roughly of same order but not degenerate) couplings and mass parameters tend to predict too small baryon asymmetry. An intuitive interpretation of the parametric dependence of these results is shown in section 3.3.2 based on the (generalized) Nanopoulos-Weinberg theorem. Finally, in section 3.3.3, we identify a few possibilities that can give rise to successful (sub-)TeV scale leptogenesis with small lepton-number breaking. Conclusions similar to ours are obtained in the numerical analysis of ref. [62].

3.3.1 Leptogenesis in TeV scale inverse and linear seesaw

In this section, instead of studying thermal leptogenesis in the most general model [eq. (3.4) and eq. (3.5)], we illustrate the main results in two limiting cases, namely the ISS and LSS models. The Lagrangians we consider are

$$-\mathcal{L}_{\rm ISS} \supset y_{a\alpha}\Psi_a^c H\ell_\alpha + m_{\Psi_a}\Psi_a\Psi_a^c + \frac{\mu_{ab}}{2}\Psi_a\Psi_b + \text{h.c.}, \tag{3.12}$$

$$-\mathcal{L}_{\rm LSS} \supset y_{a\alpha}\Psi_a^c H\ell_\alpha + m_{\Psi_a}\Psi_a\Psi_a^c + y'_{a\alpha}\Psi_a H\ell_\alpha + \text{h.c.}, \tag{3.13}$$

where $\alpha = \{e, \mu, \tau\}$ denotes SM lepton flavor index and a, b are the generation indices for Ψ. Without loss of generality, we work in the basis where m_Ψ is diagonal and real. For both models, we demand the singlet neutrinos come in two generations ($a, b = \{1, 2\}$), which is the minimum number of generations required to achieve the realistic neutrino mass matrix. Qualitative results in such two-generation model will not differ much from three-generation one. In the rest of this section, we demand that $y \gtrsim 0.01$ and define[7]

$$\varepsilon \equiv \mu/m_\Psi \ll 1, \qquad \varepsilon' \equiv y'/y \ll 1. \tag{3.14}$$

These are the natural choice of parameters for both seesaw models to obtain the SM neutrino masses and testable collider signals. The smallness of neutrino mass is controlled by the smallness of ε or ε' [see eq. (3.9)].

[7]Since we mostly assume couplings and masses are anarchic in this section, we will simply use variables without generation or flavor indices to show the parametric dependence.

To be concrete here we will present the case of the ISS model. Similar conclusions can be drawn for the LSS model, as we emphasize at the end of section 3.3.1 and a more quantitative analysis is shown in the appendix A. Starting from eq. (3.12), we can write

$$\mu = \begin{pmatrix} \mu_1 & \bar{\mu} \\ \bar{\mu} & \mu_2 \end{pmatrix}, \tag{3.15}$$

where we define $\mu_a(\bar{\mu})$ as the diagonal (off-diagonal) parts of μ matrix. In general, the μ matrix is complex. However, since we assume all the phases of each element are order one, and yet we will be doing order of magnitude parametric estimation, including those will make at most $O(1)$ changes, but will not modify the parametrics of our estimations. For the sake of simplicity, then we simply treat all elements as real numbers. Assuming $\mu_a \sim \bar{\mu} \ll m_{\Psi_a}, |m_{\Psi_2} - m_{\Psi_1}|$, we can diagonalize the Ψ, Ψ^c mass matrix to first order in $\varepsilon_a \equiv \mu_a/m_{\Psi_a} (a = 1, 2)$ and $\bar{\mu}/m_{\Psi_a}$. Defining four Majorana states $(\tilde{\Psi}_i,\ i = 1, 2, 3, 4)$ with real masses $(m_i,\ i = 1, 2, 3, 4)$ we have

$$-\mathcal{L}_{\rm ISS}^{\rm mass} \supset h_{i\alpha}\tilde{\Psi}_i H \ell_\alpha + \frac{1}{2} m_i \tilde{\Psi}_i \tilde{\Psi}_i + \text{h.c.}. \tag{3.16}$$

To first order in ε_a and $\bar{\mu}/m_\Psi$, their masses and couplings $h_{i\alpha}$ are given as (ref. [69])

$$\begin{aligned}
m_1 &\simeq m_{\Psi_1}\left(1-\frac{\varepsilon_1}{2}\right) \quad ; \quad h_{1\alpha} \simeq \frac{i}{\sqrt{2}}\left(y_{1\alpha}+\frac{\varepsilon_1}{4}y_{1\alpha}+\bar{\varepsilon}_1 y_{2\alpha}\right)\\
m_2 &\simeq m_{\Psi_1}\left(1+\frac{\varepsilon_1}{2}\right) \quad ; \quad h_{2\alpha} \simeq \frac{1}{\sqrt{2}}\left(y_{1\alpha}-\frac{\varepsilon_1}{4}y_{1\alpha}-\bar{\varepsilon}_1 y_{2\alpha}\right)\\
m_3 &\simeq m_{\Psi_2}\left(1-\frac{\varepsilon_2}{2}\right) \quad ; \quad h_{3\alpha} \simeq \frac{i}{\sqrt{2}}\left(y_{2\alpha}+\frac{\varepsilon_2}{4}y_{2\alpha}-\bar{\varepsilon}_2 y_{1\alpha}\right)\\
m_4 &\simeq m_{\Psi_2}\left(1+\frac{\varepsilon_2}{2}\right) \quad ; \quad h_{4\alpha} \simeq \frac{1}{\sqrt{2}}\left(y_{2\alpha}-\frac{\varepsilon_2}{4}y_{2\alpha}+\bar{\varepsilon}_2 y_{1\alpha}\right),
\end{aligned} \tag{3.17}$$

where

$$\bar{\varepsilon}_1 = \frac{\bar{\mu} m_{\Psi_2}}{m_{\Psi_2}^2 - m_{\Psi_1}^2} \quad , \quad \bar{\varepsilon}_2 = \frac{\bar{\mu} m_{\Psi_1}}{m_{\Psi_2}^2 - m_{\Psi_1}^2}. \tag{3.18}$$

From eq. (3.17), we see that $(\tilde{\Psi}_1, \tilde{\Psi}_2)$ and $(\tilde{\Psi}_3, \tilde{\Psi}_4)$ form pseudo-Dirac pairs with small Majorana mass splitting. The mass splitting between a pseudo-Dirac pair is only controlled by diagonal μ_a while both μ_a and $\bar{\mu}$ modify the Yukawa couplings. Taking the limit $\mu_a, \bar{\mu} \to 0$, one can easily find that $m_1 = m_2$, $m_3 = m_4$ and $h_{1\alpha} = i h_{2\alpha}$, $h_{3\alpha} = i h_{4\alpha}$, as expected for pure Dirac states.

3.3.1.1 CP asymmetry

Now we are ready to calculate the CP asymmetry from the decay of each Majorana state $\tilde{\Psi}_i \to \ell_\alpha H, (\ell_\alpha H)^*$. After summing over SM lepton flavor α, we

get:[8]

$$\epsilon_i \equiv \frac{\sum_\alpha \left[\Gamma(\tilde{\Psi}_i \to \ell_\alpha H) - \Gamma(\tilde{\Psi}_i \to \bar{\ell}_\alpha H^*)\right]}{\sum_\alpha \left[\Gamma(\tilde{\Psi}_i \to \ell_\alpha H) + \Gamma(\tilde{\Psi}_i \to \bar{\ell}_\alpha H^*)\right]} = \frac{1}{8\pi} \sum_{j \neq i} \frac{\mathrm{Im}[(hh^\dagger)^2_{ij}]}{(hh^\dagger)_{ii}} f_{ij}, \tag{3.19}$$

where $f_{ij} \equiv f^{\rm v}_{ij} + f^{\rm self}_{ij}$ comprises a contribution from vertex corrections [73]

$$f^{\rm v}_{ij} = g\left(\frac{m_j^2}{m_i^2}\right) \quad ; \quad g(x) = \sqrt{x}\left[1 - (1+x)\ln(1+\frac{1}{x})\right], \tag{3.20}$$

as well as a self energy correction to the decay [60, 61]

$$f^{\rm self}_{ij} = \frac{(m_i^2 - m_j^2) m_i m_j}{(m_i^2 - m_j^2)^2 + m_i^2 \Gamma_j^2}. \tag{3.21}$$

Here $\Gamma_j \equiv (hh^\dagger)_{jj} m_j/(8\pi)$ is the decay width of $\tilde{\Psi}_j$.

Let's take a close look at ϵ_1 and ϵ_2 in eq. (3.19):

$$\begin{aligned} \epsilon_1 &= \frac{1}{8\pi (hh^\dagger)_{11}} \mathrm{Im}[(hh^\dagger)^2_{12} f_{12} + (hh^\dagger)^2_{13} f_{13} + (hh^\dagger)^2_{14} f_{14}], \\ \epsilon_2 &= \frac{1}{8\pi (hh^\dagger)_{22}} \mathrm{Im}[(hh^\dagger)^2_{21} f_{21} + (hh^\dagger)^2_{23} f_{23} + (hh^\dagger)^2_{24} f_{24}]. \end{aligned} \tag{3.22}$$

Given that the pseudo-Dirac pairs are almost degenerate in mass, the number density of two states are approximately the same. As a result (see appendix D), it is appropriate to consider $\epsilon_1 + \epsilon_2$ and $\epsilon_3 + \epsilon_4$ as the effective CP asymmetry for each

[8] Assuming anarchy of Yukawa couplings $h_{i\alpha}$, the lepton asymmetry produced will be distributed among all the lepton flavors in roughly equal proportion. For simplicity, we ignore the small differences in the various flavor asymmetries and sum over α. When couplings are hierarchical flavor effects [70–72] could play a more relevant role, and we will briefly mention about it in section 3.3.3.

generation. Due to the pseudo-Dirac nature, one finds that

$$(hh^\dagger)^2_{13} \simeq -(hh^\dagger)^2_{23} \simeq -(hh^\dagger)^2_{14} \simeq (hh^\dagger)^2_{24} \; ; \; f_{13} \simeq f_{14} \simeq f_{23} \simeq f_{24} \, . \tag{3.23}$$

This means that when we consider the sum of ϵ_1 and ϵ_2, parts involving f_{13} and f_{14} in ϵ_1 will cancel against the corresponding parts with f_{23} and f_{24} in ϵ_2 to first order. Also, if we consider the generic parameter region of the ISS, i.e.,

$$\mu_a \sim \bar{\mu} \ll \Gamma_i \ll m_{\Psi_a} \sim |m_{\Psi_2} - m_{\Psi_1}|, \tag{3.24}$$

and no hierarchies in mass or couplings among singlet generations and SM flavors, we would get $\bar{\varepsilon}_{1,2} \sim \bar{\mu}/m_{\Psi_{1,2}}$ and

$$\begin{aligned} -f^{\rm self}_{12} \simeq f^{\rm self}_{21} \sim \varepsilon_1 \left(\frac{m_{\Psi_1}}{\Gamma_2}\right)^2 \; , \; f^{\rm v}_{12} - f^{\rm v}_{21} \sim \varepsilon_1, \\ (f_{13} - f_{14}) \sim \varepsilon_2 \; , \; (f_{13} - f_{14} - f_{23} + f_{24}) \sim \varepsilon_1 \varepsilon_2. \end{aligned} \tag{3.25}$$

Therefore, the terms involving $f^{\rm self}_{12}$ and $f^{\rm self}_{21}$ dominate in $\epsilon_1 + \epsilon_2$, giving [see eq. (3.22)]

$$\begin{aligned} \epsilon \equiv \epsilon_1 + \epsilon_2 \; &\sim \; \frac{{\rm Im}[(yy^\dagger)^2_{12}]}{(yy^\dagger)^2_{11}} \bar{\varepsilon}_1 \frac{\mu_1/m_{\Psi_1}}{(yy^\dagger)_{11}/(16\pi)} + O\left(\varepsilon^2 \frac{\Gamma}{m_\Psi}\right) + O\left(\bar{\varepsilon}^2 \frac{\Gamma}{m_\Psi}\right) \\ &\sim \; \frac{\bar{\mu}}{m_\Psi} \frac{\mu}{\Gamma} \end{aligned} \tag{3.26}$$

where we have dropped the family indices for μ and Γ to show only the parametric dependence. To go from the first line of eq. (3.26) to the second line, we only kept the dominant piece based on our choice of parameter region of ISS in eq. (3.24).

Similarly, $\epsilon_3 + \epsilon_4$ can be obtained by changing index $1 \to 2$ and $2 \to 1$ in eq. (3.26), resulting in the same parametric dependence.

For completeness, we also show the parametric dependence of $\epsilon_{1,2}$:

$$\epsilon_1 \approx -\epsilon_2 = O\left(\frac{\bar{\mu}}{m_\Psi}\frac{\mu}{\Gamma}\right) + O\left(\frac{\mu}{m_\Psi}\frac{\Gamma}{m_\Psi}\right) + O\left(\frac{\bar{\mu}}{m_\Psi}\frac{\Gamma}{m_\Psi}\right). \tag{3.27}$$

We only use $\epsilon_1 + \epsilon_2$ instead of individual ϵ_1 or ϵ_2 in our study of leptogenesis. However, they are relevant for the argument in appendix D.

If we assume $\mu \sim \bar{\mu}$ and enforce $m_\nu \sim 0.05$ eV via eq. (3.9), eq. (3.26) becomes (see also refs. [60, 61])

$$\epsilon \sim \frac{\mu}{m_\Psi}\frac{\mu}{\Gamma} \sim \frac{16\pi m_\nu^2 m_\Psi^2}{y^6 v^4} \sim 10^{-10}\left(\frac{m_\Psi}{\text{TeV}}\right)^2\left(\frac{10^{-2}}{y}\right)^6. \tag{3.28}$$

As we will see shortly [eq. (3.29)], $|\epsilon|$ should be $\gtrsim 10^{-7}$ to generate the observed baryon asymmetry via leptogenesis and eq. (3.28) falls short by three orders of magnitude. From eq. (3.28), it seems that one can obtain a larger value by reducing Yukawa couplings y. However, this approach will not allow us to obtain sufficient baryon asymmetry once we, as required, include the washout effects. We will discuss this in the following section.

3.3.1.2 Washout and baryon asymmetry

The final baryon asymmetry through leptogenesis from decays of $\tilde{\Psi}_i \to \ell_\alpha H, (\ell_\alpha H)^*$ can be parametrized as follows

$$Y_{\Delta B} \equiv \frac{n_B - n_{\bar{B}}}{s} \sim 10^{-3} \epsilon \, \eta, \tag{3.29}$$

where $n_{B(\bar{B})}$ is the number density of baryons (anti-baryons) and s is the total entropy density of the thermal bath. The pre-factor $\sim 10^{-3}$ comes from relativistic number density of $\tilde{\Psi}_i$ normalized to the entropy density s. The efficiency factor η is always less than unity and parametrizes the effect of washout processes. It is obtained by solving the Boltzmann equations. The efficiency of leptogenesis can be parametrized by the so-called washout factor [40]

$$K_i \equiv \frac{\Gamma_i}{H(T = m_i)} \tag{3.30}$$

where $H(T) \sim \sqrt{g_*} T^2 / M_{\rm Pl}$ is the Hubble rate with T being the thermal bath (photon) temperature, g_* the number of relativistic degrees of freedom and $M_{\rm Pl} = 1.22 \times 10^{19}$ GeV the Planck mass. In the ISS scenario, due to the approximate lepton

number conservation, the washout from inverse decay is actually controlled by [74][9]

$$K^{\rm eff} \sim K\delta^2, \tag{3.31}$$

where $\delta \equiv |\Delta m|/\Gamma \simeq \mu/\Gamma$ with $\Delta m = m_2 - m_1$ or $m_4 - m_3$. Also, we dropped generation index for simplicity of notation and we will do so below when there is no chance of confusion. Consistently, this quantity vanishes in the lepton number conserving limit. Notice that we can express eq. (3.26) as

$$\epsilon \sim \frac{\Gamma}{m_\Psi}\delta^2, \tag{3.32}$$

where we have taken $\bar{\mu} \sim \mu$.

If $K^{\rm eff} >$ a few, the washout from inverse decay $(H\ell_\alpha, (H\ell_\alpha)^* \to \tilde{\Psi}_i)$ is efficient (strong washout regime) and $\eta \sim 1/K^{\rm eff}$ (see appendix B.2.2). In this regime, substituting eqs. (3.32) and (3.31) into eq. (3.29), the baryon asymmetry is estimated to be

$$Y_{\Delta B} \sim 10^{-3}\sqrt{g_*}\frac{m_\Psi}{M_{\rm Pl}} \sim 10^{-18}\left(\frac{m_\Psi}{1{\rm TeV}}\right), \tag{3.33}$$

where we have taken $\sqrt{g_*} \sim 10$. This analytic estimation was first obtained in our

[9]The appearance of δ^2 may be understood as follows. In the limit $\mu \to 0$, since lepton number is preserved, no process can washout (or produce) the asymmetry. Therefore, the effective washout factor must vanish as $\mu \to 0$. Another (more technical) way to see this is to recall that the washout from the inverse decay can be obtained by the on-shell part of $\Delta L = 2$ $H\ell \leftrightarrow (H\ell)^*$ scattering. Due to the near degeneracy, this scattering gets contribution from both s-channel $\tilde{\Psi}_1$ and $\tilde{\Psi}_2$ and importantly, most of their contributions cancel. The surviving piece comes from interference of the two and is proportional to δ^2.

earlier paper [54]. Clearly, a TeV scale m_Ψ will result in a too small asymmetry compared to the observed value $Y_{\Delta B}^{\rm obs} \approx 9 \times 10^{-11}$ [75]. Remarkably, in the strong washout regime, the final baryon asymmetry ($Y_{\Delta B}$) for the ISS model with anarchic couplings and masses reduces to the simple formula [eq. (3.33)] which does not depend on μ and y.

To complete our discussion, we also need to consider the weak washout regime, where $K^{\rm eff} < 1$. ISS model has a peculiar feature that the production of singlets is controlled by K [eq. (3.30)], whereas the washout is controlled by $K^{\rm eff}$ [eq. (3.31)]. Assuming no initial abundance of $\tilde{\Psi}_i$, there are two cases in weak washout region and the corresponding efficiency factors η are

$$\eta \sim \begin{cases} K^{\rm eff} & (K^{\rm eff} < 1 \text{ and } K > 1 \text{ with no initial } \tilde{\Psi}_i) \\ K \times K^{\rm eff} & (K^{\rm eff} < 1 \text{ and } K < 1 \text{ with no initial } \tilde{\Psi}_i), \end{cases} \tag{3.34}$$

as derived in appendix B.2.1. We emphasize that such parametric dependence of η is qualitatively different from that of usual type I seesaw (i.e., $\eta \sim K^2$). To the best of our knowledge, this analytic result, especially which of $K^{\rm eff}$, K should appear in η, has not been discussed in the literature. The intuitive understanding of this parametric dependence is as follows. Firstly note that neglecting the washout, there will be opposite and equal amounts of asymmetry generated during the production and decay of singlets $\tilde{\Psi}_i$. These opposite sign asymmetries would cancel each other resulting in zero asymmetry. However, including the effect of washout, the asymmetry generated earlier (i.e. during the production of the singlets) expe-

riences more washout and the cancellation among the opposite sign asymmetries is not perfect anymore. The net asymmetry is therefore suppressed by the washout factor $K_{\rm eff}$. This factor is seen in both lines of eq. (3.34). Secondly, the asymmetry generated during production and decay of singlets are each proportional to the maximum yield of the singlets or equivalently to their yield when $T = m_\Psi$, which is $O(1)$ for $K > 1$ while parametrically suppressed by K when $K < 1$. This explains the extra suppression by K in the second line of eq. (3.34). See appendix B.2.1 for more detail.

If we, on the other hand, assume $\tilde{\Psi}_i$ acquires thermal initial abundance with zero initial asymmetry,[10] the efficiency factor is of the order

$$\eta \sim O(1) \quad (K^{\rm eff} < 1 \text{ with thermal initial } \tilde{\Psi}_i). \tag{3.35}$$

Putting everything together, in the weak washout regime, we have

$$Y_{\Delta B} \sim 10^{-3}\epsilon\,\eta \sim \begin{cases} 10^{-3}\sqrt{g_*}\frac{m_\Psi}{M_{\rm pl}}(K^{\rm eff}) & (K^{\rm eff} < 1 \text{ with thermal initial } \tilde{\Psi}_i) \\ 10^{-3}\sqrt{g_*}\frac{m_\Psi}{M_{\rm pl}}(K^{\rm eff})^2 & (K^{\rm eff} < 1 \text{ and } K > 1 \text{ with no initial } \tilde{\Psi}_i) \\ 10^{-3}\sqrt{g_*}\frac{m_\Psi}{M_{\rm pl}}(K^{\rm eff})^2 K & (K^{\rm eff} < 1 \text{ and } K < 1 \text{ with no initial } \tilde{\Psi}_i). \end{cases} \tag{3.36}$$

We see that in all cases the final baryon asymmetry in the weak washout regime $K^{\rm eff} < 1$ is smaller compared to that of strong washout in eq. (3.33). Therefore,

[10] For instance, if $\tilde{\Psi}_i$ is charged under new gauge symmetries (e.g. $U(1)_{B-L}$), they can acquire an initial thermal abundance.

Model	CP asymmetry (ϵ)	Efficiency (η)	Baryon asymmetry ($Y_{\Delta B}$)
Inverse seesaw	$\frac{\Gamma}{m_\Psi}\delta^2$	$\lesssim \left(\frac{\Gamma}{H}\delta^2\right)^{-1}$	$\lesssim 10^{-3}\sqrt{g_*}\frac{m_\Psi}{M_{\rm pl}} \sim 10^{-18}\left(\frac{m_\Psi}{1\text{TeV}}\right)$
Linear seesaw	$\frac{\Gamma}{m_\Psi}\varepsilon'^2$	$\lesssim \left(\frac{\Gamma}{H}\varepsilon'^2\right)^{-1}$	$\lesssim 10^{-3}\sqrt{g_*}\frac{m_\Psi}{M_{\rm pl}} \sim 10^{-18}\left(\frac{m_\Psi}{1\text{TeV}}\right)$

Table 3.2: Summary of the parametric dependence of CP asymmetry, washout, baryon asymmetry in inverse [see eq. (3.12)] and linear seesaw [see eq. (3.13)]. The parameters $\varepsilon, \varepsilon'$ are defined in eq. (3.14), wheres δ below eq. (3.31).

the TeV scale ISS model with anarchic mass and coupling cannot provide successful leptogenesis.

An analogous calculation for the LSS model is shown in appendix A and the parametric dependences of the final baryon asymmetry of the two seesaw models are in fact the same, as we summarize in table 3.2. Therefore, we conclude that TeV scale ISS and LSS model with anarchic parameters (y, m_Ψ, μ or y') and sizable y cannot give rise to successful leptogenesis.

3.3.2 Nanopoulos-Weinberg theorem

As discussed in the previous section, the CP asymmetries in TeV scale ISS and LSS models are small because they are respectively $\epsilon \propto \delta^2$[11] and ε'^2, where δ, ε' are the tiny parameters characterizing the small lepton number violation. We will argue in this section that this feature can indeed be anticipated due to Nanopoulos-Weinberg (NW) theorem (ref. [76]) and similar conclusions can be drawn in some

[11] One might wonder why the lepton-number violation is captured by $\varepsilon \sim \mu/m_\Psi$ in the case of the neutrino mass, and by $\delta \sim \mu/\Gamma$ in the case of CP-violation (and leptogenesis). This may follow from the fact that while the generation of m_ν is off-shell phenomenon (i.e. simply integrate out $\tilde{\Psi}$'s), that of CP-violation and related asymmetry generation occurs near on-shell. Especially, when the genesis goes through the resonance-enhancement, on top of parametric lepton-number violation ε, it acquires extra kinematic (resonance-)enhancement $\sim m_\Psi/\Gamma$, yielding the associated net breaking parameter $\sim \left(\frac{\mu}{m_\Psi}\right)\left(\frac{m_\Psi}{\Gamma}\right) \sim \delta$.

variations of ISS or LSS models, or combination of both.

The NW theorem states that, in the CP-violating decay process, if the particle can decay only through baryon (lepton) number violating parameters (e.g. Type-I), a nonzero CP asymmetry can be generated starting at third order in baryon (lepton) number violating parameters. In addition, the generalized version of the NW theorem (refs. [77, 78]) says that, if the decaying particle, on the other hand, can decay through both baryon (lepton) number violating and conserving couplings, the CP asymmetry may be generated at second order in baryon (lepton) number violating parameters.

Now we apply both theorems to check our results for the ISS and LSS models. The CP asymmetry in decay width is given in eq. (3.26) for ISS and eq. (A.9) for LSS:

$$\sum_i \sum_f |\Gamma(\tilde{\Psi}_i \to f) - \Gamma(\tilde{\Psi}_i \to \bar{f})| \propto \begin{cases} \mathrm{Im}[(yy^\dagger)^2_{12}]\delta^2 & \text{(ISS)} \\ \\ \mathrm{Im}[(yy^\dagger)_{12}(y'y'^\dagger)_{12}] & \text{(LSS)}, \end{cases} \tag{3.37}$$

where we sum over almost degenerate $\tilde{\Psi}_i$ states and all final states f.

For the ISS, if we assign the lepton number charges $L(\ell) = L(\Psi) = -L(\Psi^c) = 1$, the Yukawa coupling y is lepton number conserving and μ is the only lepton number violating parameter. Then Ψ, Ψ^c can decay also via number-conserving interactions and, following the extended version of the NW theorem, the CP asymmetry should be $O(\mu^2)$. The CP asymmetry in eq. (3.37) indeed contains δ^2, hence

$\propto \mu^2$.

Similarly for the LSS, we can always assign lepton number such that only one of y or y' violates lepton number. Since Ψ, Ψ^c can decay through either y or y', it always follows the extended NW theorem. Therefore, we expect the CP asymmetry is proportional to two powers of y and two powers of y', which matches the result in eq. (3.37).

In general, NW theorem forces the CP asymmetry from singlets decay to be $O(\delta^2)$ or $O(\varepsilon'^2)$, which is suppressed in models with small lepton number breaking. Adding further lepton number conserving decay channels or new generations of leptons would not alter this result.

3.3.3 Possible variations to achieve successful leptogenesis

Our discussion so far assumed anarchic couplings and masses and considered either a small μ or a small y', separately. In this subsection we relax these assumptions with the aim of looking for models with small $U(1)_{B-L}$ violation that can result in larger final asymmetry compared to eq. (3.33).

3.3.3.1 Inverse seesaw with degeneracy among different generations

We first consider the possibility that the singlet masses are quasi-degenerate among different *generations*:

$$\Delta m_\Psi \equiv |m_{\Psi_2} - m_{\Psi_1}|, \tag{3.38}$$

with $\mu \ll \Delta m_\Psi \ll m_{\Psi_1}, m_{\Psi_2}$ so that our previous formulae in section 3.3.1 still apply. Although quasi-degeneracy in mass within a pseudo-Dirac pair is naturally obtained due to approximate lepton number, to realize quasi-degeneracy in mass among singlets of different generations in a natural way, an approximate family symmetry is necessary as was done, for example, in the resonant leptogenesis scenario [79–81]. In scenarios with minimal flavor violation, even if Δm_Ψ is set to zero at the tree level, generally Yukawa couplings might break the family symmetry, generating Δm_Ψ at loop level of the size[12]

$$\frac{\Delta m_\Psi}{m_\Psi} \gtrsim \frac{y^2}{16\pi^2}. \tag{3.39}$$

In this case, the $\bar{\varepsilon}_{1,2}$ which parametrically is given by (see eq. (3.18))

$$\bar{\varepsilon}_1 \sim \bar{\varepsilon}_2 \sim \frac{\bar{\mu}}{\Delta m_\Psi}, \tag{3.40}$$

can be enhanced. Substituting eq. (3.40) into eq. (3.26), one has

$$\epsilon \sim \frac{\mu}{m_\Psi}\frac{\mu}{\Gamma}\frac{m_\Psi}{\Delta m_\Psi}. \tag{3.41}$$

When two generations are nearly degenerate, thus, the CP asymmetry is enhanced compared to eq. (3.26) by a factor of $\frac{m_\Psi}{\Delta m_\Psi}$. The washouts are nevertheless un-

[12]For recent work on leptogenesis in minimal flavor violation models with degeneracy among different generations of singlets, see for example, [82].

changed.[13] So the final result scales as

$$Y_{\Delta B} \sim 10^{-3}\sqrt{g_*}\frac{m_{\Psi_1}}{M_{\rm pl}}\frac{m_\Psi}{\Delta m_\Psi}. \tag{3.42}$$

The right size of $Y_{\Delta B}$ may be obtained by choosing the right size for $\frac{m_\Psi}{\Delta m_\Psi}$. However, we are not completely free to choose its value here. In particular, our analysis is done under the assumption that $\Delta m_\Psi \gg \mu$[14] and (technical) naturalness indicates that $\Delta m_\Psi/m_\Psi \gtrsim y^2/16\pi^2$. Combining these two with the constraint from the neutrino mass, i.e. $m_\nu \sim y^2v^2\mu/m_\Psi^2$, gives rise to an upper bound on the enhancement factor $m_\Psi/\Delta m_\Psi \ll 10^7$. Therefore, we conclude that while degeneracy among different singlet generation can induce a significant enhancement in the final asymmetry, whether or not the actual observed quantity can be accounted requires a careful numerical study. We find it quite likely that the observed asymmetry may be explained by this effect, but only in a small corner of the parameter space with $y \sim 10^{-3}$ for $m_\Psi \sim$ TeV.

[13]The contribution to $K^{\rm eff}$ has two pieces in the non-degenerate case: $K^{\rm eff} = K\left[O(\frac{\mu^2}{\Gamma^2}) + O(\frac{\mu^2}{m_\Psi^2})\right]$. The second term is suppressed compared to the first one and thus we only keep the first term in the previous estimation. In the case we discussed here, where there is degeneracy among different generations, the first term is still unchanged. This is because the first term is controlled by the mass splitting within each generation, which will not be modified by the degeneracy among different generations. The second term, however, is enhanced by $\frac{m_\Psi^2}{\Delta m_\Psi^2}$: $K\frac{\mu^2}{m_\Psi^2}\frac{m_\Psi^2}{\Delta m_\Psi^2}$. Now these two terms are comparable due to the assumption in eq. (3.39) and the parametric dependence of $K^{\rm eff}$ remain the same as in eq. (3.31).

[14]Implicitly, we also assumed $\Gamma \gg \mu$ to get a concrete expression. However, a straightforward check can confirm that while CP and washout factor will change (basically replacing μ/Γ with Γ/μ), the final asymmetry will be the same as the one we show above.

3.3.3.2 Inverse seesaw + linear seesaw

ISS and LSS models were treated separately in the previous discussions, see eqs. (3.12) and (3.13). Now we consider scenarios in which both μ, y' are non-vanishing:[15]

$$-\mathcal{L}_{\text{ISS+LSS}} \supset y_{a\alpha}\Psi^c_a H\ell_\alpha + (m_\Psi)_a \Psi_a \Psi^c_a + \frac{(\mu)_{ab}}{2}\Psi_a\Psi_b + y'_{a\alpha}\Psi_a H\ell_\alpha + \text{h.c.}. \quad (3.43)$$

For this model we will only consider one generation of singlets. Nothing qualitatively new happens when more generations are included (unless they are nearly degenerate, in which case one can use the results of the previous subsection). As previously shown in ref. [74], the CP asymmetry is parametrized as

$$\epsilon \sim \frac{\Gamma}{m_\Psi}\left(O(\delta^2) + O(\delta\varepsilon'\frac{m_\Psi}{\Gamma}) + O(\varepsilon'^2)\right). \quad (3.44)$$

Following the analysis in ref. [74], the washout can be worked out as

$$K^{\text{eff}} \sim \frac{\Gamma}{H}\left(O(\delta^2) + O(\varepsilon'^2) + O(\varepsilon\varepsilon')\right). \quad (3.45)$$

Based on eqs. (3.44) and (3.45), it is obvious that in the limit where $y' \to 0$ or $\mu \to 0$, we recover the results for the ISS or LSS (at tree level) models (see table 3.2).

Now we would like to find if there exists a range of parameters where the

[15] In principle there could also be $\mu'\Psi^c\Psi^c$ term, see eq. (3.5). However, such a term does not enter neutrino mass formula and has similar effects as μ in leptogenesis. Therefore we neglect it in this study.

asymmetry is larger than eq. (3.33). To do this, let us first focus on the strong washout regime for definiteness. Under this hypothesis the final asymmetry is given by $\epsilon/K^{\rm eff}$ and

$$Y_{\Delta B} \sim 10^{-3}\sqrt{g_*}\frac{m_\Psi}{M_{\rm pl}} \times \left[\frac{1+\mathcal{O}\left(\frac{\varepsilon'^2}{\delta^2}\right)+\mathcal{O}\left(\frac{\varepsilon' m_\Psi}{\delta\Gamma}\right)}{1+\mathcal{O}\left(\frac{\varepsilon'^2}{\delta^2}\right)+\mathcal{O}\left(\frac{\varepsilon'\Gamma}{\delta m_\Psi}\right)}\right]. \tag{3.46}$$

For $\varepsilon'/\delta \ll \Gamma/m_\Psi$ or $\varepsilon'/\delta \gg m_\Psi/\Gamma$ one can readily see that the square bracket in eq. (3.46) becomes of order unity. In these limits, one can check that terms only involving μ (when $\varepsilon'/\delta \ll \Gamma/m_\Psi$) or y' (when $\varepsilon'/\delta \gg m_\Psi/\Gamma$) will be dominant in both neutrino mass formula [eq. (3.8)] and leptogenesis [see eqs. (3.44) and (3.45)]. Clearly, these limits correspond to the cases studied above, namely the ISS and LSS respectively.

The only unexplored region of parameter space is $\Gamma/m_\Psi \ll \varepsilon'/\delta \ll m_\Psi/\Gamma$, where we have

$$[\cdots] \sim \frac{m_\Psi}{\Gamma}\frac{\mathcal{O}\left(\frac{\varepsilon'}{\delta}\right)}{1+\mathcal{O}\left(\frac{\varepsilon'^2}{\delta^2}\right)}. \tag{3.47}$$

Here $[\cdots]$ refers to the expression inside the square bracket in eq. (3.46) and is maximized at $\varepsilon' \sim \delta$. Interestingly, in this regime, the neutrino mass formula is dominated by terms containing y', whereas both μ and y' have a significant impact on the asymmetry. Because both y', μ are necessary here, this case does not correspond to any model we discussed before. The final asymmetry is given by $Y_{\Delta B} \sim 10^{-3}\sqrt{g_*}\frac{m_\Psi}{M_{\rm pl}}\frac{m_\Psi}{\Gamma}$. This result is enhanced by a factor m_Ψ/Γ compared to the

typical value in eq. (3.33).

Let us therefore consider $\delta \sim \varepsilon'$. First of all, such condition might be realized quite naturally starting with a LSS framework and generating a μ term from radiative corrections. This way one expects [see eq. (3.7)]

$$\delta = \frac{\mu}{\Gamma} \sim \frac{yy' m_\Psi}{16\pi^2} \times \frac{16\pi}{y^2 m_\Psi} \sim \frac{1}{\pi}\varepsilon',$$

which is not far from the required relation. Then we can relax the assumption of strong washout ($K^{\rm eff} > 1$) and estimate the final baryon asymmetry more generally. In this regime $K^{\rm eff} \propto y'^2$, $K \propto y^2$ and the SM neutrino mass $m_\nu \propto yy'$. This implies that in the weak washout region (i.e., $K^{\rm eff} < 1$) we always have $K > 1$ for $m_\Psi \sim$ TeV. We thus have only two of the options previously considered in eq. (3.36). Finally, the baryon asymmetry scales as

$$\begin{aligned} &\epsilon \sim \varepsilon'^2, \qquad K^{\rm eff} \sim \frac{\Gamma}{H}\varepsilon'^2, \\ \Rightarrow \quad Y_{\Delta B} &\sim \begin{cases} 10^{-3}\frac{\epsilon}{K^{\rm eff}} \sim 10^{-3}\sqrt{g_*}\frac{m_\Psi}{M_{\rm pl}}\frac{m_\Psi}{\Gamma} & (K^{\rm eff} > 1) \\ 10^{-3}\epsilon K^{\rm eff} & (K^{\rm eff} < 1 \text{ with no initial } \tilde\Psi_i) \\ 10^{-3}\epsilon & (K^{\rm eff} < 1 \text{ with thermal initial } \tilde\Psi_i). \end{cases} \end{aligned} \tag{3.48}$$

These values are shown in figure 3.2 as a function of y with $m_\Psi = 1$ TeV. Figure 3.2 indicates the observed baryon asymmetry can be obtained if $y = O(10^{-5} - 10^{-4})$.

To conclude, we found that successful leptogenesis is achievable in scenarios of ISS + LSS with $\delta \sim \varepsilon'$, provided the Yukawa couplings are small enough. The

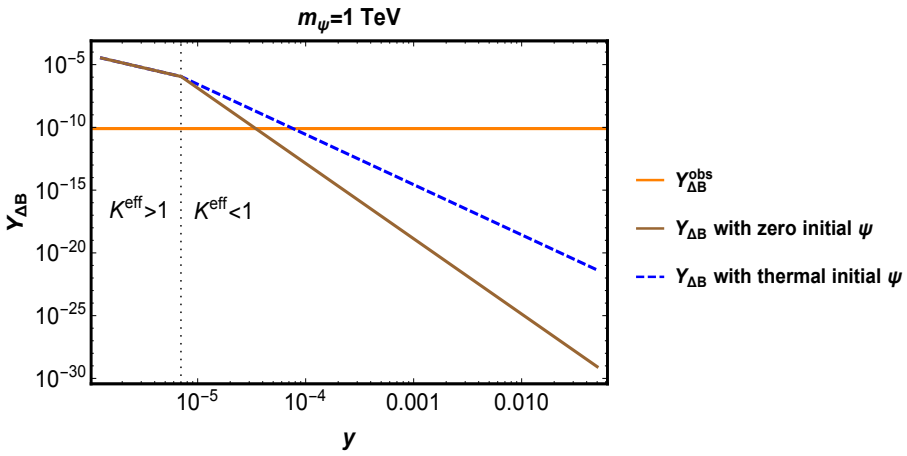

Figure 3.2: The baryon asymmetry $Y_{\Delta B}$ as a function of y in the case where $\delta \sim \varepsilon'$ in ISS+LSS models. Here m_Ψ is fixed to be 1 TeV. The blue dashed line shows result with initial thermal abundance of $\tilde{\Psi}_i$ while the solid brown line shows the results with no initial $\tilde{\Psi}_i$ abundance. The vertical dotted lines indicate the border between the strong and weak washout regions. The orange line shows where the observed baryon asymmetry is obtained. Here we only plot the region where $y > y'$, meaning $y > \sqrt{yy'} \sim \sqrt{m_\nu m_\Psi / v^2} \approx 10^{-6}$. When $y < y'$, the results can be simply obtained by the exchange the role of y and y'.

Yukawa coupling needed for leptogenesis, $y = O(10^{-5} - 10^{-4})$, clearly lies outside of the window of our naturalness criteria and is also too small to provide signals at colliders. Therefore, we will not consider this option any further.

3.3.3.3 Other mechanisms

There are several alternative options that may allow us to achieve a successful TeV scale (or lower) leptogenesis in scenarios with small $U(1)_{B-L}$ breaking. We here mention a few that were originally realized in the context of type I seesaw model with singlet fermions. We will however not discuss them in detail because they all require unnatural couplings or flavor symmetries.

As a first option, if there is certain hierarchical structure in the Yukawa coupling $y_{a\alpha}$ (i.e. deviations from anarchical as well as natural values), lepton flavor

effects can play an important role [70–72] in enhancing the efficiency since an optimal regime can be realized by having the lepton asymmetry stored in the lepton flavors that suffer the least washout. As we have touched upon earlier, a second option is allowing quasi-degeneracy in singlet mass of different generations—as in resonant leptogenesis [79–81]. This can be realized by imposing approximate family symmetry. In ref. [83], while total lepton number violation can be very small (or even conserved), both lepton flavor effects and quasi-degenaracy among mass of singlets have been utilized to achieve leptogenesis at around TeV scale.

Finally we should mention an alternative mechanism for leptogenesis. While the present work focuses on leptogenesis from decays of singlets, the lepton asymmetry can also be realized via flavor oscillation among singlets, as first pointed out by Akhmedov, Rubakov and Smirnov (ARS) [84]. One distinguishing feature of the ARS mechanism is that leptogenesis must occur at a scale higher than the singlet mass, $T > m_{\rm NP}$, when oscillations among sterile neutrinos can be important. Although the total lepton number is approximately conserved, flavor oscillation among singlets can create an asymmetry in some singlet flavor. The singlets that are in thermal equilibrium can subsequently transfer their asymmetry to the SM lepton doublets and finally, via the EW sphalerons, to the baryon sector. Requiring the generation of lepton asymmetry takes place while the EW sphalerons are still active ($T \gtrsim 100$ GeV), implies the mass of new singlets involved in ARS leptogenesis must be well below the weak scale, $m_{\rm NP} < 100$ GeV. They may hence be probed in neutrinoless double beta decay experiments and high intensity beam experiments. In this scenario, a hierarchy in $y_{a\alpha}$ is needed such that at least one of the singlets

does not reach thermal equilibrium until after EW sphaleron processes freeze out to prevent the washout of the asymmetry. According to our earlier definition, a certain amount of unnaturalness is thus required to realize this mechanism as well. In the context of ISS model, ARS leptogenesis with GeV scale singlets has been studied in refs. [85, 86].

3.4 General idea of the hybrid seesaw

Low-scale seesaw models with small lepton-number violation are confronted with several issues that make them not fully satisfactory. In particular, the required smallness of lepton-number breaking terms, the central ingredient for the seesaw mechanism, is often left unexplained. Even though the requirement $C \ll 1$ is consistent with the criteria of technical naturalness, one finds it not fully convincing because it has no clear origin within that description. In this sense the smallness of neutrino masses is not truly explained. The second major issue was discussed in section 3.3 and corresponds to the difficulty with regard to the question of explaining the observed baryon-anti-baryon asymmetry of the Universe via leptogenesis.

In this work, we will show that there exists a rather simple and motivated extension that addresses *both* issues. Before we get to more technical discussions, however, in this section we present a qualitative description of our model. We hope this makes the big picture and expected outcomes more transparent, which often could be obscured by otherwise essential details. For concreteness of discussion, in the rest of the chapter, we will focus on an extension of the inverse seesaw model.

3.4.1 Natural μ term and successful leptogenesis

Our hybrid seesaw model (proposed in [54] and also discussed in [55]) is based on the following Lagrangian:

$$-\mathcal{L} \supset y_{a\alpha}\Psi^c_a H \ell_\alpha + \kappa_a \Psi^c_a \Phi_\kappa \Psi_a + \lambda_{ia} N_i \Phi_\lambda \Psi_a + \frac{1}{2} M_{N_i} N_i N_i + \text{H.c.}, \quad (3.49)$$

where H and ℓ_α ($\alpha = e, \mu, \tau$) are the SM Higgs and lepton doublets and the $SU(2)_L$ contraction is left implicit. The new fermions N_i, (Ψ^c_a, Ψ_a) and the two complex scalars Φ_κ and Φ_λ are SM gauge singlets. We assume Φ_κ and Φ_λ have masses and develop vacuum expectation values of order the TeV scale. As a result (Ψ^c_a, Ψ_a) get a mass of that order as well. On the other hand we will take $M_{N_i} \gg$ TeV. Our model is therefore the marriage of a TeV scale module $(\Psi, \Psi^c, \Phi_\lambda, \Phi_\kappa)$ and a heavy module (N_i).

The model in eq. (3.49) represents a very special combination of the standard type I and the inverse seesaw. Specifically, the fermions N_i are analogous to those of the type I seesaw, whereas (Ψ^c_a, Ψ_a) play the role of the pseudo-Dirac fermions present in the usual inverse seesaw model of section 3.2. However, to realize our hybrid version of the seesaw it is crucial that there is *no* direct coupling between the heavy module N and the SM, i.e. ℓH. The heavy sector interacts with the SM only via the TeV module, see figure 3.1. This ensures that the virtual exchange of N_i does not generate neutrino masses, but rather a small Majorana mass term for Ψ_a (after the scalar Φ_λ acquires VEV).

To be more specific, the connection with eqs. (3.4) and (3.5) in section 3.2 or eq. (3.12) in section 3.3 can be made clear by noting that integrating out the heavy Majorana singlet N, we get

$$\mu_{ab} = \sum_i \frac{\lambda_{ia}\lambda_{ib}\left\langle\Phi_\lambda\right\rangle^2}{M_{N_i}} \tag{3.50}$$

$$m_{\Psi_a} = \kappa_a \left\langle\Phi_\kappa\right\rangle . \tag{3.51}$$

Using this in eq. (3.9), the SM neutrino mass is found to be (dropping flavor indices for simplicity)

$$m_\nu \sim \left[\frac{(yv)^2}{M_N}\right]\left(\frac{\lambda\langle\Phi_\lambda\rangle}{\kappa\langle\Phi_\kappa\rangle}\right)^2 . \tag{3.52}$$

The first factor in eq. (3.52) is the usual neutrino mass formula in high-scale type-I seesaw, i.e., the one we would have obtained *had* N directly coupled to ℓH. Instead, here the TeV-scale particles $\Psi, \Psi^c, \Phi_\lambda, \Phi_\kappa$ mediate lepton number violation from the heavy singlet N to the SM sector: see LHS of figure 3.1. This is the origin of the second factor in the SM neutrino mass formula above, which may thus be viewed as a "modulation" by TeV-scale physics.

Moving on to the leptogenesis, we have seen in section 3.3 that generically models with $C \ll 1$ and natural couplings and masses fail to produce the observed baryon asymmetry. Hence, the inverse seesaw should be equipped with a primordial baryon asymmetry. In the hybrid model of eq. (3.49) the latter in fact originates

from the decays

$$N_i \;\rightarrow\; \Phi_\lambda \Psi_a. \tag{3.53}$$

These do not induce an asymmetry in the SM ℓ directly, but first in Ψ. The asymmetry in Ψ is then distributed to Ψ^c via sizable κ and then eventually into SM lepton number asymmetry via a large Yukawa y in eq. (3.49). Again, just like in the case of neutrino mass generation, we see that the TeV-scale particles ($\Psi, \Psi^c, \Phi_\kappa$ and Φ_λ) acts as a mediator of lepton number violation from N_i to the SM (see RHS of figure 3.1). In addition, decays of Ψ, Ψ^c can lead to washout of the UV asymmetry. Thus, this process is completed through an interesting and subtle interplay between physics at UV and IR (details of which are discussed in the following two sections). Remarkably, with a single move, we have cured the two most important hurdles of the inverse seesaw model. Namely, the structure of the hybrid seesaw model is such that the small neutrino masses are controlled by the small Majorana mass of Ψ as in the usual inverse seesaw model. The twist here is that the smallness of this Majorana mass is explained by a version of high-scale type I seesaw and baryogenesis is then primarily achieved by the decay of the associated heavy fermions (as in the standard type I high-scale seesaw).

There are, however, several aspects that tell us eq. (3.49) is incomplete. (a) We introduced new scalar fields that undergo symmetry breaking phase transition[16]

[16] As we will discuss in detail later, *dynamical* scalars, as opposed to their VEVs, are required in order to be able to set thermal equilibrium between the SM and the singlet sectors in the early Universe and enable leptogenesis within the singlet sector.

and, given that phenomenologically the size of their VEV needs to be $O(\text{TeV})$, those scalars suffer from a naturalness problem. Unless we can explain why the new scalars are at the TeV scale, we have provided no convincing explanation of why the neutrinos are light. To achieve this the ultimate theory must therefore be able to solve the hierarchy problem. (b) As we emphasized above, the Lagrangian eq. (3.49) is not the most general one involving the SM and the new fields introduced here. Symmetries or new mechanisms must be invoked in order to avoid other interaction terms (for example, a direct coupling of N to SM lepton and Higgs or bare Majorana mass terms for Ψ, Ψ^c) that would otherwise completely spoil our conclusions. This problem is much easier to solve than the previous one, since the required global symmetries may for example emerge as accidental symmetries of an underlying UV completion of eq. (3.49) with gauge symmetries (as demonstrated in appendix E).

Interestingly, the hybrid seesaw structure can be realized in warped/composite seesaw in chapter 2. First of all, elementary N_R in composite seesaw (see eq. (2.1)) is roughly analogous to that N in eq. (3.49). In the hybrid seesaw model, N mixes with Ψ (once Φ_λ acquires VEV), which matches on to elementary N_R mixing with composite singlet interpolated by $\mathcal{O}_N$ (via the $\lambda\overline{N_R}\mathcal{O}_N$ coupling). The VEVs of Φ_κ and Φ_λ represent the confinement scale of composite Higgs sector. In particular, there could be a *composite* scalar associated with "fluctuations" of the confinement scale (dilaton), which can play the role of the *physical* scalar Φ_λ with its mass being naturally $\sim$ TeV, i.e., the compositeness scale. So, the issue (a) mentioned above, i.e., hierarchy problem for scalars, is absent. Moving on, as we have already briefly mentioned in section 2.1, due to the fact that theory consists of a weakly coupled

(external) sector and a CFT sector, the absence of any other interaction terms but the linear coupling $\lambda N\mathcal{O}_N$ is completely natural. Therefore, in the toy version, hybrid seesaw, a direct coupling of N (corresponds to elementary N_R) to SM Higgs (composite) and SM lepton is forbidden. Similarly, (bare) Majorana mass terms for Ψ, Ψ^c are not allowed since CFT sector preserves lepton-number. Thus, the issue (b) of the hybrid seesaw model, i.e., the particular structure of the Lagrangian, is solved.

Finally, regarding the neutrino mass, the TeV-modulation factor mentioned in eq. (3.52), corresponds to an RG running in composite seesaw. Matching eq. (2.8) with eq. (3.52) using eq. (2.6) and identifying M_N with $M_N^{\rm bare}$, we get

$$\left(\frac{\langle\Phi_\lambda\rangle}{\kappa\langle\Phi_\kappa\rangle}\right)^2 \leftrightarrow \left(\frac{\rm TeV}{M_{\rm Pl}}\right)^{2[\mathcal{O}_N]-5}, \tag{3.54}$$

and thus can naturally be much larger or smaller than 1. Specifically, if this modulation factor is (much) larger than unity, then $M_N^{\rm bare}$ as large as $M_{\rm Pl}$ can still give the required SM neutrino mass.

Rather than focusing on a specific solution of the above issues (a) and (b), in this work we will take a more model-independent approach and analyze in detail the physics of the low energy picture eq. (3.49). In our minds eq. (3.49) should be interpreted as a toy model capturing the main qualitative features of the warped realization or any other UV completion of the hybrid framework.

Before moving on to study the details of our toy model, we mention that the same Lagrangian eq. (3.49) was considered previously in [64] with $M_{N_i} = O(\text{TeV})$.

From our results, however, $M_{N_i} \gg O(\text{TeV})$ turns out to be a necessary condition to achieve a successful baryogenesis. We will hence not consider that possibility.

3.5 Formalism for the hybrid genesis

Our hybrid seesaw model is defined by the Lagrangian in eq. (3.49). Without loss of generality, we work in the basis where κ and M_N are real positive and diagonal. For definiteness, we have chosen a minimal model $a = 1, 2, 3$ and $i = 1, 2$ required to explain two light neutrino mass differences and leptogenesis.[17] The hybrid seesaw model consists of states at high scale, $\sim M_N$, and states at $\sim$ TeV scale. As we will discuss in detail, the entire process of genesis is comprised of two steps: high scale leptogenesis (both generation and washout) at $T \sim M_N$ and low scale washout at $T \sim m_\Psi$. In particular, one important result that we show in section 3.5.2.3 and section 3.5.2.4 is that seemingly complicated physics at intermediate scales does not induce additional washout of the asymmetry generated at $T \sim M_N$, and hence establishing a clean two-step structure of hybrid genesis.

We begin with a general discussion of generation of asymmetries in particle number based on symmetry argument in section 3.5.1, which is valid for *any* model. In section 3.5.2, we provide a qualitative assessment of leptogenesis specific to our hybrid seesaw model, and then present a quantitative study in section 3.5.3. The formalism developed in this section will be used in section 3.6 to map out in detail the parameter space which works for leptogenesis in our hybrid model.

[17] In section 3.6.2.2, when we consider certain hierarchy in y, three generation of N_i is required to obtain a realistic neutrino mass matrix.

3.5.1 Generalities

Before delving into the specifics of our hybrid seesaw model, we provide a brief discussion on generic aspects of the generation of particle number asymmetries viewed from symmetries of the underlying physics. Once the Lagrangian is given, all the symmetries (and corresponding charges of fields) of the theory can be analyzed. In particular, all the $U(1)$ symmetries can be identified and as we will demonstrate below, they will play an important role in understanding particle asymmetry generation.

Viewing each parameter in the Lagrangian as symmetry breaking parameter, by comparing the rates of processes to the Hubble rate, one realizes that the notion of symmetry can be more general than the symmetry of the Lagrangian. Namely, some of $U(1)$ symmetries unseen in the Lagrangian may arise when processes mediated by couplings that break those symmetries are slow compared to the Hubble rate. In this sense, the notion of symmetry in the history of the Universe, now including those already seen from the Lagrangian, are to be understood as temperature dependent concept. In particular, they would be broken or restored, depending on the temperature T. Let us take the case of the EW sphaleron processes as an example to illustrate this idea. Due to the mixed $SU(2)_L$ anomaly, the EW sphaleron configuration breaks $B + L$ [89] while preserving $B - L$. At high temperatures its rate is given approximately by $\Gamma_{\not{B+L}} \sim 250\alpha_W^5 T$. At temperature $T \gtrsim 10^{12}$ GeV, the EW sphaleron processes are slower than the Hubble rate and hence inactive. In that regime, $U(1)_B$ and $U(1)_L$ are separately good symmetries. At intermediate

temperatures, 100 GeV $\lesssim T \lesssim 10^{12}$ GeV, on the other hand, the EW sphaleron processes are fast and only the $B-L$ remains as a good symmetry. At even lower temperature, $T \lesssim 100$ GeV, the process gets Boltzmann suppressed, $\Gamma_{\rm sph} \propto e^{-E_{\rm sph}/T}$ where $E_{\rm sph} \sim m_W/\alpha_W$, again making both $U(1)_B$ and $U(1)_L$ good symmetries.

To be more specific, now we will define *exact*, *effective* and *approximate* symmetries as follows. Let us take $\Gamma_{\not x}$ to be the rate of a process that violates a specific $U(1)_x$. For example, the EW sphaleron processes contribute to $\Gamma_{\not B+\not L}$. At a given temperature T^*, $\Gamma_{\not x}(T^*)$ falls into one of the following three possibilities: (i) $\Gamma_{\not x}(T^*) \gg H(T^*)$; (ii) $\Gamma_{\not x}(T^*) \ll H(T^*)$; and (iii) $\Gamma_{\not x}(T^*) \sim H(T^*)$. For case (i), the x-violating process is fast enough and thus the corresponding $U(1)_x$ is broken at T^*. In case (ii), although the symmetry-violating process exists, it is very slow compared to the Hubble rate. To a good approximation, the corresponding $U(1)_x$ is a good symmetry at T^* and therefore we call it an *effective* symmetry. We emphasize that there is a special case in (ii) where $\Gamma_{\not x}(T^*) = 0$, meaning there is no x-violating process for such $U(1)_x$. Typically, gauged $U(1)$ symmetries like $U(1)_Y$ of the SM will have this property. For an obvious reason, we call such symmetry as *exact* symmetry. It is crucial to identify exact/effective symmetries because they act as conservation laws at the temperature of interest and determine the spectator effects. Finally, processes of type (iii) have rates of the order of the Hubble rate and are to be described by non-equilibrium dynamics using the Boltzmann equations (BEs). The associated symmetry is special in that it is neither a perfectly good effective symmetry nor gets completely violated.[18] Therefore, in the rest of the discussion,

[18]For these processes, two out of three Sakharov conditions i.e. the out-of-equilibrium and $U(1)_x$

we will refer to it as an *approximate* symmetry.

For a particle i, we can describe asymmetry in its *number* density as $n_{\Delta i} \equiv n_i - n_{i^*}$ with n_i and n_{i^*} respectively the number density of itself and its antiparticle. If they carry a charge q_i^x under a $U(1)_x$, they will contribute to the corresponding *charge* asymmetry:

$$n_{\Delta x} = \sum_i q_i^x n_{\Delta i}. \tag{3.55}$$

It is shown in refs. [87, 88] that one can invert the relation above to express $n_{\Delta i}$ in term of $n_{\Delta x}$ as follows[19]

$$n_{\Delta i} = \sum_x R_{ix} n_{\Delta x}, \tag{3.56}$$

where R_{ix} can be constructed from charges carried by all the particles under all $U(1)_x$ of a model. Hence the analysis of asymmetry generation which involves various particles and interactions in the thermal bath at certain range of temperature T^* boils down to identifying *exact/effective* or *approximate* $U(1)$ symmetries as discussed above. From eq. (3.56), it is clear that in the absence of $U(1)$ or only with exact/effective $U(1)$ such that $n_{\Delta x} = 0$ for all x, all particle asymmetries vanish. Hence, for successful genesis, it is necessary to have at least one approximate $U(1)$ which allows for $n_{\Delta x} \neq 0$, although existence of such $U(1)$ alone is not a sufficient condition. The actual size of final asymmetry requires further quantitative study of non-equilibrium physics via BEs. In the next section, we will discuss the viability of

violation conditions, are met. If the last ingredient i.e. C and CP violation is also met, a nonzero $U(1)_x$ asymmetry can develop.

[19] A pedagogical derivation of this result is given in ref. [88]. Explicitly, we have $R_{ix} = g_i \xi_i \sum_y q_i^y (J^{-1})_{yx}$ where $J_{yx} = \sum_i g_i \xi_i q_i^x q_i^y$ with g_i the gauge/family degrees of freedom of particle i. Also, ξ_i is the statistical factor which goes to 1 (2) for relativistic fermion (boson) and becomes exponentially suppressed for non-relativistic particle.

hybrid-genesis by identifying the *exact/effective* symmetries as well as *approximate* symmetries. The latter allows the development of nonzero asymmetries at a specific temperature regime.

3.5.2 Hybrid genesis: qualitative description

We now move on to our hybrid model: we start by discussing a crucial ingredient which is common to all leptogenesis models, namely, the EW sphaleron processes which communicate the asymmetry in the lepton sector to the baryon sector. In particular, they are active in the temperature range $T^{+}_{\rm EWSp} > T > T^{-}_{\rm EWSp}$. The upper bound is estimated to be $T^{+}_{\rm EWSp} \sim 10^{12}$ GeV [90] while the lower bound is determined from lattice simulation to be $T^{-}_{\rm EWSp} = 132$ GeV and occurs after EW phase transition at $T = 159$ GeV [91]. Generically, the genesis will occur through one of the following two scenarios:

(A) If high scale genesis takes place and completes at $T_g > T^{+}_{\rm EWSp}$, since baryon number B remains to be a good symmetry, genesis occurs through generation of an asymmetry in the approximate symmetry $U(1)_L$ (lepton number). We denote $Y_{\Delta L} \equiv n_{\Delta L}/s$ where $n_{\Delta L}$ is lepton charge asymmetry defined as in eq. (3.55) normalized by entropic density $s = \frac{2\pi^2}{45} g_\star T^3$. Here, $g_\star$ is the number of relativistic degrees of freedom of the Universe at temperature T.[20]

[20] As we will see later, in our model, we will have to extend the definition of lepton number to include particles beyond the SM. Here and for the rest of the work, we assume all lepton flavors L_α are not conserved. This is in accordance with our consideration where all the dimensionless couplings are taken to have 'natural' values $\gtrsim \mathcal{O}\left(10^{-2}\right)$. For instance, taking $|y_{a\alpha}| \sim 0.05 - 0.5$, lepton flavors are not conserved for $T \lesssim 10^{13} - 10^{15}$ GeV (for the estimation, one can use the rate calculated in for e.g. refs. [92, 93]). This allows us to assume that the asymmetry is equally distributed among the three lepton flavors, simplifying the analysis.

When the temperature drops below T^{+}_{EWSp}, while both L and B are no longer conserved by the EW sphaleron processes, $B-L$ remains conserved and the asymmetry in this conserved charge is related to the generated lepton asymmetry as $Y_{\Delta(B-L)}\left(T<T^{+}_{\mathrm{EWSp}}\right)=-Y_{\Delta L}\left(T_g\right)$.

(B) On the other hand, if leptogenesis takes place and completes at $T^{-}_{\mathrm{EWSp}}<T_g<T^{+}_{\mathrm{EWSp}}$, instead of L, the generation of asymmetry is described directly in terms of $Y_{\Delta(B-L)}\left(T_g\right)$.

Barring the low scale washout that we will discuss later in section 3.5.2.4, the baryon asymmetry will be frozen at T^{-}_{EWSp} and we have[21]

$$Y_{\Delta B}\left(T^{-}_{\mathrm{EWSp}}\right)=d\,Y_{\Delta(B-L)}, \tag{3.57}$$

where d is an order one number which depends on number of relativistic degrees of freedom at T^{-}_{EWSp}. Assuming only the SM number of relativistic degrees of freedom (excluding the top quark) at T^{-}_{EWSp} after EW symmetry breaking, we have $d=\frac{30}{97}$ [94, 95] which is the value we will use in this work.

Having understood these two cases separately, it is useful to introduce a new symbol Δ to denote asymmetry in both cases as follows:

$$\Delta=\begin{cases}-\Delta L, & \text{scenario (A)},\\ \Delta(B-L), & \text{scenario (B)}.\end{cases} \tag{3.58}$$

[21] $Y_{\Delta B}$ includes the contributions of the quarks which are in chemical equilibrium. For instance, if all quarks are in chemical equilibrium, we simply have $Y_{\Delta B}=\sum_a\left(Y_{\Delta Q_a}+Y_{\Delta u_a}+Y_{\Delta d_a}\right)$.

In principle, leptogenesis can happen across $T^{+}_{\rm EWSp}$. However, such possibility may correspond to a very small portion of the parameter space, and for simplicity, we will not consider this possibility further. In practice, for $M_{N_1} > 10^{12}$ GeV, we will assume scenario (A) while for $M_{N_1} < 10^{12}$ GeV, we will consider scenario (B).

3.5.2.1 Symmetries of the hybrid model

We now identify the exact/effective $U(1)$ symmetries as well as approximate ones of the hybrid model. From the Lagrangian eq. (3.49), we have seven types of fields $\{H, \Phi_\lambda, \Phi_\kappa, \ell_\alpha, \Psi^c_a, \Psi_a, N_i\}$. Let us first identify exact symmetries of the theory. For this, we note that the Majorana mass of N_i implies that they cannot carry any conserved charge. Together with hypercharge conservation and three interaction terms in eq. (3.49), we get five constraints and have $7 - 1 - 4 = 2$ *exact* $U(1)$ symmetries, provided the scalar potential does not break them (tree-level breaking) and they can be made gauge-anomaly free (loop-level breaking). These two symmetries are chosen to be $U(1)_{B-L}$ and $U(1)_{\lambda-B}$ with particle charge assignments shown in table 3.3. We denote the first one as $U(1)_{B-L}$ since, although it is not exactly the same as $(B-L)$ (accidental) symmetry of the SM, as far as charges of SM particles are concern, it coincides with the baryon minus lepton number of the SM. Notice that $SU(2)_L - SU(2)_L - U(1)_{B-L}$ mixed anomaly vanishes. For this reason, in scenario (B) when EW sphaleron processes are in thermal equilibrium, $U(1)_{B-L}$ remains conserved. Under $U(1)_{\lambda-B}$, the rest of SM particles carry the charges same as $U(1)_{L-B}$. One readily see that $U(1)_{\lambda-B}$ is also free from $SU(2)_L - SU(2)_L - U(1)_{\lambda-B}$

anomaly and hence is also preserved by the EW sphaleron processes.

For later purpose, we will call **fully-symmetric** those realizations in which both $U(1)$ symmetries are preserved. The model based on gauge symmetries presented in appendix E is such an example: in that case $U(1)_{B-L}$ is a gauge symmetry while $U(1)_{\lambda-B}$ arises as an accidental global symmetry. On the other hand, in the scenario where eq. (3.49) originates from warped extra dimension, the two global symmetries are absent since $\Phi_{\kappa,\lambda}$ are identified with a single *real* field — the dilaton. As we indicated in previous sections, in this case we view eq. (3.49) as a good proxy or toy version of would-be effective theory coming from warped extra dimensional theory. Scenarios like these, in which the scalars $\Phi_{\kappa,\lambda}$ are real, will be called **non-symmetric** models. We expect that a study of this case may capture main features of physics of genesis in warped extra dimensional theory. As we will see in the next section, while detailed dynamics can differ, the difference in the final asymmetry between the fully-symmetric and non-symmetric scenarios is just order one. Finally, in section 3.5.2.3 we will briefly comment on the case where only one combination of $U(1)_{B-L}$, $U(1)_{\lambda-B}$ is preserved by the scalar potential.

Having identified the exact symmetries, we now move on to finding the approximate ones. Recall that when we counted the number of constraints to figure out the exact $U(1)$'s, we used the fact that M_N disallows charges for N_i's. In the limit $\lambda_{ia} \to 0$ or $M_{N_i} \to 0$, however, a new $U(1)$ emerges. This approximate lepton number is broken by the coexistence of λ_{ia} and M_{N_i} and, as we discuss below, it is in this charge that the asymmetry gets generated via high scale genesis. We define such approximate symmetry as the *extended* lepton number L' and the associated

	$U(1)_{B-L}$	$U(1)_{\lambda-B}$
ℓ_α	-1	1
Ψ_a	0	1
Ψ_a^c	$+1$	-1
N	0	0
Φ_κ	-1	0
Φ_λ	0	-1

Table 3.3: Charge assignments of $\ell_\alpha, \Psi_a, \Psi_a^c, \Phi_\kappa, \Phi_\lambda$ under the two global symmetries of the **fully-symmetric model**. The former coincides with the baryon minus lepton number of the SM particles. Besides the lepton doublet ℓ_α, we do not show the charges of the rest of SM particles. In the gauge model presented in Appendix E, $U(1)_{B-L}$ is a gauge symmetry while $U(1)_{\lambda-B}$ remains an accidental global symmetry. Under $U(1)_{\lambda-B}$, the rest of SM particles carry the charges same as $U(1)_{L-B}$. On the other hand, the two symmetries are absent in the **non-symmetric model** originated from warped extra dimension since $\Phi_{\kappa,\lambda}$, which are identified with the dilaton, are real.

$Y_{\Delta L'}$ (hence its $U(1)$ charges) is given as[22]

$$Y_{\Delta L'} = \sum_\alpha Y_{\Delta \ell_\alpha} + \sum_\alpha Y_{\Delta e_\alpha} + \sum_a Y_{\Delta \Psi_a} - \sum_a Y_{\Delta \Psi_a^c}, \tag{3.59}$$

where e_α denotes the SM right-handed lepton for a given flavor α. It may be worth mentioning that the above extended lepton number (L') is to be distinguished from the lepton number (L) of the SM. Notice, however, that when all heavy states (Ψ_a, Ψ_a^c and also Φ_κ) eventually disappear from the thermal bath, the two coincide. Similarly to eq. (3.58) defined for general case, we define Δ for the hybrid model. Since there is little chance for confusion and we will consider only hybrid model

[22]The contribution from right-handed charged leptons e_α in eq. (3.59) will be absent if the corresponding charge lepton Yukawa interactions are out of thermal equilibrium for e.g. $T \gtrsim 10^{12}$ GeV [70–72].

from now on, we decided to use the same symbol.

$$\Delta = \begin{cases} -\Delta L', & \text{scenario (A)} \\ \Delta(B - L'), & \text{scenario (B).} \end{cases} \tag{3.60}$$

The breaking of this approximate symmetry at high temperatures is captured by the following processes: decays and inverse decays $N_i \leftrightarrow \Phi_\lambda \Psi_a, N_i \leftrightarrow (\Phi_\lambda \Psi_a)^*$ and scatterings $\Phi_\lambda \Psi_a \leftrightarrow (\Phi_\lambda \Psi_b)^*$, $\Psi_a \Psi_b \leftrightarrow (\Phi_\lambda \Phi_\lambda)^*$. Below, we discuss how these processes can be studied to understand the generation and washout of the asymmetry in the Δ charge.

3.5.2.2 High scale leptogenesis ($T \sim M_N$)

The dynamics of genesis at high scale $\sim M_N$ is essentially the same as that of the usual type-I seesaw model: the high scale leptogenesis proceeds via out of equilibrium decay of heavy N_i and if involved couplings provide needed CP-violation, non-zero asymmetry may be generated in approximate $U(1)_{L'}$ charge.

Starting with the generation, asymmetry is created via out-of-equilibrium decay of N_i: $N_i \to \Phi_\lambda \Psi_a, N_i \to (\Phi_\lambda \Psi_a)^*$. Concretely, N_i decays more often to $\Phi_\lambda \Psi_a$ than to $(\Phi_\lambda \Psi_a)^*$ if these processes occur with CP-violation. A non-zero CP-violation arises through the interference of tree and one-loop diagrams. When this happens, the number density of Ψ_a may be larger than that of Ψ_a^*, i.e. non-zero asymmetry in $Y_{\Delta\Psi_a}$ is created.

However, this immediately raises the question of erasing the asymmetry via

the inverse decay: $\Phi_\lambda \Psi_a \to N_i, (\Phi_\lambda \Psi_a)^* \to N_i$. Intuitively, if the number density of Ψ is larger than that of Ψ^*, the corresponding inverse decay will tend to occur more rapidly than the other, thus coverting more Ψ (and Φ_λ) into N_i than Ψ^*. This, combined with the above story of decay, then leads to null net asymmetry. Indeed, this reasoning can be shown to be correct if everything happens in equilibrium environment. Namely, it is non-equilibrium condition that enables actual creation of net asymmetry. This condition is met by virtue of the expansion of the Universe. That is, as the temperature cools down below the mass of N_i, unlike the decay, the inverse decay becomes Boltzmann suppressed: thermal energy that $(\Psi\Phi_\lambda)$ or $(\Psi\Phi_\lambda)^*$ carries becomes insufficient to create N_i with mass $M_N > T$. When the washout process due to the inverse decay becomes effectively inactive, a net asymmetry can eventually be generated.

However, the inverse decay is not the only washout process to consider. The scattering processes, $\Phi_\lambda \Psi_a \leftrightarrow (\Phi_\lambda \Psi_b)^*$, $\Psi_a \Psi_b \leftrightarrow (\Phi_\lambda \Phi_\lambda)^*$, violate Δ by two units and can erase the Δ asymmetry. As is well-known, by unitarity, the on-shell contribution to these scattering amplitude is the same as the inverse decay. For this reason, in order to avoid double-counting, in writing down the BEs in section 3.5.3 we will treat the inverse decay and *off-shell* part of $\Delta = 2$ scattering as separate source of washout.

3.5.2.3 Survival of the asymmetry at $T \lesssim M_N$

Having discussed generation and standard mechanisms for washout of asymmetry at high scale ($T \gtrsim M_N$), we now move on to the consideration of physics at intermediate scales, $\langle \Phi_\lambda \rangle < T < M_N$, as well as other potentially dangerous washout processes. In principle, these dynamics can erase previously created asymmetry and hence successful genesis necessitates any such washout processes, including those at intermediate scales, to be under control.

We first discuss a subtle washout effect that can potentially appear in the **fully-symmetric model**. As we mentioned earlier, there are two exact/effective symmetries $U(1)_{B-L}$ and $U(1)_{\lambda-B}$ in this model, which impose conservation laws for the global charges of $U(1)_{B-L}$ and $U(1)_{\lambda-B}$ in table 3.3. In terms of Δ that we defined in eq. (3.60), the conservation laws can be expressed as

$$Y_\Delta + \sum_a Y_{\Delta\Psi_a} - Y_{\Delta\Phi_\kappa} = 0, \tag{3.61}$$

$$Y_\Delta + Y_{\Delta\Phi_\lambda} = 0. \tag{3.62}$$

If there exists a process depleting Φ_λ, e.g. Φ_λ decaying into particles in the model, $Y_{\Delta\Phi_\lambda}$ would vanish and this will result in $Y_\Delta \to 0$ due to the conservation of $U(1)_{\lambda-B}$ [see eq. (3.62)]. For a concrete example, let's imagine $M_{N_1} \ll M_{N_2}$ and consider that the high scale genesis is mostly done by the decay of N_2 while the generation of asymmetry and washout from N_1 are negligible. At temperature $T \sim M_{N_2}$, Φ_λ could get a thermal mass $m_{\Phi_\lambda}(T) \sim T \gg M_{N_1}$ and thus the decay $\Phi_\lambda \to N_1 \Psi^*$

could be kinematically allowed. In that case, this decay is the dominant depletion process for Φ_λ at temperatures $T \gg \langle\Phi_\lambda\rangle$. If such decay is fast compared to Hubble, all asymmetry generated by N_2 will then be washed out and hence leptogenesis fails.

It is also clear from the above example that such washout process can be forbidden assuming M_{N_i} are of the same order and the high scale asymmetry is primarily generated from N_1 decay. In this case when $T \lesssim M_{N_1}$, Φ_λ cannot decay and the high scale asymmetry survives. Given that such choice of M_{N_i}'s, i.e. no hierarchy, is more natural according to our naturalness criteria, we only consider this for the rest of our discussion.

There are further washout processes that should be taken into account after Φ_λ has acquired a VEV at much lower temperatures of the order $T \sim \langle\Phi_\lambda\rangle$. We will discuss these "*low-scale washout*" processes partly below and the rest in the next section.

For **non-symmetric model**, both $U(1)_{B-L}$ and $U(1)_{\lambda-B}$ are absent, and Φ_λ cannot carry an asymmetry. Thus, once the asymmetry is generated at high scale, in contrast to the **fully-symmetric model**, one does not have to worry about the washout from depletion of Φ_λ discussed above.

Next, we briefly comment on the possibility of a scenario where only one linear combination of $U(1)_{B-L}$ and $U(1)_{\lambda-B}$ survives due to the scalar potential. Such scenario is different from both the fully-symmetric and non-symmetric models and requires a separate consideration. When one combination of two $U(1)$'s is broken, it is possible for Φ_λ to decay and thus erase the primordial asymmetry. One such an example is obtained starting from the two global symmetries in table 3.3 with

eq. (3.49) but allowing their breaking in the scalar potential. For instance, let us consider the potential interaction $\Phi_\lambda \Phi_\kappa^* |\Phi_\kappa|^2$ which preserves only $U(1)_{(B-L)+(\lambda-B)}$. In such a case, we have only one conservation law for unbroken $U(1)$, not two, and the statement that the existence of process leading to $Y_{\Delta\Phi_\lambda} \to 0$ implies $Y_\Delta \to 0$ is not generally true anymore. Instead, the fate of the asymmetry depends more on details of the dynamics. Still, it is possible to argue that since more breakings tend to enable more asymmetry transferring channel, if dynamics caused by those breakings transmit all the asymmetries eventually into the SM sector before EW sphaleron processes are turned off, genesis fails, assuming zero net primordial asymmetry. This is simply because the sum of net asymmetry in the SM sector plus net asymmetry of the singlet sector is zero by initial condition and asymmetry transmitting dynamics moved all the asymmetries to the SM sector. Importantly, the above statement is regardless of the details of asymmetry transferring physics. As long as they are efficient enough and completed above $T^-_{\rm EWSp}$, it is a correct statement. To illustrate the idea, let us take the example above with $\Phi_\lambda \Phi_\kappa^* |\Phi_\kappa|^2$-term in the scalar potential. If thermal masses for the scalars satisfy $m_{\Phi_\lambda}(T) > 3m_{\Phi_\kappa}(T)$, the decay $\Phi_\lambda \to \Phi_\kappa \Phi_\kappa \Phi_\kappa^*$ is allowed. Since Φ_κ couples to Ψ and Ψ^c with unsuppressed coupling κ, it may decay/scatter into those. Finally, asymmetry stored in Ψ and Ψ^c may get processed to the SM via Yukawa coupling either by decay or scattering process. If all this is done at temperatures above $T^-_{\rm EWSp}$, as per the argument above, we get zero net asymmetry. We will not consider these scenarios anymore, and next go back to the discussion of fully-symmetric and non-symmetric models.

We finally discuss washouts at scales below M_{N_i}. In particular, we will argue

that provided above mentioned two subtle (and easy to avoid) washouts are absent and if washout from off-shell $\Delta = 2$ scattering is small, then there is no additional washout effects at intermediate scales. Further washouts we need to consider is, therefore, those occurring at TeV scale after scalars get VEVs. Notice that this is quite a remarkable fact in that although physics happens in the entire energy range, the study of genesis can be structured in clean two steps: high scale genesis and low scale washout.

Integrating out heavy singlets N_i, the effective Lagrangian at $\langle\Phi_\lambda\rangle < T < M_N$ is given by

$$-\mathcal{L} \supset y_{a\alpha}\Psi^c_a H\ell_\alpha + \kappa_a\Psi^c_a\Phi_\kappa\Psi_a + \sum_i \frac{\lambda_{ia}\lambda_{ib}}{M_{N_i}}\Phi_\lambda\Psi_a\Phi_\lambda\Psi_b + \text{H.c.}. \tag{3.63}$$

The dimension five operator violates L' by two units which could contribute to the washout of Y_Δ. The corresponding process at high $T \sim M_N$ is that of $\Delta = 2$ scattering mediated by off-shell N and will be taken into account whenever they are relevant (see section 3.5.3.2 for details). Since the rate for this process $\Gamma_{\Delta=2} \propto T^3$, which drops faster than Hubble rate, $\Gamma_{\Delta=2} < H \propto T^2$ is always true at lower temperatures if it is enforced at a high temperature. Namely, requiring $\Gamma_{\Delta=2} < H$ at high temperature guarantees that washout from the above dimension five operator is under control at *all* intermediate temperatures.

To summarize, assuming no depletion of the asymmetry from Φ_λ decay (both kinds discussed above), once all washout processes in high scale ($T \gtrsim M_N$) involving N-exchange are taken under control, the preservation of the asymmetry is a

robust feature of our model, at least for temperatures at which $\langle \Phi_{\kappa,\lambda} \rangle = 0$ (what happens after the scalars have acquired a VEV will be discussed in the next subsection). In the model which arises from gauge symmetry we considered in appendix E (fully-symmetric model), this is ensured by assuming high scale asymmetry is generated from the lightest N decay. This is because in the gauge model, at the renormalizable level, no symmetry breaking terms in the scalar potential is allowed by gauge invariance and possible symmetry breaking higher dimensional terms are highly-Planck-suppressed. See appendix E for more detail. No new source of asymmetry violation at intermediate temperatures is possible in non-symmetric models. For scenarios with a remnant global symmetry, i.e. "intermediate models", the conclusion is however model-dependent.

3.5.2.4 Low scale washout ($T \sim m_\Psi$)

We define the temperature region $T \lesssim \langle \Phi_{\kappa,\lambda} \rangle$ as low scale or TeV scale. In principle, a large entropy production during thermal phase transition(s) of Φ_λ and/or Φ_κ can result in undesired dilution of asymmetry generated from high scale. In order to avoid this, throughout the discussion we assume that phase transition is smooth and hence no large entropy production occurs. This ensures no significant dilution of the asymmetry from phase transitions and the only washout out effects we need to consider at low scale are the dynamical processes involving relevant particles discussed below.

Once scalars get VEVs, there can be new kinds of processes generated by the

higher dimensional operator in (3.63) with some or all of scalars set to their VEVs. Washouts mediated by these processes may be significant even after suppressing those with all physical Φ_λ (as we did in section 3.5.2.3). Therefore, they need to be treated separately and we will call them as "low scale washout".

We first consider an operator with *one* of Φ_λ set to its VEV: $\sim \lambda^2 \langle \Phi_\lambda \rangle \Phi_\lambda \Psi_a \Psi_b / M_N$. This operator can generate several kinds of washout dynamics. As we now show, however, each of those new effects are automatically suppressed assuming a large separation of two physical scales: $\langle \Phi_\lambda \rangle \ll M_N$ and $m_\Psi \sim m_{\Phi_{\lambda,\kappa}} \sim \langle \Phi_{\lambda,\kappa} \rangle$. In order to see this more explicitly, we first note that the condition that $\Delta = 2$ washout from off-shell scattering at high scale module ($T \sim M_{N_1}$) is small can be expressed schematically as

$$\frac{\lambda_i^4}{16\pi^3} \frac{T^3}{M_{N_i}^2}\bigg|_{T=M_{N_1}} < \sqrt{g_\star} \frac{T^2}{M_{\rm Pl}}\bigg|_{T=M_{N_1}} \quad \Rightarrow \quad \frac{\lambda_i^4}{16\pi^3} \left(\frac{M_{N_1}}{M_{N_i}}\right)^2 < \sqrt{g_\star} \frac{M_{N_1}}{M_{\rm Pl}}. \tag{3.64}$$

where $i = 1, 2$ denotes singlet generation. As we will discuss more later, the dominant $\Delta = 2$ washout scattering in the UV module comes from off-shell exchange of N_2. Above, however, we show the condition for both N_1 and N_2 by keeping the index i general. We do this because at scales $T \ll M_N$ the local higher dimensional operator $\lambda_i^2 \langle \Phi_\lambda \rangle^2 \Psi^2 / M_i$ will be generated as a result of integrating out both N_1 and N_2, and yet the effects of the two will appear as a single operator. Assuming no degeneracy of M_{N_1} and M_{N_2}, on the other hand, we can safely drop the interference effects and the matching of effects may be done for each rate.

Next, we discuss four leading washout processes that above mentioned di-

mension 5 operator generates and argue that all of them are rather generically suppressed.

(1) The inverse decay $\Psi\Psi \to \Phi_\lambda$: The condition that this process is slower than Hubble rate at $T \sim m_{\Phi_\lambda}$ can be written as

$$\frac{\lambda_i^4}{16\pi^3}\left(\frac{M_{N_1}}{M_{N_i}}\right)^2\left[\pi^2\frac{\langle\Phi_\lambda\rangle}{M_{N_1}}\right] < \sqrt{g_\star}\frac{M_{N_1}}{M_{\rm Pl}}. \tag{3.65}$$

where we used $m_{\Phi_\lambda} \sim \langle\Phi_\lambda\rangle$. Comparing this to eq. (3.64), we see that the washout from this inverse decay is a small effect if the quantity in the square bracket is less than one:

$$\pi^2\frac{\langle\Phi_\lambda\rangle}{M_{N_1}} < 1 \tag{3.66}$$

and it is clear that with assumed gap $M_{N_1} \gg \langle\Phi_\lambda\rangle$ this condition is easily met.

(2) $\Psi\Phi_\lambda \to \Psi^c\Phi_\kappa$ and its associated t-channel $\Delta = 2$ scattering: Such process may be generated by usage of one factor of $\lambda_i^2\langle\Phi_\lambda\rangle/M_{N_i}$ from dimension 5 operator above and one factor of κ. Following similar steps, this washout can be small if

$$\kappa^2\frac{\langle\Phi_\lambda\rangle}{M_{N_1}}\frac{\langle\Phi_\lambda\rangle}{m_\Psi} < 1 \tag{3.67}$$

Again, with $M_{N_1} \gg \langle\Phi_\lambda\rangle$, $m_\Psi \sim \langle\Phi_\lambda\rangle$, and $\kappa \sim \mathcal{O}(1)$ that we are assuming, the above condition is easily satisfied.

(3) $\Psi\Phi_\lambda \to (\Psi\Phi_\lambda)^*$ and its associated t-channel $\Delta = 2$ scattering: There are two contributions to be added at the amplitude level. One is from local vertex of $\lambda_i^2\Phi_\lambda^2\Psi^2/M_i$ and we already argued in section 3.5.2.3 that it is suppressed. The other diagram can be constructed by two factors of $\lambda_i^2\langle\Phi_\lambda\rangle/M_{N_i}$ and one insertion of $\mu \sim \lambda^2\langle\Phi_\lambda\rangle^2/M_{N_1}$. Note, howerver, that the second is much more suppressed compared to the first: in the UV, it corresponds to eight-point correlator with four Φ_λ's set to VEV. Therefore, neglecting subdominant latter contribution, it is a robust fact that washout from $\Psi\Phi_\lambda \to (\Psi\Phi_\lambda)^*$ scattering is suppressed once the corresponding process at UV scale is small.

(4) scattering $\Psi\Psi \leftrightarrow (\Psi\Psi)^*$ mediated by off-shell Φ_λ: Noting that on-shell part of such scattering is the inverse decay $\Psi\Psi \to \Phi_\lambda$ and that off-shell contribution is sub-dominant to the on-shell contribution, it can be safely dropped once the inverse decay is suppressed via eq. (3.66).

With the above discussion, now the only remaining washouts to discuss are when both Φ_λ in (3.63) have a VEV. Because we will always take $\langle\Phi_\kappa\rangle \leq \langle\Phi_\lambda\rangle$, we can limit our discussion to temperatures in which both scalars have acquired VEVs. In this regime Ψ_a and Ψ_a^c form three pairs of pseudo-Dirac fermions, $\tilde{\Psi}_i\,(i = 1, ..., 6)$ with masses m_i. Their mass splitting as well as strength of washout are controlled by eq. (3.50). Notice that in this temperature range we can match our hybrid seesaw at low scale to the ISS model eq. (3.12). The scatterings controlled by μ violate L' and could erase exponentially the asymmetry Y_Δ generated at high scale. The formulas for low scale washout will be presented in section 3.5.3.

Finally, there are also new washout processes pertaining to the gauge model of appendix E. Gauge bosons associated to $U(1)_{B-L}$ could mediate new washout processes like $\tilde{\Psi}_i\tilde{\Psi}_i \to f\bar{f}$ where f is any fermion charged under $U(1)_{B-L}$. However, these processes are suppressed as μ^2/T^2 at $T > m_i$ and as μ^2/m_i^2 for T below the critical temperature at which Φ_κ gets a VEV. Unless we consider highly non-generic models in which the gauge boson mass is $\sim 2m_i$ these processes are not resonantly enhanced, and therefore do not induce significant washout.

3.5.2.5 Initial conditions and assumptions

In the standard cosmological model, it is assumed that after inflation, inflatons decay populate the Universe with particles which thermalize among themselves to a so-called reheating temperature.

For $M_N \lesssim 10^{15}$ GeV, the genesis occurs at temperatures where the SM particles could be thermalized by the SM interactions as well as new interactions in our model. There may be a few options for the reheating. When inflatons decay only to the SM particles, SM partcles thermalize themselves through gauge and Yukawa interactions. Then, singlet sector states, Ψ_a^c, Ψ_a, and Φ_κ, can be populated via interactions y and κ. The singlet scalars Φ_κ and Φ_λ can also be populated through scalar interactions like $|H|^2|\Phi_{\kappa,\lambda}|^2$. If, on the other hand, inflatons only decay to singlet sector particles, H and ℓ_α can be produced from the aforementioned interactions and then through the SM gauge and Yukawa interactions, the rest of the SM particles can be populated. When inflatons reheat both sectors simultaneously, then thermal-

ization happens naturally through various interactions metioned so far. Therefore, we see that regardless of the assumption about the reheating, both sectors will be thermalized and we will consider the contribution to the total energy density of the Universe from both the SM particles and singlet sector particles: $g_\star = 121.25$.

If genesis takes place at $M_{N_i} \gtrsim 10^{15}$ GeV, on the other hand, the SM particles might not be thermalized by the SM interactions [96]. If inflatons decay dominantly to the SM particles, we cannot describe this scenario within a standard radiation-dominated thermal bath. Since a separate treatment is called for, we will not consider this scenario further. Instead, we will consider the situation where inflatons decay only to the singlet sector particles and they are thermalized through interactions in our model eq. (3.49) as well as interactions in scalar potential. For instance, interactions with a large κ_a can thermalize Ψ_a and Ψ_a^c while the scalars Φ_λ and Φ_κ can be thermalized through interaction like $|\Phi_\kappa \Phi_\lambda|^2$. When $\Psi_a, \Psi_a^c, \Phi_\lambda$ and Φ_κ are all thermalized the total relativistic degrees of freedom is $g_\star = 14.5$[23] and we use this number to calculate the high scale genesis. When temperature cools down, interactions involving y and SM interactions will eventually be in equilibrium and thus SM particles are thermalized through coupling to singlets.

Starting from zero initial N_i, a thermalized Ψ_a and Φ_λ can generate N_i through inverse decays. In the gauge model of appendix E, Ψ_a^c and Φ_κ can also be thermalized by $U(1)_{B-L}$ gauge interaction. After $U(1)_X$ symmetry breaking at around genesis scale, if $U(1)_X$ gauge boson is not much heavier than the reheating temperature, it

[23]It is reasonable to assume that the decays of inflatons to heavy N_i are kinematically forbidden. Furthermore, since they are not relativistic, they do not contribution significantly to the energy density of the Universe.

could also thermalize N_i, Ψ_a, Φ_κ and Φ_λ. Motivated by the above considerations, we will consider two possible initial conditions for N_i abundance: zero N_i abundance and thermalized N_i abundance.

3.5.3 Hybrid genesis: quantitative description

In this section, we will discuss CP violation in section 3.5.3.1, washout processes from inverse decay and off-shell scatterings in section 3.5.3.2 and finally in section 3.5.3.3, we write down the BEs of hybrid genesis. Under reasonable assumptions, the formal solution to the BEs can be written down including both the inverse decay and off-shell $\Delta = 2$ scattering. It will be in the form of integral, which can readily be evaluated numerically. On the other hand, keeping only the inverse decay term allows us to derive approximate analytical solutions in appendix. B.2. In this way, our strategy will be to use these analytical solutions when the washout from off-shell $\Delta = 2$ scattering is negligible while evaluate numerically when it is relevant.

3.5.3.1 CP violation

To quantify the CP violation in the decays of $N_i \to \Phi_\lambda \Psi_a$ and $N_i \to (\Phi_\lambda \Psi_a)^*$, we define the CP parameter as follows [see eq. (B.12)]

$$\epsilon_{ia} \equiv \frac{\Gamma\left(N_i \to \Phi_\lambda \Psi_a\right) - \Gamma\left(N_i \to \Phi_\lambda^* \Psi_a^*\right)}{\Gamma_{N_i}}, \tag{3.68}$$

where $\Gamma(P)$ is the partial decay width for process P and the total decay width of N_i (at tree-level) is

$$\Gamma_{N_i} \equiv \sum_a \left[\Gamma\left(N_i \to \Phi_\lambda \Psi_a\right) + \Gamma\left(N_i \to \Phi_\lambda^* \Psi_a^*\right)\right] = \frac{\left(\lambda\lambda^\dagger\right)_{ii} M_{N_i}}{16\pi}. \tag{3.69}$$

The leading CP violation in the decays comes from the interference between tree-level and one-loop diagrams and eq. (3.68) can be written down as [73]

$$\begin{aligned} \epsilon_{ia} &= \frac{1}{8\pi}\frac{1}{\left(\lambda\lambda^\dagger\right)_{ii}} \sum_{j\neq i} \mathrm{Im}\left[\left(\lambda\lambda^\dagger\right)_{ij} \lambda_{ia}\lambda_{ja}^*\right] g\left(\frac{M_{N_j}^2}{M_{N_i}^2}\right) \\ &\quad + \frac{1}{16\pi}\frac{1}{\left(\lambda\lambda^\dagger\right)_{ii}} \sum_{j\neq i} \mathrm{Im}\left[\left(\lambda\lambda^\dagger\right)_{ji} \lambda_{ia}\lambda_{ja}^*\right] \frac{M_{N_i}^2}{M_{N_i}^2 - M_{N_j}^2}, \end{aligned} \tag{3.70}$$

where the loop function is given by[24]

$$g\left(x\right) = \sqrt{x}\left[\frac{1}{2}\frac{1}{1-x} + 1 - (1+x)\ln\frac{1+x}{x}\right]. \tag{3.71}$$

Assuming a modest hierarchy, $M_{N_2}/M_{N_1} \sim$ a few and that the main contribution to asymmetry generation to come from the decays of N_1, we will expand $g\left(M_{N_1}/M_{N_2}\right)$ at leading order in M_{N_1}/M_{N_2}. Furthermore we will ignore the Ψ_a flavor effect by

[24] This includes both self-energy and vertex corrections with the first term in the square bracket for the former while the rest of the terms for the latter. A factor of $\frac{1}{2}$ in the self energy term compared to the standard leptogenesis case is due to the fact that Φ_λ and Ψ_a are singlets instead of doublets under $SU(2)_L$. For the same reason, the second term in eq. (3.68) coming from self-energy diagrams also has a factor of $\frac{1}{2}$. Such term becomes CP-invariant once summed over flavor a.

summing over a.[25] Doing so, we have

$$\begin{aligned}\epsilon_1 &\equiv \sum_a \epsilon_{1a} \approx -\frac{1}{8\pi}\frac{1}{\left(\lambda\lambda^\dagger\right)_{11}}\left|\left(\lambda\lambda^\dagger\right)_{12}\right|^2 \sin\left(\phi_{12}\right)\frac{M_{N_1}}{M_{N_2}} \\ &\approx -\frac{1}{8\pi}\left(\lambda\lambda^\dagger\right)_{22}\sin\left(\phi_{12}\right)\frac{M_{N_1}}{M_{N_2}},\end{aligned} \tag{3.72}$$

where we have defined $\phi_{12} \equiv \arg\left[\left(\lambda\lambda^\dagger\right)_{12}^2\right]$. In the last approximation above (and the rest of the work), we assume

$$\lambda_{ia} \sim \lambda_{ib}, \tag{3.73}$$

for any a, b and i. However, we will allow $\lambda_{ia}/\lambda_{ja}$ with $i \neq j$ to vary within a few orders of magnitude.

3.5.3.2 Thermal averaged reaction densities

Here we will describe the thermal averaged reaction densities [defined in eq. (B.7)] which appear in the BEs to describe the decay and scattering processes (see appendix B.1 for details).

In the following, we assume N_i to be massive while all other particles to be massless. Firstly, we will consider the (inverse) decay $N_1 \leftrightarrow \Phi_\lambda \Psi_a$ (and the corresponding CP conjugate processes).[26] From eqs. (B.8) and (B.13), the total decay

[25] This is justified assuming a large κ in eq. (3.49), which results in fast flavor equilibrating scatterings $\Psi_a^c \Psi_a \leftrightarrow \Psi_b^c \Psi_b$. See section 3.5.3.3 for further discussion.

[26] This is equivalent to the on-shell part of $\Delta = 2$ scattering $\Phi_\lambda \Psi_a \leftrightarrow (\Phi_\lambda \Psi_a)^*$ mediated by N_1 where the subdominant off-shell contribution can be ignored.

reaction density is

$$\gamma_{N_1} = n_{N_1}^{\rm eq}\Gamma(N_1 \to \Phi_\lambda \Psi_a)\frac{\mathcal{K}_1(z)}{\mathcal{K}_2(z)}, \tag{3.74}$$

where $z = M_{N_1}/T$ and $\mathcal{K}_n(z)$ is the modified Bessel function of the second kind of order n. The decay term is proportional to $\frac{n_{N_1}}{n_{N_1}^{\rm eq}}\gamma_{N_1}$ which is not Boltzmann suppressed. On the other hand, inverse decay is simply proportional to γ_{N_1} and will be Boltzmann suppressed for $T < M_{N_1}$. If $\Gamma_{N_1} \ll H(T = M_{N_1})$, the decay happens at $\Gamma_{N_1} \sim H(T \ll M_{N_1})$ when the inverse decay is Boltzmann suppressed. In this case, the asymmetry is efficiently generated while washout due to inverse decay is suppressed. The degree of out-of-equilibrium decay for $N_i \to \Phi_\lambda \Psi_a$ is usually quantified by the washout factor already introduced in eq. (3.30)

$$K_i \equiv \frac{\Gamma_{N_i}}{H(T = M_{N_i})}. \tag{3.75}$$

The case of $K_i < 1$ is known as the weak washout regime (washout of the asymmetry from the inverse decay is not effective) while $K_i > 1$ as the strong washout regime (washout of the asymmetry from the inverse decay becomes relevant).

Next, as we maximize the CP parameter in eq. (3.72) by increasing λ_{2a}, the $\Delta = 2$ scatterings $\Phi_\lambda \Psi_a \leftrightarrow (\Phi_\lambda \Psi_b)^*$ and $\Psi_a \Psi_b \leftrightarrow (\Phi_\lambda \Phi_\lambda)^*$ from off-shell exchange of heavier N_2 can become relevant. We estimate the scattering rate for the processes

above for $T \sim M_{N_1} \ll M_{N_2}$ as follows [see eqs. (B.10) and (B.11)]

$$\Gamma^{ab}_{\text{scatt}} = \frac{\gamma^{ab}_{\text{scatt}}}{n^{\text{eq}}} \approx \frac{1}{16\pi^3} \frac{|\lambda_{2a}|^2 |\lambda_{2b}|^2}{M^2_{N_2}} T^3, \tag{3.76}$$

where $n^{\text{eq}} = \frac{T^3}{\pi^2}$. With the assumption eq. (3.73), we can relate the scattering rate above to the CP parameter eq. (3.72) as follows

$$\Gamma^{ab}_{\text{scatt}} \approx \frac{4}{\pi} \frac{\epsilon_1^2}{\sin^2(\phi_{12})} \frac{M_{N_1}}{z^3}. \tag{3.77}$$

From the above, it becomes clear that as one increases the CP parameter ϵ_1, the scattering washout rate will increase and vice versa. As we will see in section 3.6.2.2, requiring this washout scattering to be under control in general implies a lower bound on M_{N_1} [97, 98].

3.5.3.3 Boltzmann equations

We now study in detail the generation/washout of the asymmetry at $T \sim M_{N_1}$ and the low scale washout at $T \sim m_{\Phi_{\kappa,\lambda}}$. The high scale genesis can be described

by the following BEs:

$$sHz_{\rm UV}\frac{dY_{N_1}}{dz_{\rm UV}} = -\gamma_{N_1}\left(\frac{Y_{N_1}}{Y_{N_1}^{\rm eq}}-1\right), \tag{3.78}$$

$$\begin{aligned} sHz_{\rm UV}\frac{dY_{\Delta}}{dz_{\rm UV}} &= -\epsilon_1\gamma_{N_1}\left(\frac{Y_{N_1}}{Y_{N_1}^{\rm eq}}-1\right)+\frac{1}{2}\sum_a P_a\gamma_{N_1}\left(\frac{Y_{\Delta\Psi_a}}{Y^{\rm eq}}+\frac{1}{2}\frac{Y_{\Delta\Phi_\lambda}}{Y^{\rm eq}}\right) \\ &\quad+\sum_a\gamma_{\rm scatt}^{aa}\left(\frac{Y_{\Delta\Psi_a}}{Y^{\rm eq}}+\frac{1}{2}\frac{Y_{\Delta\Phi_\lambda}}{Y^{\rm eq}}\right) \\ &\quad+\sum_a\sum_{b\neq a}\gamma_{\rm scatt}^{ab}\left(\frac{1}{2}\frac{Y_{\Delta\Psi_a}}{Y^{\rm eq}}+\frac{1}{2}\frac{Y_{\Delta\Psi_b}}{Y^{\rm eq}}+\frac{1}{2}\frac{Y_{\Delta\Phi_\lambda}}{Y^{\rm eq}}\right), \end{aligned} \tag{3.79}$$

where $z_{\rm UV}\equiv M_{N_1}/T$, $Y_{\Delta i}\equiv Y_i - Y_{i^*}$, $P_a\equiv\frac{\lambda_{1a}\lambda_{1a}^*}{\left(\lambda\lambda^\dagger\right)_{11}}$ and $Y^{\rm eq}$ is defined in eq. (B.6). The rates γ_{N_1} and $\gamma_{\rm scatt}^{ab}$ are defined in eq. (3.74) and eq. (3.76), respectively. We also used the fact that in our case, both Ψ_a and Φ_λ are relativistic $\zeta_{\Psi_a}=1$, $\zeta_{\Phi_\lambda}=2$ and have one gauge degree of freedom $g_{\Psi_a}=g_{\Phi_\lambda}=1$. Here we take $g_\star=121.25$ since Ψ_a, Ψ_a^c, Φ_κ and Φ_λ all contribute to number of relativistic degrees of freedom.

We now discuss each terms in eq. (3.78) and eq. (3.79). In eq. (3.78), which describes the evolution of the number density of N_1, the first term on the right hand side is the reduction of number density by decay and the second term is the production of N_1 via inverse decay. In principle, several scattering terms that produce/remove N_1 appear on the right hand side of this equation and we ignore these subleading terms. Moving onto eq. (3.79), this equation determines evolution of asymmetry Δ. The first term on the right hand side proportional to the CP parameter describes the production of asymmetry via out-of-equilibrium decay of N_1. The remaining terms are for washout processes: the second, third, and fourth term respectively denoting washout from inverse decay, s-channel $\Delta=2$ scattering

$\Psi\Phi_\lambda \to (\Psi\Phi_\lambda)^*$ and its related t-channel process with *same* flavor Ψ, and the same scattering but with *different* Ψ flavors a and $b \neq a$.

Assuming that all $\Psi_a^c\Psi_a \leftrightarrow \Psi_b^c\Psi_b$ are in thermal equilibrium due to large κ, the asymmetry will be equally distributed among all generations of the Ψ_a. In this case we have $Y_{\Delta\Psi_1} = Y_{\Delta\Psi_2} = Y_{\Delta\Psi_3} \equiv \frac{1}{3}Y_{\Delta\Psi}$ where $Y_{\Delta\Psi} = Y_{\Delta\Psi_1} + Y_{\Delta\Psi_2} + Y_{\Delta\Psi_3}$. With this assumption, we can sum over flavor in the scattering rate $\gamma_{\rm scatt} \equiv \sum_{a,b}\gamma^{ab}_{\rm scatt}$ and eq. (3.79) can be simplified to

$$\begin{aligned} sHz_{\rm UV}\frac{dY_\Delta}{dz_{\rm UV}} &= -\epsilon_1\gamma_{N_1}\left(\frac{Y_{N_1}}{Y^{\rm eq}_{N_1}} - 1\right) + \frac{1}{2}\gamma_{N_1}\left(\frac{Y_{\Delta\Psi}}{3Y^{\rm eq}} + \frac{Y_{\Delta\Phi_\lambda}}{2Y^{\rm eq}}\right) \\ &\quad + \gamma_{\rm scatt}\left(\frac{Y_{\Delta\Psi}}{3Y^{\rm eq}} + \frac{Y_{\Delta\Phi_\lambda}}{2Y^{\rm eq}}\right), \end{aligned} \tag{3.80}$$

where we have made use of $\sum_a P_a = 1$.

In order to solve the equations above in closed form, we need to express $Y_{\Delta\Psi}$ and $Y_{\Delta\Phi_\lambda}$ in term of Y_Δ. According to symmetry consideration we presented in section 3.5.1, all particle asymmetries can be relate to the charge Y_Δ [see eq. (3.56)]. So, we write $Y_{\Delta\Psi} = -c_\Psi Y_\Delta$ and $Y_{\Delta\Phi_\lambda} = -c_{\Phi_\lambda}Y_\Delta$, with $c_\Phi, c_{\Phi_\lambda} > 0$. In terms of these, we can rewrite eq. (3.80) as

$$\begin{aligned} sHz_{\rm UV}\frac{dY_\Delta}{dz_{\rm UV}} &= -\epsilon_1\gamma_{N_1}\left(\frac{Y_{N_1}}{Y^{\rm eq}_{N_1}} - 1\right) - \left(\frac{1}{2}\gamma_{N_1} + \gamma_{\rm scatt}\right)\left(c_\Psi\frac{Y_\Delta}{3Y^{\rm eq}} + c_{\Phi_\lambda}\frac{Y_\Delta}{2Y^{\rm eq}}\right) \\ &\equiv -\epsilon_1\gamma_{N_1}\left(\frac{Y_{N_1}}{Y^{\rm eq}_{N_1}} - 1\right) - \left(\frac{1}{2}\gamma_{N_1} + \gamma_{\rm scatt}\right)c_{W1}\frac{Y_\Delta}{Y^{\rm eq}}, \end{aligned} \tag{3.81}$$

where we have defined

$$c_{W1} \equiv \frac{c_\Psi}{3} + \frac{c_{\Phi_\lambda}}{2}. \tag{3.82}$$

The coefficient c_{W1} will be determined by the symmetries of the model and by the particle contents in the thermal bath (see Appendix C for details). Formally, the solution to eq. (3.81) is given by

$$Y_\Delta\left(z_{\rm UV}\right) = Y_\Delta\left(z_{{\rm UV},i}\right) e^{-\frac{c_{W1}}{Y^{\rm eq}}\int_{z_{{\rm UV},i}}^{z_{\rm UV}} dz' W(z')} + \epsilon_1 \int_{z_{{\rm UV},i}}^{z_{\rm UV}} dz' \frac{dY_{N_1}}{dz'} e^{-\frac{c_{W1}}{Y^{\rm eq}}\int_{z'}^{z_{\rm UV}} dz'' W(z'')} \tag{3.83}$$

where $z_{{\rm UV},i}$ is the initial temperature, $W(z) \equiv \frac{1}{sHz}\left(\frac{1}{2}\gamma_{N_1} + \gamma_{\rm scatt}\right)$ is the total washout factor and $Y_\Delta(z_{{\rm UV},i})$ is a preexisting asymmetry. The approximate solution including only decays and inverse decays are presented in appendix B and can be summarized as

$$Y_\Delta(z_{\rm UV} \to \infty) = \epsilon_1 \eta_{N_1} Y^{\rm eq}_{N_1}(0) \tag{3.84}$$

where η_{N_1} is the efficiency factor :

$$\eta_{N_1} \sim \begin{cases} 1/(K_1 \ln K_1) & \text{for } K_1 \gg 1 \text{ [eq. (B.39)]} \\ K_1^2 & \text{for } K_1 \ll 1 \text{ with zero initial } Y_{N_1} \text{ [eq. (B.31)]} \\ O(1) & \text{for } K_1 \ll 1 \text{ with thermal initial } Y_{N_1} \text{ [eq. (B.40)]} \end{cases} \tag{3.85}$$

and K_1 is defined in eq. (3.75). When off-shell $\Delta = 2$ scatterings are relevant, we

took into account their effects numerically.

Next we will study the effect of low scale washout. For simplicity, we assume that all three pseudo-Dirac pairs $\tilde{\Psi}_i$ have comparable masses and denote the common mass scale as m_Ψ. With this assumption BE's for all three pairs of $\tilde{\Psi}_i$ can be written with a common $z_{\rm IR} \equiv \frac{m_\Psi}{T}$. We will work up to leading order in the mass difference. At low scale $T \sim m_\Psi$, the washout is described by (here we ignore the asymmetry generation from Ψ decay as it is shown to be negligible in section 3.3)

$$\begin{aligned} sHz_{\rm IR}\frac{dY_\Delta}{dz_{\rm IR}} &= \frac{1}{2}\gamma_\Psi\left(\frac{Y_{\Delta\ell}}{6Y^{\rm eq}}+\frac{Y_{\Delta H}}{4Y^{\rm eq}}\right) \\ &= -\frac{1}{2}\gamma_\Psi\left(c_\ell\frac{Y_\Delta}{6Y^{\rm eq}}+c_H\frac{Y_\Delta}{4Y^{\rm eq}}\right) \equiv -\frac{1}{2}c_{W2}\gamma_\Psi\frac{Y_\Delta}{Y^{\rm eq}}, \end{aligned} \tag{3.86}$$

where γ_Ψ describes the washout from $\ell H \leftrightarrow \bar{\ell}H^*$ with on-shell pseudo-Dirac fermions $\tilde{\Psi}_i$ and we used $g_\ell = g_H = 2$ and $\zeta_\ell = 1$, $\zeta_H = 2$. Also, as we already did above, we wrote $Y_{\Delta\ell} = -c_\ell Y_\Delta$ and $Y_{\Delta H} = -c_H Y_\Delta$, with $c_\ell, c_H \geq 0$. We have also assumed lepton flavors to equilibrate such that $Y_{\Delta\ell_e} = Y_{\Delta\ell_\mu} = Y_{\Delta\ell_\tau} \equiv \frac{1}{3}Y_{\Delta\ell}$ where $Y_{\Delta\ell} = Y_{\Delta\ell_e}+Y_{\Delta\ell_\mu}+Y_{\Delta\ell_\tau}$. We have defined $c_{W2} \equiv \frac{c_\ell}{6}+\frac{c_H}{4}$ and here we take $g_\star = 106.75$ since Ψ_a, Ψ_a^c, Φ_κ and Φ_λ no longer contribute to number of relativistic degrees of freedom. For $T_{\rm EWsp}^- < T \lesssim 10^4$ GeV, we have $c_\ell = \frac{42}{79}$, $c_H = \frac{16}{79}$ and $c_{W2} = \frac{11}{79}$. Since the eq. (3.86) is homogeneous, the solution can be obtained straightforwardly (or equivalently by keeping the first term of eq. (3.83) and setting the second term to zero)

$$Y_\Delta\left(z_{{\rm IR},f}\right) = Y_\Delta\left(z_{{\rm IR},i}\right)e^{-\frac{6}{\pi^2}c_{W2}K_\Psi^{\rm eff}f\left(z_{{\rm IR},i},z_{{\rm IR},f}\right)}, \tag{3.87}$$

where $z_{\rm IR,i}$ and $z_{\rm IR,f}$ denote respectively the initial and final temperatures within the IR physics for which eq. (3.86) is solved. The function $f(z_{\rm IR,i}, z_{\rm IR,f})$ is defined in eq. (B.20). In addition, the low scale effective washout factor is defined as [c.f. $T \ll M_{N_1}$ eq. (3.31)]

$$K_\Psi^{\rm eff} \equiv \sum_a \frac{\Gamma_{\Psi_a}}{H} \left(\frac{|\mu_{aa}|}{\Gamma_{\Psi_a}} \right)^2 \Bigg|_{T=m_{\Psi_a}} . \tag{3.88}$$

where $\Gamma_{\Psi_a} \equiv \frac{1}{16\pi}(yy^\dagger)_{aa} m_{\Psi_a}$. Since for our case $M_{N_1} \gg m_\Psi$, we can take $z_{\rm IR,i} \to 0$. The initial abundance of $Y_\Delta(z_{\rm IR,i})$ of the IR solution is obtained from the final asymmetry $Y_\Delta(z_{\rm UV,f} \to \infty)$ of the UV genesis. Namely,

$$Y_\Delta\left(z_{\rm IR,i}\right) = Y_\Delta\left(z_{\rm UV,f}\right). \tag{3.89}$$

As for $z_{\rm IR,f}$, it is bounded by $T^-_{\rm EWsp} = 132$ GeV where EW sphaleron processes cease to be effective. If $m_\Psi \gg T^-_{\rm EWsp}$, we can take $z_{\rm IR,f} \to \infty$ and use $f(0,\infty) = \frac{3\pi}{2}$. Already for $m_\Psi = 1$ TeV, we have $f(0, \frac{1000}{132}) = 4.564$ which is only about 3 % different from $\frac{3\pi}{2}$. On the other hand, taking $m_\Psi = 500$ GeV, we have $f(0, \frac{500}{132}) = 3.058$. After the low scale washout, when the EW sphaleron processes get out of equilibrium at $T^-_{\rm EWSp} = 132$ GeV, the baryon asymmetry is frozen as given in eq. (3.57). To summarize, the complete formula for the baryon asymmetry generated in our hybrid seesaw model is given as

$$Y_{\Delta B} = d \times \epsilon_1 \eta_{N_1} Y_{N_1}^{\rm eq}(0) \times e^{-\frac{6}{\pi^2} c_{W2} K_\Psi^{\rm eff} f(z_{\rm IR,i}, z_{\rm IR,f})}. \tag{3.90}$$

This equation clearly demonstrates the interplay of the high scale and low scale physics in hybrid-genesis. The part $\epsilon_1 \eta_{N_1} Y_{N_1}^{\rm eq}(0)$ shows the generation of the asymmetry from the high scale N_1 decay [eq. (3.84)], while the exponential factor encodes the washout effect from the low scale [eq. (3.87)]. The coefficient d is the factor related to the EW sphaleron processes shown in eq. (3.57).

3.6 Results

In this section we will use the formalism developed in section 3.5 to identify the region of parameter space of our model that accounts for the observed baryon asymmetry. Most of the results of this section are based on *analytic* expressions derived in section 3.5 and appendix B; however, when the washout effects from off-shell scattering become significant we used numerical methods. Fortunately, most of the plots given below can be understood analytically. For the readers' convenience, we provide a list of formulae relevant to leptogenesis in table 3.4. In particular, we show the parametric dependence of each quantity on the two main parameters of the effective theory in the IR, i.e., m_Ψ and y, and present most of the plots in the plane $y - m_\Psi$.

We discuss the results only for our **fully-symmetric model** for concreteness. Noticing that the main difference between **fully-symmetric** and **non-symmetric** models are the existence of exact $U(1)$ symmetries and that this will mainly lead to a difference in spectator effects, we conclude based on the argument in appendix C that their final asymmetry will differ only up to an order one factor.

SM neutrino mass in hybrid seesaw				
No.	Quantity	Expression	Dependence on model parameters	Ref.
T1	Neutrino mass	$m_\nu \sim \frac{y^2 v^2}{m_\Psi^2}\mu$	$\mu \sim \frac{m_\nu}{v^2}\left(\frac{m_\Psi^2}{y^2}\right)$	eq. (3.8)
T2	μ	$\mu \sim \frac{\lambda_2^2\langle\Phi_\lambda\rangle^2}{M_N}$	$\lambda_2^2 \sim \frac{m_\nu M_N}{v^2\langle\Phi_\lambda\rangle^2}\left(\frac{m_\Psi^2}{y^2}\right)$	eq. (3.50)
Leptogenesis in high scale module				
No.	Quantity	Expression	Dependence on model parameters	Ref.
T3	CP parameter	$\epsilon_1 \sim \frac{\lambda_2^2}{8\pi}$	$\epsilon_1 \sim \frac{m_\nu M_N}{8\pi v^2\langle\Phi_\lambda\rangle^2}\left(\frac{m_\Psi^2}{y^2}\right)$	eq. (3.72)
T4	Washout factor	$K_1 \equiv \frac{\Gamma_{N_1}}{H(T=M_{N_1})} \sim \frac{\lambda_1^2}{16\pi\sqrt{g_\star}}\frac{M_{\rm pl}}{M_N}$	$K_1 \sim \frac{r^2 M_{\rm pl} m_\nu}{16\pi\sqrt{g_\star}v^2\langle\Phi_\lambda\rangle^2}\left(\frac{m_\Psi^2}{y^2}\right)$	eq. (3.75)
T5	Asymmetry in strong washout	$Y_\Delta^s(z_{{\rm UV},f}) \sim 10^{-3}\frac{\epsilon_1}{K_1 \ln K_1}$	$Y_\Delta^s(z_{{\rm UV},f}) \sim \frac{\sqrt{g_\star}}{r^2}\frac{M_N}{M_{\rm pl}}/\ln K_1$	eq. (B.39)
T6	Asymmetry in weak washout	$Y_\Delta^w(z_{{\rm UV},f}) \sim 10^{-3}\epsilon_1 K_1^2$ $(Y_{N_1}(z_{{\rm UV},i})=0)$	$Y_\Delta^w(z_{{\rm UV},f}) \sim \frac{r^4 M_{\rm pl}^2 m_\nu^3 M_N}{g_\star v^6\langle\Phi_\lambda\rangle^6}\left(\frac{m_\Psi^6}{y^6}\right)$	eq. (B.31)
T7		$Y_\Delta^{\rm th,w}(z_{{\rm UV},f}) \sim 10^{-3}\epsilon_1$ (thermal $Y_{N_1}(z_{{\rm UV},i})$)	$Y_\Delta^{\rm th,w}(z_{{\rm UV},f}) \sim \frac{m_\nu M_N}{8\pi v^2\langle\Phi_\lambda\rangle^2}\left(\frac{m_\Psi^2}{y^2}\right)$	eq. (B.40)
T8	Off-shell N_2 scattering	$K_{N_2}^{\rm scatt} = \frac{\Gamma_{N_2}^{\rm scatt}}{H(T=M_{N_1})} \sim \frac{\lambda_2^4}{16\pi^3\sqrt{g_\star}}\frac{M_{\rm pl}}{M_N}$	$K_{N_2}^{\rm scatt} \sim \frac{1}{\sqrt{g_\star}}\frac{M_{\rm pl} m_\nu^2 M_N}{v^4\langle\Phi_\lambda\rangle^4}\left(\frac{m_\Psi^4}{y^4}\right)$	eq. (3.77)
The washout in TeV scale module				
No.	Quantity	Expression	Dependence on model parameters	Ref.
T9	Effective washout factor	$K_\Psi^{\rm eff} \sim \frac{\Gamma_\Psi}{H(T=m_\Psi)}\left(\frac{\mu}{\Gamma_\Psi}\right)^2$	$K_\Psi^{\rm eff} \sim \frac{16\pi}{\sqrt{g_\star}}\frac{M_{\rm pl} m_\nu^2}{v^4}\left(\frac{m_\Psi}{y^6}\right)$	eq. (3.88)
T10	Low scale washout	$Y_\Delta(z_{{\rm IR},f}) \sim Y_\Delta(z_{{\rm IR},i})e^{-K_\Psi^{\rm eff}}$	$Y_\Delta(z_{{\rm IR},f}) \sim Y_\Delta(z_{{\rm IR},i})e^{-\frac{16\pi}{\sqrt{g_*}}\frac{M_{\rm pl} m_\nu^2}{v^4}\left(\frac{m_\Psi}{y^6}\right)}$	eq. (3.87)
Constraints				
No.	Quantity	Expression	Dependence on model parameters	Ref.
T11	$\mu \to e\gamma$	${\rm BR}(\mu\to e\gamma) \simeq \frac{3\alpha_{\rm em}}{8\pi}\left\lvert\left(y^t\frac{v^2}{m_\Psi^\dagger m_\Psi}y^*\right)_{\mu e}\right\rvert^2$	${\rm BR}(\mu\to e\gamma) \sim \frac{3\alpha_{\rm em}}{8\pi}v^4\left(\frac{y^4}{m_\Psi^4}\right)$	eq. (3.11)

Table 3.4: Summary of formulae for hybrid-leptogenesis with $r \equiv \lambda_1/\lambda_2$. High scale and TeV scale modules are defined in eq. (3.92). Generally we assume that $M_N \sim M_{N_1} \sim M_{N_2}$ and $r \leq 1$

3.6.1 General parameter space

As discussed in section 3.5, there are two scales relevant for leptogenesis in our model. The asymmetry is first generated at high temperatures through decays of the Majorana singlet N_i. This primordial asymmetry is then prone to further washout at the TeV scale. In other words, the asymmetry that is generated and survives the high temperature washout effects can be taken as an initial condition for the TeV-scale leptogensis. As was shown in section 3.3, the asymmetry generated at the TeV scale by itself is generically negligible, so we only take into account the washout processes at this scale. Furthermore, as we discuss in detail in section 3.6.2, the allowed range for M_N in our hybrid model is roughly of order $10^6 - 10^{16}$ GeV. This corresponds to relaxed bounds on both (upper and lower) sides compared to the standard Type I scenario, and in what follows, we will study this full mass range.

In order to avoid technical details obscuring the main physics, we assume two generations of N_i ($i = 1, 2$) and their Yukawa couplings to be anarchic, except for the specific cases described below. In particular, Ψ_a flavor effects can be ignored due to the assumption in eq. (3.73) as well as fast flavor equilibrating scatterings mentioned in footnote 25. The same assumption as in eq. (3.73) allows us to simply denote their Yukawa couplings as λ_i ($\lambda_i \sim \lambda_{ia}$ for all a). As we discuss in section 3.6.2.2, in order to lower the scale of high scale leptogenesis down to 10^6 GeV, hierarchies in the couplings λ_i are required and the third generation of N is also needed to fit neutrino observables. For this reason it is useful to define the ratio $r \equiv \frac{\lambda_1}{\lambda_2}$. The mass of N_i is denoted as M_{N_i} or simply M_N when all M_{N_i} are of the same order but

not degenerate. For the other couplings y and κ, we assume anarchical structure and for simplicity, we treat them as numbers rather than matrices.

Under the reasonable assumptions mentioned above, our hybrid model can be parametrized by six parameters:

$$y,\ m_\Psi\ \lambda_2,\ r,\ M_N, \langle\Phi_\lambda\rangle. \tag{3.91}$$

Since hybrid-genesis intrinsically features two scales, it is convenient to classify these parameters in two modules :

$$\begin{aligned} \text{High scale module} \quad &: \quad \lambda_i N_i \Phi_\lambda \Psi + \frac{1}{2} M_{N_i} N_i N_i + \text{h.c.}, \\ \text{TeV scale module} \quad &: \quad y \Psi^c H \ell + m_\Psi \Psi^c \Psi + \frac{1}{2} \mu \Psi \Psi + \text{h.c.} \end{aligned} \tag{3.92}$$

Here the high scale module is the part of the full Lagrangian in eq. (3.49) which only contains particles relevant to high scale leptogenesis and has three parameters: λ_2, r, M_N. (Note that $\langle\Phi_\lambda\rangle$ does not affect high scale genesis, so it is not included here.) The TeV scale module is basically the ISS model (eq. (3.12)) with $m_\Psi = \kappa\langle\Phi_\kappa\rangle$ and μ determined by high scale parameters as in T2 in table 3.4. Because $\langle\Phi_\lambda\rangle$ is a more fundamental quantity than μ, we interpret the former as independent.

There are two constraints on six parameters in eq. (3.91): one is the observed neutrino mass m_ν and the other the observed baryon asymmetry. This leaves us with four independent parameters. The above simplifications allow us to write down simple relations as in Table 3.4.

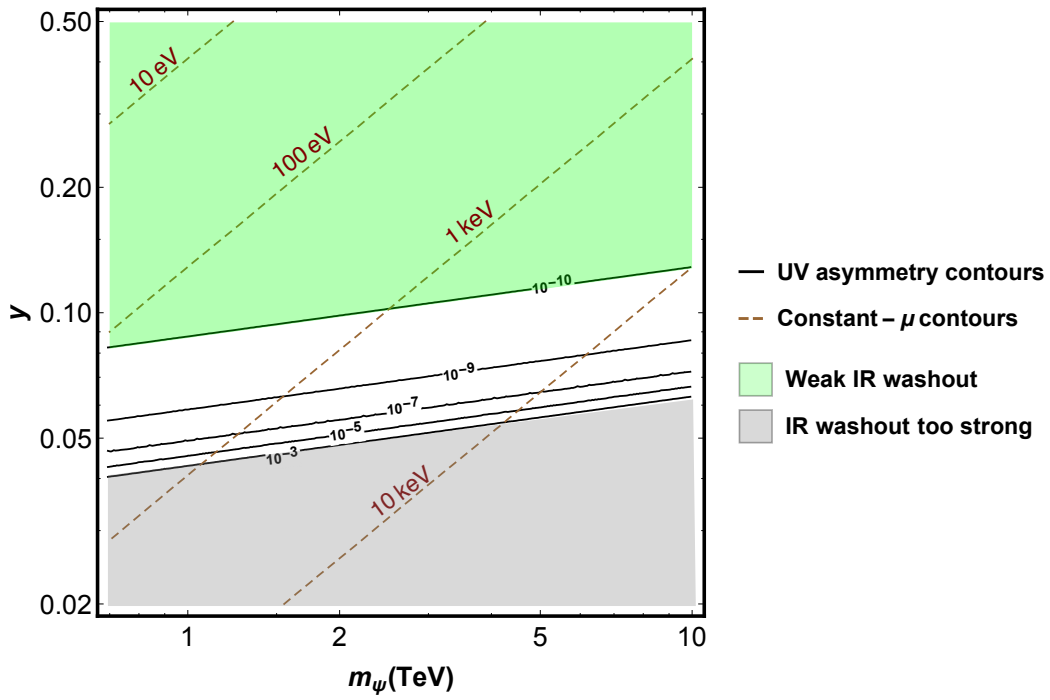

Figure 3.3: Contours of needed UV asymmetry (solid black lines) and μ (dashed brown lines) in the (m_Ψ, y) plane to obtain the observed baryon asymmetry $Y_{\Delta B} \sim 10^{-10}$ and $m_\nu = 0.05$ eV. In the green shaded region, washout at the TeV scale is negligible so that the UV asymmetry needs to be the observed baryon asymmetry $\sim 10^{-10}$. On the other hand, for smaller values of y, due to exponential sensitivity in y and m_Ψ, UV asymmetry lines get closer to each other. In the gray shaded region, TeV scale washout becomes so large that even saturating maximal allowed $Y_\Delta(z_{_{UV},f}) \sim 10^{-3}$ results in too small final asymmetry to explain the observation.

3.6.1.1 TeV scale module

We first study the impact of our parameters in the TeV scale module in eq. (3.92). Consider figure 3.3, where y and m_Ψ are treated as independent. For a chosen m_Ψ and y, the quantity μ will be fixed by the SM neutrino mass m_ν via T1 in table 3.4. This is presented in figure 3.3, where the dashed lines on the plot are contours of constant μ and we have fixed $m_\nu = 0.05$ eV. From table 3.4, we see that $\mu \sim m_\Psi^2/y^2$.

Once m_Ψ, y and m_ν are fixed, the low scale effective washout factor (T9 in table 3.4) is fixed as well. Therefore, we can determine the required amount of asymmetry generated at the high scale $Y_\Delta(z_{\text{UV},f})$ (using T9 in table 3.4) in order to match the observed value $Y_{\Delta B} \sim 10^{-10}$ [75] through eq. (3.57). Contours of the needed UV asymmetry are shown as solid lines in figure 3.3. As can be seen from table 3.4, the required $Y_\Delta(z_i)$ depends on (m_Ψ, y) via $K_\Psi^{\text{eff}} \sim \frac{16\pi}{\sqrt{g_\star}} \frac{M_{\text{Pl}} m_\nu^2}{v^4} \left(\frac{m_\Psi}{y^6}\right)$. Therefore, the required UV asymmetry lines will simply be parallel to constant $\sim \frac{m_\Psi}{y^6}$. In the green shaded region of the plot, the washout effect at the TeV scale is negligible and hence the UV asymmetry will need to be of order the observed size. For smaller y values, on the other hand, the washout from the TeV scale is exponentially strong so the final asymmetry becomes sensitive to TeV scale parameters: this is reflected in the UV asymmetry contours getting closer and closer to each other as y gets smaller. For the gray shaded region, $y \lesssim 0.04$, the washout is so strong that even the maximal $Y_\Delta(z_{\text{UV},f}) \sim 10^{-3}$ would not be enough. For this reason no UV asymmetry contours are present in that region.

3.6.1.2 High scale module

The high scale module in eq. (3.92) has four parameters: λ_2, r, M_N and $\langle \Phi_\lambda \rangle$. Besides determining the generated UV asymmetry $Y_\Delta(z_{\text{UV},f})$, they also control the TeV scale mass μ as T2 in table 3.4. Fixing two of the four parameters, we can plot contours of constant μ and $Y_\Delta(z_{\text{UV},f})$ in the plane defined by the remaining two. For instance, fixing $\langle \Phi_\lambda \rangle$ and r, we obtain contours of constant μ and $Y_\Delta(z_{\text{UV},f})$ in

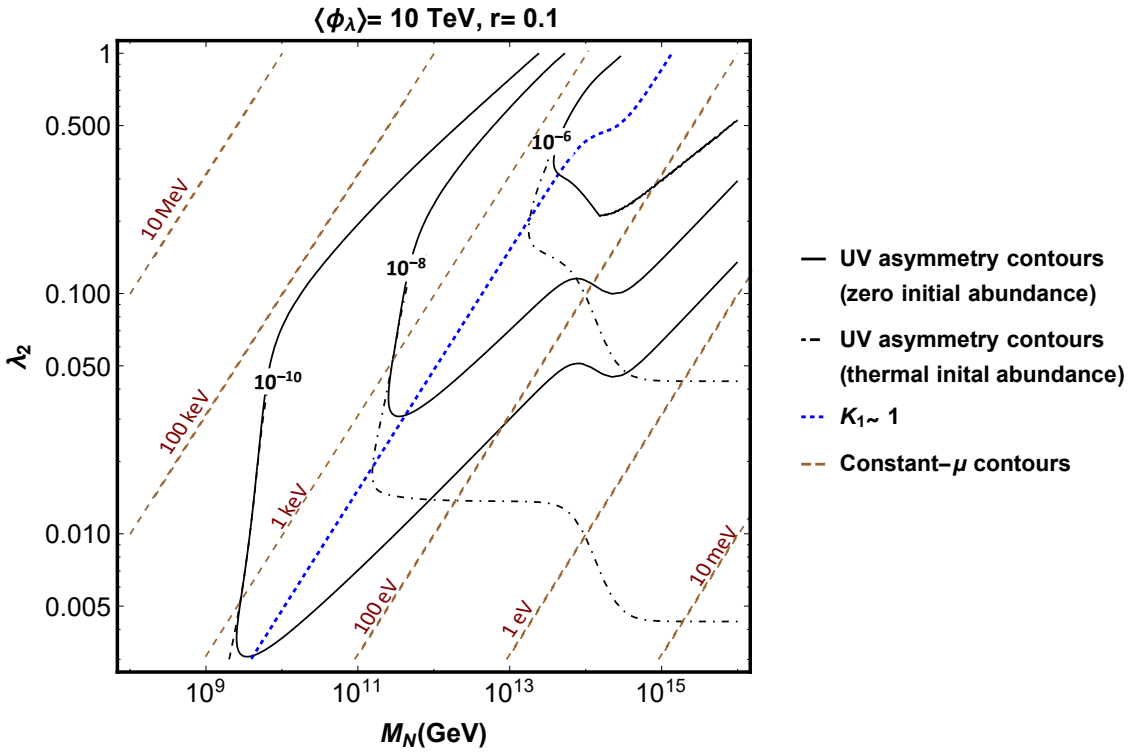

Figure 3.4: Contours of UV asymmetry and μ generated in the high scale module in the (M_N, λ_2) plane for $\langle\Phi_\lambda\rangle = 10$ TeV and $r = 0.1$. Solid curves are contours of UV asymmetry assuming zero initial abundance of N and dot-dashed curves are contours of UV asymmetry with the assumption of thermal initial abundance for N. The brown dashed lines are contours of constant μ. The blue dotted line sets the boundary between strong washout regime (to the left of the line) and weak washout regime (to the right of the line) for the high scale module.

the (M_N, λ_2) plane. These contours are shown in figure 3.4. As seen from T2 in table 3.4, constant μ simply gives straight lines (brown, dashed). Moving onto UV asymmetry, the blue dotted curve in the plot separates the regions of strong and weak UV washout. The transition seen in this curve around $M_N \sim 10^{14}$ GeV is due to the change in $g_\star$ as discussed in section 3.5.2.5. In the region to the left of the blue dotted curve, washout in the UV is strong and the UV asymmetry is a function mainly of M_N with only a logarithmic dependence on λ_2 (T5 in table 3.4), as long as the washout from off-shell scattering is negligible (i.e. as long as λ_2 is

not too large). So, in this region UV asymmetry contours (solid, black lines) are almost vertical lines until λ_2 becomes so large that washout from off-shell scattering becomes important. For such high λ_2 values, the UV asymmetry is very sensitive to $K_{N_2}^{\rm scatt}$ and contours of constant asymmetry roughly follow constant $K_{N_2}^{\rm scatt} \propto \frac{\lambda_2^4}{M_N}$ lines. In the weak washout region (to the right of the blue dotted curve) and with zero initial abundance for N, the UV asymmetry is $\propto \frac{\epsilon_1 K_1^2}{g_*} \propto \frac{\lambda_2^6}{g_* M_N^2}$. Therefore, as long as g_* does not vary significantly, solid curves in this region follow constant $\frac{\lambda_2^3}{M_N}$ lines. The dot-dashed black curves are contours of constant UV asymmetry assuming thermal initial abundance for N. They differ from the solid curves only in the weak washout regime where the UV asymmetry is $\propto \frac{\lambda_2^2}{g_*}$ and follow constant λ_2 lines if g_* is constant. The transition in both cases seen around $M_N \sim 10^{14}$ GeV is due to the change in g_* mentioned earlier.

3.6.1.3 Combining high scale and TeV scale modules

Here, we will combine the results of sections 3.6.1.1 and 3.6.1.2 in order to get a better picture of the allowed parameter space. For given values of (y, m_Ψ), we can find from figure 3.3 the required values of μ (for the right SM neutrino mass) and UV lepton asymmetry. Then, we can "match" these values to those generated by the high scale module from figure 3.4: for a given $\langle \Phi_\lambda \rangle$ and r, we can determine the necessary (M_N, λ_2). To make the parametric dependence more explicit, we fix (at a time) values of two parameters out of (M_N, $\langle \Phi_\lambda \rangle$ and r) and present viable contours for various values of the 3rd parameter in the 2D $y - m_\Psi$ plane. We show some of

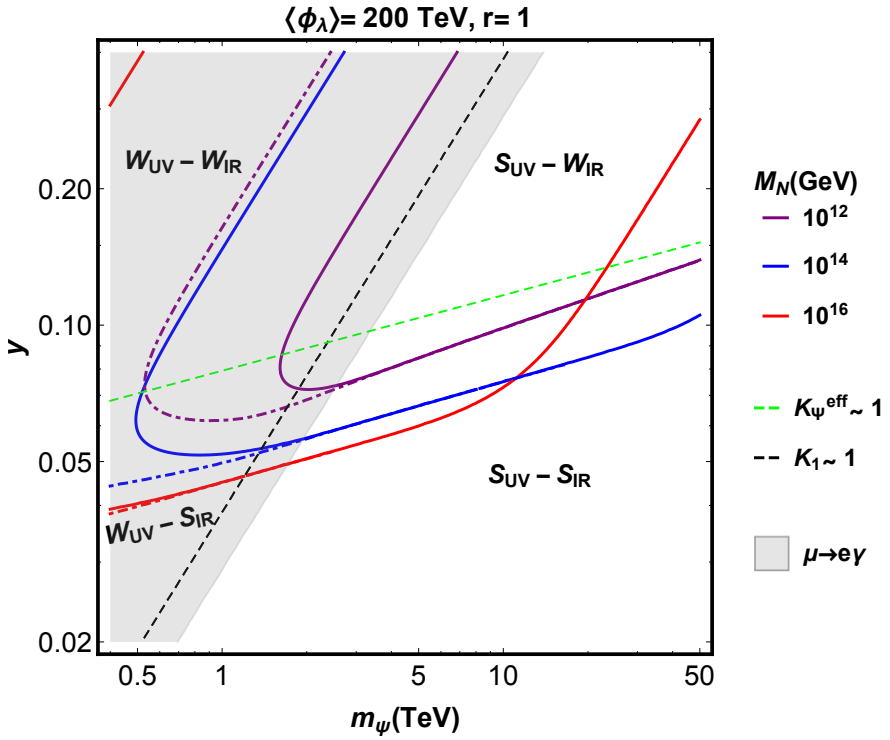

Figure 3.5: Interplay of high-scale washout and asymmetry generation with TeV scale washout. Solid (dot-dashed) curves are contours on which observed baryon asymmetry and SM neutrino masses are produced for fixed r and $\langle\Phi_\lambda\rangle$ and different choices of M_N, assuming zero (thermal) initial abundance for N . The dashed green line sets the boundary between the weak washout and strong washout regimes in the IR (around the TeV scale), and the dashed black line is the boundary of weak and strong washout regimes in UV. The gray shaded region is constrained by $\mu \to e\gamma$.

the curves in figures 3.5 and 3.6: more details are given below.

First of all, we mention some of the *general* ingredients going into these plots. In order to generate them, we have assumed anarchic, non-degenerate Majorana singlet masses. We have estimated the CP asymmetry, UV washout factor and effective IR washout factor as shown in table 3.4 and have used the analytic approximate expressions of appendix B. Whenever washout from off-shell scattering becomes important (for regions in parameter space where $K_{N_2}^{\rm scatt} > 0.1$), we take it into account by calculating the efficiency factor numerically. The solid curves in

figures 3.5 and 3.6 are produced under the assumption of *zero* initial N_1 abundance and dot-dashed curves are obtained assuming thermal initial N_1 abundance. These differ only in the weak UV washout regime since in the strong UV washout regime any asymmetry generated at the early time is efficiently erased and the final result only depends on the equilibrium abundance of N_1 at a time when the inverse decays freeze out. As already noted above, on each curve, we have fixed the SM neutrino mass (to $m_\nu = 0.05$ eV) and the final baryon asymmetry matches the observed one. Finally, the region constrained by lepton flavor violating process $\mu \to e\gamma$ (T11 in table 3.4) is shaded in gray, see the upper left corner of each plot. As discussed in section 3.2, such constraint can be further relaxed with flavor symmetries.

We now discuss in more detail some of the *specfic* features in these plots. Interestingly, there is an important *interplay* between the asymmetry generation/washout effects in high scale and washouts in TeV scale modules. In order to see this, consider first figure 3.5, where we fix r and $\langle\Phi_\lambda\rangle$ and show working contours for several values of M_N: we observe that it is divided into four regions by two dashed lines: the green dashed line denotes the $K_\Psi^{\rm eff} \sim 1$ boundary (of strong/weak washout in the IR) and the black dashed line is for $K_1 \sim 1$ (i.e., boundary of strong/weak washout in the UV). From table 3.4, we see that $K_\Psi^{\rm eff} \sim m_\Psi/y^6$ and $K_1 \sim m_\Psi^2/y^2$. The region above (below) the green dashed line has $K_\Psi^{\rm eff} < 1$ ($K_\Psi^{\rm eff} > 1$), is identified as the weak (strong) IR washout region and labelled by $W_{\rm IR}$ ($S_{\rm IR}$). The dashed black line, on the other hand, separates the high scale strong ($S_{\rm UV}$) and weak ($W_{\rm UV}$) washout regimes. The high scale washout is strong ($K_1 > 1$) below this line and weak ($K_1 < 1$) above it. One can identify four regimes from these combination: $S_{\rm UV} - S_{\rm IR}$, $S_{\rm UV} - W_{\rm IR}$,

$W_{\rm UV} - W_{\rm IR}$ and $W_{\rm UV} - S_{\rm IR}$:

(i) $S_{\rm UV} - S_{\rm IR}$: In this regime, the high scale asymmetry generation happens in the strong washout regime and the UV asymmetry generated is determined primarily by M_N and has only a very weak dependence on other parameters. Fixing all other parameters besides $\{m_\Psi, y\}$, from T5 in table 3.4, we see that the UV asymmetry has only logarithmic (mild) UV dependence on K_1. On the other hand, the final asymmetry is exponentially sensitive to TeV-scale washout, i.e. $K_\Psi^{\rm eff} \sim m_\Psi/y^6$ and hence a constant final asymmetry will lie along the constant $K_\Psi^{\rm eff}$ lines i.e. parallel to $K_\Psi^{\rm eff} \sim 1$ line. Eventually no curves will appear simply because TeV-washout becomes so strong that it is not possible to render the observed size of asymmetry for any choice of M_N.

Furthermore, one may notice from the red curve in figure 3.5 that its behavior differs from the others for larger m_Ψ. This may be understood by recalling that for larger M_N washout in the UV from scattering by off-shell exchange of N_2 becomes larger (parametrized by $K_{N_2}^{\rm scatt}$ in T5 of table 3.4) and at some point it becomes a significant factor in determining the final asymmetry. In this regime, the final asymmetry will follow a constant $K_{N_2}^{\rm scatt}$ line. Moreover, $K_{N_2}^{\rm scatt} \sim m_\Psi^4/y^4$ and so the asymmetry curve appears to be parallel to constant K_1 line.

(ii) $S_{\rm UV} - W_{\rm IR}$: In this region washout at the TeV scale is negligible and the final asymmetry is set by the high scale parameters as T5 in table 3.4. So the curves in this region follow a constant K_1 curve except for some choice of parameters

when washout due to scattering from off-shell N_2 exchange becomes relevant, in which case the curves are determined by a constant $K_{N_2}^{\rm scatt}$ line that coincides with a constant K_1 line.

(iii) $W_{\rm UV} - W_{\rm IR}$: In this region, washout at the TeV scale is negligible and the final asymmetry will be mainly dictated by the UV asymmetry. The asymmetry generated at the high scale, as shown in T6 or T7 in table 3.4, will be proportional to powers of m_Ψ/y and they will lie on constant K_1 lines (for both zero and thermal initial N_1 abundance).

(iv) $W_{\rm UV} - S_{\rm IR}$: The generation of asymmetry at the high scale occurs in the weak washout regime and the washout at the TeV scale is strong. The curves in this region interpolate between strong-strong and weak-weak regions, starting from a constant $K_\Psi^{\rm eff}$ line near the $S_{\rm UV} - S_{\rm IR}$ region and ending roughly on constant K_1 lines near the $W_{\rm UV} - W_{\rm IR}$ region.

Useful complementary information can be found in figure 3.6, where we show two plots with fixed $(M_N, \langle\Phi_\lambda\rangle)$ instead, while varying r and with fixed (M_N, r), for several choices of $\langle\Phi_\lambda\rangle$, respectively. Analyses similar to that done for figure 3.5 can be performed here also, but for brevity, we will not repeat it. As seen from T4 in table 3.4, $K_1 \propto \frac{r^2}{\langle\Phi_\lambda\rangle^2}$ and thus as we change either r or $\langle\Phi_\lambda\rangle$ (as we do in figure 3.5), the $K_1 \sim 1$ boundary will also change. To avoid too much complication in plots, therefore, we decided not to show $K_1 \sim 1$ lines for each case. For a discussion of other phenomenology of this model (such as collider and cosmological signals), see ref. [54].

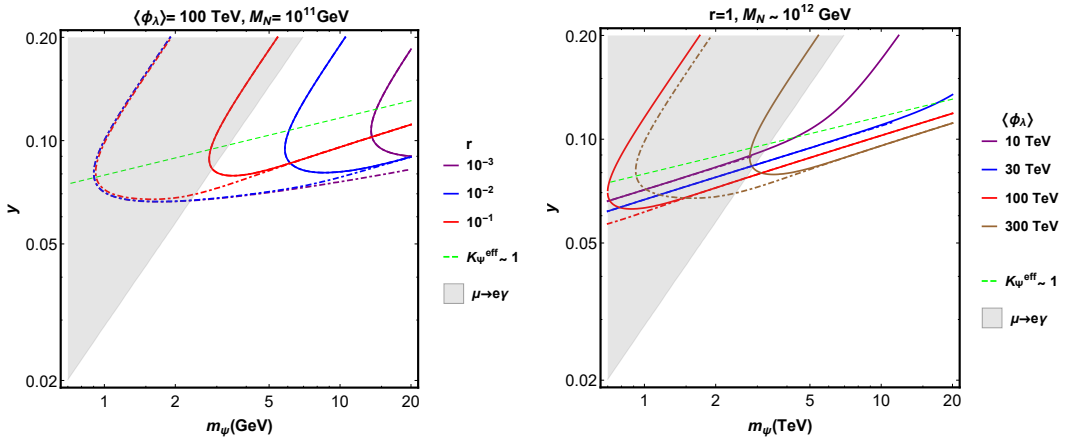

Figure 3.6: Solid (dot-dashed) curves are contours in (m_Ψ, y) plane on which the observed neutrino mass and baryon asymmetry is produced assuming zero (thermal) initial abundance for N, similar to figure 3.5. In the left panel, we vary r and keep M_N and $\langle\Phi_\lambda\rangle$ fixed, while the right panel shows the results with varying $\langle\Phi_\lambda\rangle$ while keeping M_N and r fixed. The gray shaded region is constrained by $\mu \to e\gamma$.

3.6.2 Selected benchmark points

In this section we are going to focus on some representative benchmark points. We categorize the possibilities based on M_N, the size of mass of heavy Majorana singlet. Specifically we present the choice of parameters that make leptogenesis possible for $M_N > 10^{15}$ GeV and $M_N < 10^9$ GeV, i.e., outside the usual range of Majorana singlet mass in type I seesaw leptogenesis scenarios.

3.6.2.1 Super-heavy singlet: $\gtrsim 10^{15}$ GeV

We start with singlet masses close to the upper bound on the reheating temperature from BICEP, i.e., $M_N \sim 10^{16}$ GeV [99].[27] In type I seesaw, leptogenesis fails in this regime because it suffers from too large washout due to off-shell scattering mediated by the Majorana singlet. This washout has a rate proportional to λ^4

[27] The constraint is on the Hubble scale during inflation, which with the assumption of instantaneous reheating, can be translated into a bound on the reheating temperature.

and as one increases M_N, one also has to increase λ in order to generate sufficient SM neutrino mass (in the type I seesaw $m_\nu \sim \lambda^2 v^2/M_N$). When $\lambda > 1$, the washout becomes strong and efficiently erases the asymmetry. On the other hand, in our hybrid model, we can keep λ small enough to suppress the washout from scattering and adjust other parameters to obtain the SM neutrino mass even for such large values of M_N. Indeed, taking into account the above considerations, it was shown in [54] that the upper bound on M_N in hybrid model is given by

$$M_N \lesssim \left(\frac{16\pi^3\sqrt{g_*}\, v^4}{M_{\rm Pl}\, m_\nu^2}\right) \times \left(\frac{y\langle\Phi_\lambda\rangle}{\kappa\langle\Phi_\kappa\rangle}\right)^4 \sim 10^{14}\ \text{GeV} \times \left(\frac{y\langle\Phi_\lambda\rangle}{\kappa\langle\Phi_\kappa\rangle}\right)^4, \tag{3.93}$$

where the first factor is the bound for standard type I seesaw due to strong washout from scattering as discussed earlier. We see that the second factor, which can be interpreted as a TeV-modulation effect, buys us extra freedom and allows to relax the usual upper bound of $10^{14} \sim 10^{15}$ GeV. Initial conditions for leptogenesis in this high temperature regime are discussed in section 3.5.2.5.

In order to illustrate successful leptogenesis for $M_{N_1} \gtrsim 10^{15}$ GeV, as a benchmark point we choose $M_{N_1} = 10^{16}$ GeV and $M_{N_2} = 3 \times 10^{16}$ GeV (shown in table 3.5). A choice of $\lambda \sim 0.5$ allows for N_1 decays and inverse decays to be in equilibrium around $T = M_{N_1}$ while keeping the off-shell scattering mediated by N's out of equilibrium. With this choice of parameters, high scale leptogenesis happens in the strong washout regime ($K_1 \approx 10$), and it generates a UV baryon asymmetry of $\sim 10^{-5}$. The washout at the TeV scale is then needed to dilute it down to the observed baryon asymmetry of $\sim 10^{-10}$. For this to happen we must have $K_\Psi^{\rm eff} \approx 27$.

M_{N_1} (GeV)	λ_2	$r = \frac{\lambda_1}{\lambda_2}$	$\frac{M_{N_2}}{M_{N_1}}$	$\langle\Phi_\lambda\rangle$ (TeV)	m_Ψ (TeV)	y	K_1	K_Ψ^{eff}	μ (keV)
10^{16}	0.5	1	3	400	3	0.05	10	27	5
10^{11}	0.04	0.3	3	20	8	0.1	30	0.2	6
10^7	0.01	0.001	20	4	20	0.2	0.6	0.03	15

Table 3.5: Three different benchmark points consistent with neutrino mass data and leptogenesis, organized by Majorana singlet mass scale.

This value of K_Ψ^{eff} can be obtained by a choice of $m_\Psi \sim 3$ TeV and $y \sim 0.05$, which is also consistent with the $\mu \to e\gamma$ bound. To get the observed neutrino mass with the chosen parameters, we then take $\langle\Phi_\lambda\rangle \sim 400$ TeV.[28]

Note that since we have not introduced any significant hierarchies in any of the mass or Yukawa matrices, we obtain an anarchic SM neutrino mass matrix in the SM flavor basis as is sufficient to fit to the observed neutrino masses and mixing angles.

3.6.2.2 Going below Davidson-Ibarra bound of $\sim 10^9$ GeV

At the other extreme we consider Majorana singlet masses below 10^9 GeV. In standard type I seesaw model, one can not have successful leptogenesis for singlet masses below 10^9 GeV unless one employs flavor effects or resonant leptogenesis which requires hierarchical parameters and/or new ingredients as discussed in section 3.3.3.3. This lower limit on the Majorana singlet mass is known as Davidson-Ibarra bound [40]. However, as shown in [54], the lower bound in hybrid seesaw is

[28] As discussed in section 3.4 and chapter 2, such a value for $\langle\Phi_\lambda\rangle$, i.e., $\gg$ TeV, can be "effectively" obtained with*out* any hierarchies in the *fundamental* parameters in the warped/composite UV completion of the hybrid model.

relaxed

$$M_N \gtrsim 10^{-7} \frac{8\pi v^2}{m_\nu} \left(\frac{y \langle \Phi_\lambda \rangle}{\kappa \langle \Phi_\kappa \rangle} \right)^2 \sim 10^9 \text{ GeV} \times \left(\frac{y \langle \Phi_\lambda \rangle}{\kappa \langle \Phi_\kappa \rangle} \right)^2 , \tag{3.94}$$

where the first factor is the Davidson-Ibarra lower bound for the case of standard type-I seesaw and the second factor is due to the TeV-modulation. Therefore, in our model we can have successful leptogenesis with Majorana singlet masses $\ll 10^9$ GeV , even if we ignore flavor effects and without any degeneracy between singlet masses. However, there exists another rather generic lower bound $M_N \gtrsim 10^5$ GeV. This is derived by the simultaneous requirements of large enough CP violation and small enough $\Delta = 2$ washout due to scattering. In order to see this more explicitly, we note that to suppress potentially dangerous washout by the $\Delta = 2$ scattering from the off-shell N_2 mediation, we need to impose its rate to be smaller than the Hubble rate at $T = M_{N_1}$. Using eq. (3.72) and (3.77) this gives us the following condition:

$$\begin{aligned} M_{N_1} &\gtrsim \frac{4}{\pi} \frac{\epsilon_1^2}{\sin^2(\phi_{12})} \frac{M_{\rm Pl}}{1.66\sqrt{g_\star}} \\ &= 8.5 \times 10^4 \frac{1}{\sin^2(\phi_{12})} \left(\frac{\epsilon_1}{10^{-7}} \right)^2 \sqrt{\frac{121.25}{g_\star}} \text{ GeV}. \end{aligned} \tag{3.95}$$

Hence we see that the requirement that the scatterings $\Phi_\lambda \Psi_a \leftrightarrow (\Phi_\lambda \Psi_a)^*$ be out of equilibrium set a lower bound on the mass of N_1 [97, 98]. The value $\epsilon \sim 10^{-7}$ is chosen because this is the minimum value of ϵ to get successful leptogenesis.

To achieve leptogenesis for the lowest value $M_{N_1} \sim 10^5$ GeV, we however need

a hierarchy in $\lambda_{1a}/\lambda_{2a}$. This can be seen by checking the allowed range of λ_{1a} and λ_{2a}. Since the value of ϵ_1 is already saturated to its minimum value for $M_{N_1} \sim 10^5$ GeV, we can not afford additional washout effects. As we saw in eq. (3.85), the maximum efficiency of the washout can be achieved if $K_1 \lesssim 1$, and this leads to

$$\begin{aligned} \left(\lambda\lambda^\dagger\right)_{11} &\lesssim 1.66\sqrt{g_\star}16\pi\frac{M_{N_1}}{M_{\rm Pl}} \\ &= 7.5\times 10^{-12}\sqrt{\frac{121.25}{g_\star}}\left(\frac{M_{N_1}}{10^5\,{\rm GeV}}\right). \end{aligned} \tag{3.96}$$

On the other hand, to have $|\epsilon_1| \gtrsim 10^{-7}$, from eq. (3.72), we require

$$\begin{aligned} \left(\lambda\lambda^\dagger\right)_{22} &\gtrsim 8\pi 10^{-7}\frac{M_{N_2}}{M_{N_1}}\frac{1}{|\sin\left(\phi_{12}\right)|} \\ &= 2.5\times 10^{-5}\left(\frac{M_{N_2}}{M_{N_1}}\frac{1}{10}\right)\frac{1}{|\sin\left(\phi_{12}\right)|}. \end{aligned} \tag{3.97}$$

The above estimation shows that to achieve leptogenesis for $M_{N_1} \sim 10^5$ GeV, we need $\lambda_{1a}/\lambda_{2a} \sim 5\times 10^{-4}$ (i.e. a small value of r),[29] but not among different generations of Ψ's.

The relaxation of the lower bound on the singlet Majorana masses, thus lowering the required reheating temperature of the Universe, may alleviate the gravitino overproduction problem [100–104] of SUSY models. Namely, for gravitino masses (SUSY breaking scale) $\sim$ TeV (which is the "natural" range), we typically need reheating temperatures below $\sim 10^9$ GeV in order to avoid BBN bounds from excessive late decays of (very weakly-coupled) gravitinos [105, 106]. In the usual type

[29] As discussed in [54], with the choice of *anarchic* parameters instead, we can only go down to $M_N \sim 10^{11}$ GeV.

I seesaw model, this might be in tension with leptogenesis.

We now present a specific choice of parameters consistent with leptogenesis for Majorana singlet mass $M_{N_1} \sim 10^7$ GeV (see table 3.5). We choose $\lambda_1 \sim 10^{-5}$ such that we get $K_1 \sim 1$ in order to optimize the efficiency factor η. As already mentioned, we need to allow for a hierarchy between the Yukawa couplings of N_1 and N_2, which we choose to be $r = \frac{\lambda_1}{\lambda_2} \sim 10^{-3}$ corresponding to $\lambda_2 \sim 0.01$. This provides an enhancemnet in the UV asymmetry by a factor of $\frac{1}{r^2} \sim 10^6$, compared to the anarchic ($r = 1$) case (see T5 in table 3.4), which is enough to account for the observed asymmetry. Note that with $\lambda_2 \gg \lambda_1$, the decay rate of N_2 is much larger than the Hubble rate, and so washout from inverse decay of N_2 can be potentially dangerous for leptogenesis. However, since at temperatures below the mass of N_2, the rate for this inverse decay is Boltzmann suppressed, a small hierarchy between M_{N_2} and M_{N_1} is sufficient for N_2 inverse decay to be out of equilibrium at $T \approx M_{N_1}$. The condition we demand is

$$e^{-\frac{M_{N_2}}{M_{N_1}}} < \frac{\Gamma_{N_1}}{\Gamma_{N_2}} \sim r^2. \tag{3.98}$$

We choose $M_{N_2} \approx 20 M_{N_1}$ as our benchmark value which gives a Boltzmann suppression of $e^{-20} \sim 10^{-9} \ll r^2$. With the chosen values for M_{N_2} and λ_2, washout from off-shell scattering, mediated by N_2, is out of equilibrium when asymmetry generation happens. A choice of $m_\Psi \sim 20$ TeV and $y \sim 0.2$ would result in weak washout at the TeV scale ($K_\Psi^{\text{eff}} \sim 0.03$) and is consistent with the $\mu \to e\gamma$ bound. We then can pick $\langle \Phi_\lambda \rangle = 3$ TeV to obtain the right SM neutrino mass scale.

One might worry that with the hierarchies introduced it may not be possible to obtain a relatively anarchic SM neutrino mass matrix. We should however note that even though we are discriminating different N generations (labeled by $i, j, ...$), we are not introducing any hierarchies distinguishing different Ψ families (labeled by $a, b, ...$) or SM lepton flavors (labeled by $\alpha, \beta, ...$), and this results in an anarchic SM neutrino mass matrix in the flavor basis. Still, in the limit of $r \to 0$ the rank of the λ matrix is reduced by one. This in turn reduces the rank of μ and SM neutrino mass matrices. So in order to have a realistic neutrino mass matrix in scenarios with small r, we need to consider at least three generations of N_i. We take N_3 to have Yukawa couplings comparable to those of N_2. Choosing M_{N_3} larger than M_{N_2} by a factor of a few ensures that contributions of N_3 to the CP asymmetry and to off-shell scattering washout are subdominant compared to those of N_2. Note that this scenario with small $r \sim 10^{-3}$ and three generations of N results in one of the SM neutrino mass eigenvalues being much smaller than the other two, by a factor of $\sim r^2 \sim 10^{-6}$. Such a small mass for the lightest neutrino mass eigenstate is of course consistent with the current neutrino data.

3.6.2.3 Intermediate scales: $\sim 10^9 - 10^{15}$ GeV

The region of parameter space with $M_N \sim 10^9 - 10^{15}$ GeV works in our model as well as in the usual type I case. An example of a working point is presented, for $M_N \sim 10^{11}$ GeV, in table 3.5. No hierarchies in the Yukawa or mass matrices nor small Yukawa coupling are needed for this case.[30] For the presented benchmark

[30] As mentioned in footnote 29, this is the smallest value of M_N which works with anarchy.

point, the asymmetry in the UV is generated in strong washout regime ($K_1 \sim 30$) and the washout at the TeV scale is negligible ($K_\Psi^{\rm eff} \sim 0.2$).

Chapter 4: Fast phase transition in Randall-Sundrum models

4.1 Introduction

As illustrated in the previous chapters, the RS/CH model is an attractive solution to the Planck-EW hierarchy problem and could allow further modifications to address neutrino mass and baryon asymmetry problems, like warped/composite seesaw mentioned above. Most of the analysis related to warped/composite seesaw is done in the zero temperature limit, which is sufficient to study SM neutrino mass. However, as shown in chapter 3 based on simplified hybrid seesaw, the dynamics at high temperature $T \gg$ TeV is necessary to achieve successful leptogenesis. Therefore, in order to study leptogenesis in full warped/composite seesaw, it is also crucial to understand high temperature behavior, as well as cosmological evolution of the model. In this chapter, we will focus on one important stage of the early cosmological evolution of warped/composite seesaw (or general RS/CH models)—the phase transition (PT).

It is known that at sufficiently high temperature, the strongly coupled sector of CH models is in a deconfined phase, similar to high temperature quark gluon phase of QCD [21]. Whereas at low temperature, it undergoes confinement and composite states (e.g. SM Higgs) are generated, similar to the low temperature

hadron phase of QCD. So this class of models features a deconfined to confined PT. Due to the non-perturbative nature of such phase transition, it is extremely hard to determine the nature of the transition (i.e. first or second order PT or cross-over), as well as the transition rate. Taking QCD as an example, although we know its the group structure and the fermion content very well, we only get some sense of its cosmological PT with the help of non-perturbative lattice calculation [107–110]. It seems almost impossible to understand the PT in CH models since we have no clue of its UV dynamics.

Remarkably, as mentioned earlier, the strongly coupled 4D theory with conformal symmetry is dual to a weakly coupled 5D AdS spacetime including gravity according to AdS/CFT duality. This opens a window to study some non-perturbative physics of 4D CH models using analytic 5D calculations. It is known that the high temperature deconfined phase of 4D CH model is dual to a large black hole configuration in 5D AdS described by the AdS-Schwarzschild (AdS-S) geometry [111], with a UV brane. While the low temperature RS phase has both UV and IR branes. The free energy of these two phase can be calculated analytically and we can robustly argue that the phase transition is *first order* (see section 4.2). The phase transition occurs by bubble nucleation and the rate can be estimated by the Euclidean 4D bounce action. Since the low temperature RS phase has a IR brane, the bounce configuration should capture the feature that the IR brane "emerges" from the black hole horizon. As discussed in ref. [112], one ansatz of such bounce is the horizon moving to AdS boundary and then a IR brane emerging from the boundary to the equilibrium place. The authors of ref. [112] calculated the bounce action of this

ansatz and derived the phase transition rate per unit volume Γ:

$$\Gamma \sim T^4 e^{-cN^2/\epsilon^\alpha}, \tag{4.1}$$

where T is the temperature of the universe and ϵ is the 5D mass of GW scalar in units of AdS curvature k (or the anomalous dimension of the dual 4D CFT operator). It is assumed that the dual CFT theory has a $SU(N)$ gauge structure and thus N is related to 5D Planck mass M_5 as $N^2/(16\pi^2) = (M_5/k)^3$. c is an order one factor and the power α is model dependent but generally order unity. Since the Planck-EW hierarchy is also controlled by ϵ (see eq. (1.1)), it is straight forward to show that this transition rate is too slow compared to Hubble expansion at the critical temperature T_c (defined in section 4.2) for large N (required by the validity of 5D EFT) and $\epsilon = O(0.1)$ (required by achieving Planck-EW hierarchy in the standard GW mechanism). Later, it was realized that the phase transition rate goes up as the temperature goes down, and the transition could complete but the temperature where the nucleation happens is much smaller than T_c, thus called supercooling [113–118]. Allowing supercooling enlarges the controlled parameter space of the 5D model, but the universe is stuck in the false vacuum before transition starts, whose vacuum energy density dominates the universe and drives the low scale inflation. All pre-existing abundance will be exponentially diluted and thus the asymmetry generated from high scale, e.g. leptogenesis of our warped/composite seesaw, will be negligible today if the universe supercools.

A faster phase transition rate can be achieved for a larger ϵ in eq. (4.1) .

Since ϵ is the anomalous dimension of the $\mathcal{O}_{\rm GW}$, ϵ may not be a constant but can grow from UV to IR if there is a non-trivial RG equation (RGE) for $\mathcal{O}_{\rm GW}$. The relevant ϵ entering eq. (4.1) is at the scale of phase transition, which can be very different from that at the UV scale, and thus both large hierarchy and fast phase transition can be simultaneously obtained [118,119].[1] In section 4.4 of this chapter, we propose a general modification of the standard stabilization mechanism where the deformation of CFT $\mathcal{O}_{\rm GW}$ has both UV and IR fixed points. In our model, the anomalous dimension of this deformation near UV fixed point (denoted as ϵ) controls the large hierarchy between UV scale and confinement scale, whereas the phase transition rate is determined by the anomalous dimension near IR fixed point (denoted as ϵ'). Thus a fast phase transition near the critical temperature and a large Planck-EW hierarchy can be realized if $\epsilon \ll \epsilon' \lesssim 1$. In this case, leptogenesis along the lines of chapter 3 will be successful due to no dilution of the primordial asymmetry after the phase transition.

However, the estimation of the bounce action and phase transition rate in [112] assumes $\epsilon' \ll 1$, which may not be directly applicable to models with $\epsilon' \lesssim 1$. The reason is that such an ansatz always involves a region where temperature is higher than the IR brane scale and thus KK particles or even physics above the 5D UV cutoff must be considered. This region may have negligible contribution to the bounce action for $\epsilon' \ll 1$, but in general it is not true for $\epsilon' \lesssim 1$. We then propose a new ansatz of the bounce in section 4.3: the deconfined phase is the usual AdS-S

[1] There are also other ways to reduce the bounce action and enhance the transition rate (see, for example, [120–123]).

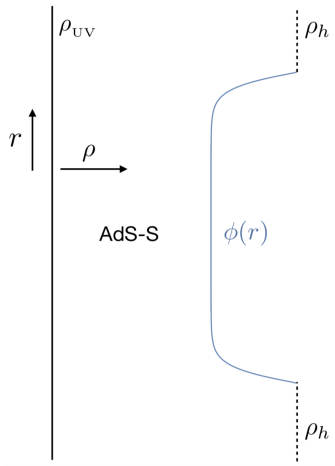

Figure 4.1: The ansatz of the bubble configuration in 5D. The bulk geometry is AdS-S everywhere and the black solid (dashed) line indicates the position of the UV brane scale $\rho_{\rm UV}$ (horizon ρ_h). The deconfined phase is outside of the bubble, where it is purely AdS-S. Inside the bubble (the confined phase), $\phi(r)$ cuts off the spacetime and smoothly connects to ρ_h at the end of the bubble.

geometry with a horizon, while the confined phase is now modeled as the AdS-S geometry in the bulk with an IR brane cutting off the spacetime in front of the horizon. This is also a solution of the background Einstein equation and can reduce to RS configuration if the IR brane is much away from the horizon. In our ansatz, the dynamical IR brane moves from the equilibrium position to the horizon (see figure 4.1),where the full bounce configuration is smooth and can be calculated within the 5D EFT even for $\epsilon' \lesssim 1$. We also demonstrate that this ansatz can set a robust bound on the phase transition rate. Furthermore, we briefly discuss the phenomenological signals of our model in section 4.6. Our model predicts an interesting correlation between the radion mass, which may be probed at colliders, and the amplitude and frequency of stochastic gravitational waves from the phase transition, which may be probed by e.g. Laser Interferometer Space Antenna (LISA) experiment [124].

4.2 4D Equilibrium description of the two phases

We can understand some qualitative features of the PT by studying it from a 4D perspective. In particular, we can estimate the critical temperature of the PT as follows.

We model the deconfined phase as a $SU(N)$ gauge theory at a temperature T. Since there are N^2 degrees of freedom in the thermal bath, we can write quite generally,

$$F_{\text{deconfined}} \equiv E - TS = -CN^2T^4, \tag{4.2}$$

where $E\,, S\,, T$ is the energy density, entropy density and temperature of the thermal bath respectively and C is some $\mathcal{O}(1)$ constant that can be determined once the CFT is explicitly specified.

At low enough temperature the QFT can potentially confine giving rise to massive, hadronic states. Quite generally, there can also exist a (almost) massless degree-of-freedom (d.o.f) in the confined phase—the Goldstone boson corresponding to spontaneous breaking of scale symmetry, namely the dilaton. At temperatures parametrically smaller than the confinement scale, it is sufficient to consider the dilaton as the only dynamical d.o.f in the EFT.

For phenomenological viability, the dilaton has to have a mass which can be achieved by having a (small) explicit breaking of scale invariance in the "CFT". This can be done by deforming the CFT by an operator $\Delta\mathcal{L}_{\text{CFT}} = g\mathcal{O}$. Such a

deformation will result in an effective potential for the dilaton μ [125, 126]:

$$V_{\text{eff}} = \lambda\left(g(\mu)\right)\mu^4, \tag{4.3}$$

where the explicit breaking is characterized by the "running" quartic coupling $\lambda\left(g(\mu)\right)$. For small deformation g, we can expand the beta function as $\beta(g) \equiv \frac{dg}{d\ln\mu} \approx \epsilon g$. The solution the above RGE is given by,

$$g(\mu) = g_0\left(\frac{\mu}{\Lambda_{\text{UV}}}\right)^{\epsilon}, \tag{4.4}$$

where g_0 is the deformation at scale Λ_{UV}. Thus the deformation corresponds to the operator $\mathcal{O}$ having a scaling dimension $4+\epsilon$. The potential for radion then becomes (up-to first order in g),

$$V_{\text{eff}} = \left(\lambda(0) + \lambda'(0)g_0\left(\frac{\mu}{\Lambda_{\text{UV}}}\right)^{\epsilon}\right)\mu^4, \tag{4.5}$$

where $\lambda(0) = \lambda(g=0)$, and $\lambda'(0) = \frac{d\lambda}{dg}|_{g=0}$. The above potential has a minimum at $\langle\mu\rangle = \Lambda_{\text{UV}}\left(-\frac{\lambda(0)}{\lambda'(0)g_0}\right)^{\frac{1}{\epsilon}}$. A large hierarchy between $\langle\mu\rangle$ and Λ_{UV} can be obtained for small ϵ. It will be convenient to re-express the dilaton potential in terms of $\langle\mu\rangle$,

$$V_{\text{eff}} = \lambda(0)\mu^4\left(1 - \frac{1}{1+\epsilon/4}\left(\frac{\mu}{\langle\mu\rangle}\right)^{\epsilon}\right). \tag{4.6}$$

According to the dilaton EFT, this effective potential gives the free energy of the confined phase i.e. $F_{\text{confined}} \underset{T\ll\mu}{\approx} V_{\text{eff}}(\mu)$.

Having estimated the free energies of the two phases, we can now calculate the temperature at which they become equal, namely the critical temperature for the PT, T_c:

$$\begin{aligned} F_{\text{deconfined}}(T_c) &= V_{\text{eff}}(\langle\mu\rangle) \\ \Rightarrow \frac{T_c}{\langle\mu\rangle} &= \left(\frac{\epsilon\lambda(0)}{C(4+\epsilon)N^2}\right)^{1/4}. \end{aligned} \tag{4.7}$$

We see that T_c is self-consistently and parametrically smaller than $\langle\mu\rangle$ for small ϵ and(or) small $\bar{\lambda}$. This justifies the effective description of the confined phase involving only the dilaton. Furthermore, the above fact indicates that at the temperature T_c we can have a simultaneous existence of both the confined and the deconfined phase, and thus the PT under consideration is first order in nature. As will be explained below, T_c is *not* suppressed compared to $\langle\mu\rangle$ by N, contrary to what eq. (4.7) might indicate at first sight.

We can also *estimate* the rate of PT from the 4D perspective. A cosmological PT completes when the bubble nucleation rate per unit volume, Γ, gets bigger than H^4 where H is the Hubble scale. For $T \leq T_c$, H roughly remains constant (being dominated by the cosmological constant corresponding to the false vacuum) and is given by $H^2 \sim \frac{N^2 T_c^4}{M_{\text{pl}}^2}$. Γ can be computed in terms of the Euclidean bounce action S_E as,

$$\Gamma \sim T^4 e^{-S_E}. \tag{4.8}$$

Thus for the PT to complete one needs roughly $S_E < 4\ln\left(\frac{M_{\text{Pl}}}{T_c}\right) \sim 140$. Given this

stringent constraint, to really answer the question whether the PT completes or not, we need to calculate the bounce action S_E precisely. This is difficult to do within a 4D framework since the 4D theory under consideration is strongly coupled. Thus to make progress, we will now utilize the AdS/CFT duality and consider the 5D dual of the entire set-up considered so far.

4.3 5D geometry and the structure of the bounce

The 5D dual of the confined phase corresponds to an RS geometry at finite temperature with a UV and an IR boundary. The dual of the deconfined phase corresponds to a AdS-S geometry with a UV boundary and a horizon (instead of a IR boundary) cutting off the extra-dimension. To compute the bounce action from 5D, in principle, one has to look for a solution of the 5D Einstein equations which smoothly interpolates between the two above mentioned geometries. Although it is a mathematically well-posed question, finding the true solution is difficult in practice. Instead, we will identify the dynamical degrees of freedom for the two phases and make an *ansatz* about the 5D geometry of the bounce. Although our ansatz may not be the true bounce solution, we will argue later that,

$$S_{\text{ansatz}}^{\text{thin wall}} > S_{\text{true}}^{\text{thin wall}}. \tag{4.9}$$

Along with a lower bound on $S_{\text{true}}^{\text{thin wall}}$ that we will derive below, this will enable us to estimate $S_{\text{true}}^{\text{thin wall}}$ reliably in some part of our parameter space.

To this end, we now describe 5D geometry of our ansatz. The dual of the

deconfined phase is described by the 5D metric,

$$ds^2 = -\left(\rho^2 - \frac{\rho_h^4}{\rho^2}\right) dt^2 + \frac{d\rho^2}{\rho^2 - \frac{\rho_h^4}{\rho^2}} + \rho^2 \sum_i dx_i^2, \tag{4.10}$$

where $\rho_{\rm UV} > \rho > \rho_h$ with $\rho_{\rm UV}(\rho_h)$ being the position of the UV brane (horizon). The AdS curvature has been set to 1.The confined phase can be described by the same geometry but with an IR boundary cutting off the extra dimension so that $\rho_{\rm UV} > \rho > \phi$ where ϕ denotes the location of the IR boundary. There is another solution of the Einstein equation with two branes at finite temperature: RS configuration with time compactified. This is often used as the dual of the confined phase. These two solutions are approximate the same when $\phi \gg \rho_h$.

To have a smooth geometry describing the bounce, we promote ϕ to be a function $\vec{r}$ such that it interpolates between some value $> \rho_h$ inside the bubble to $\phi = \rho_h$ outside. We can then calculate the action for ϕ using the 5D action:

$$\begin{aligned} S = S_{\rm GR} + S_{\rm GW} &= 2M_5^3 \int_\phi^\Lambda dy \int d^4x \sqrt{-g}\,(R_5[g] + 12) \\ &+ 4M_5^3 \int d^4x \sqrt{-\gamma} K - 12 M_5^3 \int d^4x \sqrt{-\gamma} + S_{\rm GW}, \end{aligned} \tag{4.11}$$

where $K = g^{\mu\nu} K_{\mu\nu}$ is the trace of the extrinsic curvature $K_{\mu\nu}$ of the IR boundary. In the above, the boundary terms are present for both the UV ($\rho = \rho_{\rm UV}$) and the IR ($\rho = \phi$) boundaries and, to avoid clutter, we have used γ to denote induced metrics on both of them. $S_{\rm GW}$ denotes the action of a Goldberger-Wise (GW) field that stabilizes the extra dimension.

We start by evaluating $S_{\rm GR}$. By $O(3)$ symmetry we expect the action to be a function of the $r = |\vec{x}|$ only. To calculate the extrinsic curvature K, we need the normal to the surface $\rho = \phi(r)$,

$$n_\mu = \left(\frac{\rho^2}{\rho^4 - \rho_h^4 + \phi'^2}\right)^{1/2} (0, -\phi', 0, 0, 1). \tag{4.12}$$

Then induced metric on that surface is given by,

$$ds^2_{\rm ind} = -\left(\frac{\rho^2}{L^2} - \frac{\rho_h^4}{\rho^2 L^2}\right) dt^2 + \left(\rho^2 + \frac{\phi'^2}{\rho^2 - \frac{\rho_h^4}{\rho^2}}\right) dr^2 + \rho^2(r^2 d\theta^2 + r^2 \sin^2\theta d\phi^2). \tag{4.13}$$

From the above the trace of the extrinsic curvature and the determinant of the induced metric can be calculated as,

$$\sqrt{\gamma} = r^2 \sin\theta \phi^2 \left(\phi^4 - \rho_h^4 + \phi'^2\right)^{1/2}, \tag{4.14}$$

$$\begin{aligned}\sqrt{\gamma} K = r^2 \sin\theta &\frac{1}{\phi^4 - \rho_h^4 + \phi'^2} \times \\ &[2\phi(\rho_h^4 - \phi^4)\frac{\phi'}{r} + (6\phi^4 - 2\rho_h^4)\phi'^2 - 2\phi\frac{\phi'^3}{r} \\ &+ (\phi^4 - \rho_h^4)(4\phi^4 - 2\rho_h^4 - \phi\phi''(r))].\end{aligned} \tag{4.15}$$

Given the Goldberger-Wise action, $S_{\rm GW} = \int_\phi^\Lambda dy \int d^4x \left(\frac{1}{2}(\partial\Psi)^2 - \frac{1}{2}M^2\Psi^2\right)$, we can evaluate its contribution to the effective action for ϕ by solving for the extra-dimensional profile of Ψ and substituting that back into $S_{\rm GW}$. We propose an ansatz to calculate $S_{\rm GW}$: first, we will ignore the backreaction of Ψ on the background AdS-

S geometry eq. (4.10) and second, we will make the simplifying assumption that Ψ lives in an AdS geometry as opposed to the actual AdS-S geometry. In this ansatz, the effective contribution of $S_{\rm GW}$ yields the standard result which has the same form as eq. (4.6) (with $\mu = \phi$), where $\lambda = \bar{\lambda}\frac{3}{4\pi^2}N^2$ and $\frac{3}{4\pi^2}N^2$ is upper limit for $\lambda(0)$ demanding the small back reaction to the 5D geometry. A larger $N^2 \equiv \frac{M_5^3}{16\pi^2}$ denotes a better control of the effective GR description of the 5D physics. In passing, we note that using the value of λ and $C = \frac{\pi^2}{8}$, which follows from 5D, we can rewrite eq. (4.7) as,

$$\frac{T_c}{\langle\mu\rangle} = \left(\frac{12\epsilon\bar{\lambda}(0)}{\pi^4(4+\epsilon)}\right)^{1/4}. \tag{4.16}$$

From the above we finally get the effective action for ϕ,

$$\begin{aligned} S_\phi =& \frac{4\pi}{T}\int dr r^2 \Bigg[2M_5^3 \Big(\frac{2}{\phi^4 - \rho_h^4 + \phi'^2}\Big[2\phi(\rho_h^4 - \phi^4)\frac{\phi'}{r} + (6\phi^4 - 2\rho_h^4)\phi'^2 - 2\phi\frac{\phi'^3}{r} \\ &+ (\phi^4 - \rho_h^4)(4\phi^4 - 2\rho_h^4 - \phi\phi'')\Big] + \rho_h^4 - 2\phi^4 - 6\phi^2\left(\phi^4 - \rho_h^4 + \phi'^2\right)^{1/2}\Big) + V_{\rm eff}(\phi)\Bigg]. \end{aligned} \tag{4.17}$$

where $V_{\rm eff}(\phi)$ is the dilaton potential given in eq. (4.6).

The 5D bounce is then specified by a solution $\phi(r)$ to the equation of motion that follows from the above action and we show such an example in fig. 4.1.

For the present ansatz the 5D geometry, as required, is smooth everywhere by construction except the potentially problematic region where the IR boundary merges into the AdS-S horizon. To see whether this merging is smooth, we can

evaluate the induced metric in the near-horizon region by writing $\phi(r) = \rho_h(1 + \delta\phi(r))$. Assuming $\rho_h^2\delta\phi \ll \phi'^2$, we get

$$\begin{aligned} ds^2_{\text{ind}} =& 4\rho_h^2\delta\phi dt^2 + \frac{\phi'^2}{4\rho_h^2\delta\phi}dr^2 \\ =& 4\rho_h^2 y^2 dt^2 + dy^2 \end{aligned} \tag{4.18}$$

where we have made a variable change $y = \sqrt{\delta\phi}$. This is same as the metric of 2D flat space (with correct time periodicity). The choice of $\rho_h^2\delta\phi \ll \phi'^2$ is guaranteed by a fall off $\delta\phi(\delta r) \sim \delta r^n$ with $n < 2$. We also note that just the assumption of $\rho_h^2\delta\phi \ll \phi'^2$ is not enough to render the radion action finite. We first note the near horizon behavior of $\sqrt{\gamma}$ and K:

$$\sqrt{\gamma} = r^2 \sin\theta \rho_h^2 \delta\phi' \tag{4.19}$$

$$K \sim \frac{1}{\sqrt{\gamma}} \sim \frac{1}{\delta\phi'}. \tag{4.20}$$

So for $\delta\phi \sim \delta r^n$ behavior we need $0 < n < 1$ to ensure a finite radion action.

4.3.1 Phase transition in thin-wall regime

We can numerically solve the equation of motion following from eq. (4.17) and plug the solution back into eq. (4.17) to obtain the bounce action and hence the rate of the PT. However in the thin wall regime, namely when $T_n \approx T_c$, one can obtain an analytical expression for the transition rate if $\epsilon \ll 1$ or $\bar{\lambda} \ll 1$. Under such an approximation, $\rho_h \ll \langle\mu\rangle$, as follows from eq. (4.16), and most of the bounce action

is determined by the radion/dilaton potential. To see this more explicitly, we take the limit of $\phi \gg \rho_h$ and $\phi' \ll \phi^2$ of the effective action (4.17) to get,

$$S_\phi \approx \frac{4\pi}{T} \int dr r^2 \Big[6M_5^3 \phi'^2 + V_{\text{eff}}(\phi) \Big]. \tag{4.21}$$

The above is the standard dilaton/radion potential that follows in the presence of a stabilized RS geometry. Under this approximation of radion dominance,

$$S_{3,\text{true}} \geq S_{3,\text{radion dominance}}. \tag{4.22}$$

This is because the true bounce action might involve contributions of degrees of freedom *additional* to the radion and such contributions can only make the bounce action bigger, i.e. the radion dominance ansatz underestimates the bounce action. For an $O(3)$ symmetric bounce solution, the bounce action can be rewritten quite generally as,

$$\frac{S_3}{T} = \frac{16\pi}{3} \frac{S_1^3}{(\Delta F)^2 T}, \tag{4.23}$$

where ΔF is the difference of the free energy in two phases and S_1 is given by,

$$\begin{aligned} S_1 \equiv \int dr \Bigg[2M_5^3 \Big(& \frac{2}{\phi^4 - \rho_h^4 + \phi'^2} \Big[(6\phi^4 - 2\rho_h^4)\phi'^2 + (\phi^4 - \rho_h^4)(4\phi^4 - 2\rho_h^4 - \phi\phi'') \Big] \\ & + \rho_h^4 - 2\phi^4 - 6\phi^2 \left(\phi^4 - \rho_h^4 + \phi'^2 \right)^{1/2} \Big) + V_{\text{eff}}(\phi) \Bigg] \\ \overset{\epsilon \text{ and/or } \bar{\lambda} \ll 1}{\approx} & \int_{\rho_h}^{\langle \mu \rangle} d\tilde{\phi} \sqrt{2V_{\text{eff}}(\tilde{\phi})}, \end{aligned} \tag{4.24}$$

where $\tilde{\phi}$ is the canonically normalized field. Such a form of S_1, with a potential $V_{\text{eff}}(\tilde{\phi})$ that is bounded from below, implies that extremizing the bounce action is equivalent to *minimizing* the bounce action. Hence this implies, $S_{1,\text{ansatz}} < S_{1,\text{true}}$ and equivalently, eq. (4.9). Then combining eqs. (4.9) and (4.22) and using the fact that $S_{\text{ansatz}} \approx S_{\text{radion dominance}}$, we get a reliable estimate of the true bounce action.

Under the approximations mentioned above, we calculate the bounce action:

$$\frac{S_3}{T} \approx 16 \left(\frac{8}{3}\right)^{1/4} \left(\frac{(1+\epsilon/4)}{\bar{\lambda}\epsilon}\right)^{\frac{3}{4}} \times N^2 \frac{T_c/T}{\left(1-(T/T_c)^4\right)^2}. \tag{4.25}$$

The RHS is a function of temperature and is minimized at $T = \frac{T_c}{\sqrt{3}}$ so that,

$$\frac{S_3}{T} > 45 \left(\frac{(1+\epsilon/4)}{\epsilon}\right)^{\frac{3}{4}} \frac{N^2}{\bar{\lambda}^{3/4}}. \tag{4.26}$$

Using $\epsilon = 1/20$, as to ensure a correct Planck-Weak hierarchy, and $\bar{\lambda} = 1$, this gives the upper bound $N < 1$ for a viable bounce. For theoretical control of the 5D EFT we need $N > 1$ and for such cases the PT does not complete. Staying within the regime of small backreaction (i.e. $\bar{\lambda} \lesssim 1$), looking at eq. (4.26) we are lead to the conclusion that one way of ensuring a smaller bounce action is to increase the value of ϵ. However, since $\epsilon = 1/20$ gives the correct electroweak hierarchy, the challenge is to increase ϵ that appears in (4.26) while still maintaining the correct value of the hierarchy.

4.4 A non-trivial RG flow between a UV and an IR fixed point

Earlier in eq. (4.3) we approximated the beta function as $\beta(g) \approx \epsilon g$ where we were expanding the coupling constant around the trivial fixed point $g = 0$. However, another interesting possibility arises if g flows into a nontrivial IR fixed point (F.P.) at $g = g_\star$. Such a RGE having two F.P.s takes the following general form:

$$\frac{dg}{d\ln\mu} = \beta_g(g) = -g(g_\star - g)f(g) \tag{4.27}$$

where $f(g)$ is a function that is positive at both F.P.s and has no zeros between $g = 0$ and $g = g_\star$. Expanding around the UV and the IR F.P.s we get, respectively,

$$\frac{d\ln g}{d\ln\mu} \approx -\epsilon \quad \text{near UV F.P. } (g = 0) \tag{4.28}$$

$$\frac{d\ln(g_\star - g)}{d\ln\mu} \approx \epsilon' \quad \text{near IR F.P. } (g = g_\star) \tag{4.29}$$

where $\epsilon = g_\star f(0)$ and $\epsilon' = g_\star f(g_\star)$. The RGE solutions near the IR and the UV F.P.s are respectively

$$g = g_0 \left(\frac{\mu}{\Lambda_{\text{UV}}}\right)^{-\epsilon} \quad \text{near UV F.P.,} \tag{4.30}$$

$$g = g_\star - \left(\frac{\mu}{\Lambda_{\text{IR}}}\right)^{\epsilon'} \quad \text{near IR F.P..} \tag{4.31}$$

The above solutions captures the running of $g(\mu)$ which takes a value g_0 at the UV scale Λ_{UV} and grows in the IR (we will choose $\epsilon > 0$). Around a "matching" scale

$\Lambda_{\rm IR}$ the coupling transitions from the basin of attraction of the UV F.P. to that of the IR F.P. and thus, the above solutions (4.30) are valid everywhere except for a narrow range around $\Lambda_{\rm IR}$. This matching scale is can be estimated in terms of the UV parameters by,

$$\frac{\Lambda_{\rm IR}}{\Lambda_{\rm UV}} \sim \left(\frac{g_\star}{g_0}\right)^{\frac{1}{\epsilon}}, \tag{4.32}$$

and hence for small values of ϵ and $g_0/g_\star$, it is exponentially smaller than the UV cutoff.

The μ-dependence of λ near the two F.P.s are given by:

$$\lambda(\mu) = \begin{cases} \lambda(0) + \lambda'(0) g_0 \left(\frac{\mu}{\Lambda_{\rm UV}}\right)^{-\epsilon} + \cdots & \text{near the UV F.P.,} \\ \lambda(g_*) - \lambda'(g_*) g_* \left(\frac{\mu}{\Lambda_{\rm IR}}\right)^{\epsilon'} + \cdots & \text{near the IR F.P.,} \end{cases} \tag{4.33}$$

[2] We see for $\lambda(g_*), \lambda'(g_*) g_* < 0$ and $|\lambda(g_*)| < |\lambda'(g_*) g_*|$ the dilaton potential can have a minima at

$$\langle \mu \rangle \sim \Lambda_{\rm IR} \left(-\frac{\lambda(g_*)}{\lambda' g_*}\right)^{1/\epsilon'}. \tag{4.34}$$

Combining this with the previous estimate of $\Lambda_{\rm IR}$ given in eq. (4.32) we get,

$$\langle \mu \rangle \sim \Lambda_{\rm IR} \left(-\frac{\lambda(g_*)}{\lambda' g_*}\right)^{1/\epsilon'} \sim \Lambda_{\rm UV} \left(\frac{g_\star}{g_0}\right)^{\frac{1}{\epsilon}} \left(-\frac{\lambda(g_*)}{\lambda' g_*}\right)^{\frac{1}{\epsilon'}}. \tag{4.35}$$

Thus for $1 > \epsilon' \gg \epsilon$, $\langle \mu \rangle$ is not too far below $\Lambda_{\rm IR}$ and the Planck-weak hierarchy is still guaranteed by the smallness of ϵ as in before. We can rewrite the potential

[2] Note that in the case of $\lambda_{IR} < 0$ which is needed to stabilize the dilation near the IR F.P., the F.P. CFT may not stand on its own, and the CFT+ deformation should be consider together as an EFT.

in terms of $\langle\mu\rangle$ using the parameters at the IR F.P.,

$$V_{\rm eff}(\mu) = \lambda(g_*)\left(1 - \frac{1}{1+\epsilon'/4}\left(\frac{\mu}{\langle\mu\rangle}\right)^{\epsilon'}\right)\mu^4 \tag{4.36}$$

This has the identical form as the potential in eq. (4.6) except the proximity to the IR F.P. has replaced ϵ with ϵ' and correspondingly the bounce action for the thin-wall transition becomes parametrically smaller. This allows for the PT to complete for parametrically larger N in the the thin-wall regime. In particular, one can get the numerical result of S_1 from the first line of eq. (4.24) and show that, using $\epsilon' = 0.5, \bar{\lambda} = 0.5$, the PT can complete for $N \lesssim 2$. Although this is a parametric improvement, it shows even for slightly larger values of N, the PT does not complete in the thin-wall regime and thus one has to go over to the thick-wall regime.

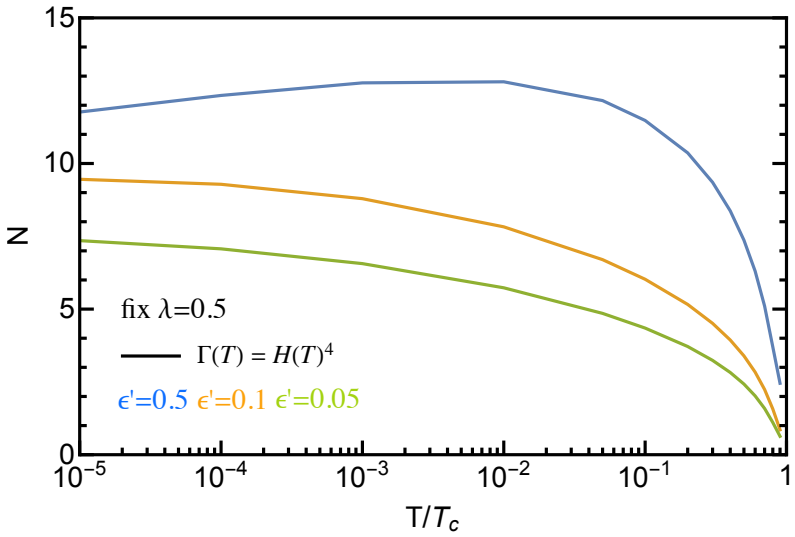

Figure 4.2: The contour plot for $\Gamma = H^4$ in N and T/T_c plane with fixed $\bar{\lambda} = 0.5$ and different ϵ'

4.5 Phase transition in thick wall regime

There is another limit $T \ll T_c$ where we can have an analytic estimation of the bounce (usually referred as the thick-wall approximation [127]). For $\lambda \ll 1$, the relevant scale for the bounce ϕ_r can be estimated as the scale where the free energy of the two phases are equal

$$\frac{3}{4\pi^2}\bar{\lambda}(\phi_r)\phi_r^4 \sim \frac{\pi^2}{8}T^4. \tag{4.37}$$

It is clear from the above equation that $\phi_r \gg T$ for $\lambda \ll 1$. Together with assumption $\phi' \ll \phi^2$, the action in Eq. (4.17) can be reduce to standard radion potential in Eq. (4.21). The $O(3)$ symmetry action in this case can then be approximated as

$$S_B \sim \frac{N^2}{\bar{\lambda}(\phi_r)^{3/4}}. \tag{4.38}$$

In order to complete the phase transition, the following inequality needs to be satisfied at some temperature: (see Eq. (4.1))

$$S_B/4 + \ln\frac{T_c}{T} \leq \ln\frac{M_{\rm Pl}}{T_c}. \tag{4.39}$$

To see if for a given set of parameters the phase transition completes, one can minimize the left hand side of the above inequality and then compare the minimum with the right hand side. The boundary of the parameter space where the phase transition completes is obtained by equating the minimum of this equation to RHS.

This boundary gives the maximum N for a given ϵ' and $\bar{\lambda}(0)$ for which the phase transition completes.

The left-hand side of Eq. (4.39) is minimized at T given by

$$\ln \frac{T_c}{T} \sim \frac{1}{\epsilon'} \ln \frac{\epsilon' N^2}{4\bar{\lambda}(0)^{3/4}}, \tag{4.40}$$

where we have used the approximation $\frac{\phi_r}{\langle\phi\rangle} = \left(\frac{4+\epsilon'}{\epsilon'}\right)^{1/4} \frac{T}{T_c}$.Then we get the following parametric dependence for $N_{\max}$:

$$\frac{N_{\max}^2}{4\bar{\lambda}(0)^{3/4}} \approx \ln \frac{M_{\rm Pl}}{T_c} - \frac{1}{\epsilon'} \ln \left(\epsilon' \ln \frac{M_{\rm Pl}}{T_c} \right) \tag{4.41}$$

It can be seen in Eq. (4.40) that for a given $N \leq N_{\max}$ and λ, the phase transition temperature T_n can be estimated as $\ln \frac{T_C}{T_n} \gtrsim \frac{1}{\epsilon'} \ln \frac{\epsilon' N^2}{4\bar{\lambda}(0)^{3/4}}$. Then it is clear to see that a larger ϵ' leads to a larger T_n/T_c and $N_{\max}$, as shown in fig. 4.2.

4.6 Phenomenology

Amplitude of gravity waves is larger (smaller) the longer (shorter) the duration of the phase transition is. This duration can be captured by the temperature variation of the bounce action near T_n,

$$\frac{\beta}{H} = -\frac{T}{\Gamma}\frac{d\Gamma}{dT} \sim T\frac{dS}{dT}\bigg|_{T_n} \tag{4.42}$$

In our context we can relate this to the RG running of the radion quartic,

$$\frac{\beta}{H} \sim \frac{S_3}{T}\frac{\mu}{\lambda}\frac{d\lambda}{d\mu} \sim \frac{S_3}{T}\epsilon'. \tag{4.43}$$

Since radion mass in our model is also proportional to ϵ' [125, 126], the anomalous dimension near the IR fixed point, there is an interesting correlation between the radion mass, which may be probed at colliders and the amplitude and frequency of stochastic gravitational waves (controlled by $\frac{\beta}{H}$) from the PT, which may be probed by LISA experiment.

Chapter 5: Conclusions

The SM of particle physics is so far the most successful theoretic model which has passed extensive experimental tests. However, it is still imperfect due to its own theoretic limitation and lack of explanation of some experimental results. In chapter 1 of this thesis, we reviewed one of the theoretic problem, Planck-EW hierarchy problem, and two problems related to non-zero neutrino masses and the observed baryon anti-baryon asymmetry of the universe. In order to address all of these problems, it is necessary to consider theories beyond the SM.

In chapter 1, we also reviewed some existing solutions to the above three problems. Composite Higgs models, and the AdS/CFT dual RS models with a warped extra dimension, provide a plausible way to address the Planck-EW hierarchy problem. In such models there exists a strongly interacting sector with approximate conformal symmetry undergoing confinement at around TeV scale, of which SM Higgs originates as the composite state. The big hierarchy between the UV scale (e.g. Planck scale) and the confinement scale is naturally explained by the small perturbation to the conformal symmetry. Moreover, we discussed seesaw mechanism to solve neutrino mass problem. For type I seesaw, the tiny but non-zero SM neutrino mass is generated via the exchange of heavy right-handed singlet neutrinos

with unsuppressed couplings to SM left-handed neutrinos. Seesaw models predict SM neutrinos are Majorana and the lepton number symmetry is broken. Due to the presence of the lepton number violation and heavy singlets in seesaw models, it is also an attractive model which can produce the observed baryon asymmetry via leptogenesis. In such mechanism, lepton asymmetry is generated from the out-of-equilibrium decay of heavy singlets, which subsequently is converted into baryon asymmetry via SM sphaleron process.

In chapter 2, based on RS/CH framework, we studied a natural embedding of high scale type I seesaw, named warped/composite seesaw, which can address all three problems mentioned before in one shot. Remarkably, the type I seesaw structure of warped/composite seesaw model at UV scale appears as TeV scale inverse seesaw after confinement. We justified the robustness of such feature from both 4D (section 2.1) and 5D (section 2.2) point of view.

We moved on to study leptogenesis in chapter 3. To avoid technical difficulty in analyzing leptogenesis in full warped/composite seesaw, we presented the results based on a simplified 4D version, hybrid seesaw. We set up the formalism to study leptogenesis in hybrid seesaw and demonstrated that successful leptogenesis can be realized in a larger parameter space compared to type I seesaw models. Furthermore, leptogenesis inherits the hybrid structure of the hybrid seesaw, which has an interesting interplay of high scale asymmetry generation and TeV scale washout.

We believe leptogenesis in the full warped/composite seesaw has similar qualitative features as that in hybrid seesaw. To justify this argument, we also studied the phase transition in the RS/CH models in chapter 4. The phase transition in

CH models in the early universe is hard to estimate due to strong couplings. Such deconfined to confined phase transition is usually modeled in the dual 5D theory as the transition between a black hole phase and RS phase with two branes. It is usually believed that this transition is too slow at the critical temperature due to approximate conformal symmetries, which is required to achieve large Planck-EW hierarchy (see section 4.3.1). This leads to a large amount of supercooling and dilution of pre-existing asymmetries generated via leptogenesis. We presented a modification of standard Goldberger-Wise stabilization mechanism with both UV and IR fixed points. The phase transition rate in this case is controlled by the physics near IR fixed point while the Planck-EW hierarchy is still controlled by the UV fixed point. Therefore, this modification allows a fast phase transition at the critical temperature, still maintaining the large Planck-EW hierarchy (see section 4.4). This result is justified using our new ansatz of the geometric configuration of the bubbles nucleated in the phase transition, where the transition rate can be robustly calculated in the perturbative region of 5D EFT. Thus in this scenario, primordial asymmetry from leptogenesis will survive after the phase transition until today, accompanied by interesting gravitational wave signals (see section 4.6).

Appendix A: Leptogenesis in TeV scale linear seesaw

In section 3.3, we discussed leptogenesis in TeV scale inverse seesaw model in detail. Now we move on to study another well-motivated seesaw model, the linear seesaw. The Lagrangian is

$$-\mathcal{L}_{\rm LSS} \;=\; y_{a\alpha}\Psi^c_a H\ell_\alpha + (m_\Psi)_{ab}\Psi_a\Psi^c_b + y'_{a\alpha}\Psi_a H\ell_\alpha + \text{h.c.}, \tag{A.1}$$

where α is the SM lepton flavor index and $a, b = 1, 2$ denotes the generations of Ψ, Ψ^c. By redefining the fields, the $(m_\Psi)_{ab}$ matrix can be made real and diagonal whereas $y_{a\alpha}$ and $y'_{a\alpha}$ are complex. In the mass basis, we get the same form as in eq. (3.16), but the parameters are changed to

$$\begin{aligned} m_1 = m_2 = m_{\Psi_1} \quad &; \quad h_{1\alpha} = \frac{y_{1\alpha} + y'_{1\alpha}}{\sqrt{2}} \;,\; h_{2\alpha} = \frac{i(y_{1\alpha} - y'_{1\alpha})}{\sqrt{2}} \\ m_3 = m_4 = m_{\Psi_2} \quad &; \quad h_{3\alpha} = \frac{y_{2\alpha} + y'_{2\alpha}}{\sqrt{2}} \;,\; h_{4\alpha} = \frac{i(y_{2\alpha} - y'_{2\alpha})}{\sqrt{2}}. \end{aligned} \tag{A.2}$$

The condition for small lepton number breaking in this case is $\varepsilon'_{a\alpha} \ll 1$, where we define $\varepsilon'_{a\alpha} \equiv y'_{a\alpha}/y_{a\alpha}$. It is clear that taking $\varepsilon'_{1\alpha} \to 0$ limit, $h_{1\alpha} = ih_{2\alpha}$ and thus $(\tilde{\Psi}_1, \tilde{\Psi}_2)$ become a Dirac pair.

In this section, we only focus on the effect from the Lagrangian in eq. (A.1).

Loops will generate a mass spitting between singlets within the same generation, which will effectively generate a μ term as in the ISS models. Though the size of this μ term is loop suppressed, it might change the parametric dependance of the final baryon asymmetry. We have studied the models with both y' and μ turned on in section 3.3.3.2.

CP asymmetry

According to the definition of the CP asymmetry parameter for $\tilde{\Psi}_i$, denoted as ϵ_i in eq. (3.19), we have

$$\begin{aligned}\epsilon_1+\epsilon_2 &= \frac{1}{8\pi(hh^\dagger)_{22}}\left(\sum_{i\neq 1}\mathrm{Im}[(hh^\dagger)^2_{1i}]f_{1i}+\sum_{j\neq 2}\mathrm{Im}[(hh^\dagger)^2_{2j}]f_{2j}\right)\\ &\quad+\frac{1}{8\pi}\frac{(hh^\dagger)_{22}-(hh^\dagger)_{11}}{(hh^\dagger)_{11}(hh^\dagger)_{22}}\left(\sum_{i\neq 1}\mathrm{Im}[(hh^\dagger)^2_{1i}]f_{1i}\right),\end{aligned} \tag{A.3}$$

Notice that $f_{ij}=f^{\rm v}_{ij}+f^{\rm self}_{ij}$, where $f^{\rm v}_{ij}$ and $f^{\rm self}_{ij}$ are defined in eqs. (3.20) and (3.21) respectively. lt is easy to show that in pure linear seesaw [eq. (A.2)] with singlets in different generations being non-degenerate (i.e., $|m_{\Psi_2}-m_{\Psi_1}|>\Gamma_i$),

$$\left.\begin{aligned} f^{\rm v}_{12}&=f^{\rm v}_{21}\\ f^{\rm self}_{12}&=f^{\rm self}_{21}=0\end{aligned}\right\}\quad\Rightarrow\quad f_{12}=f_{21}$$

$$\left.\begin{aligned} f^{\rm v}_{13}&=f^{\rm v}_{14}=f^{\rm v}_{23}=f^{\rm v}_{24}\\ f^{\rm self}_{13}&\approx f^{\rm self}_{14}\approx f^{\rm self}_{23}\approx f^{\rm self}_{24}\end{aligned}\right\}\quad\Rightarrow\quad f_{13}\approx f_{14}\approx f_{23}\approx f_{24} \tag{A.4}$$

Using such relation and $\mathrm{Im}[(hh^\dagger)^2_{12}] = \mathrm{Im}[(hh^\dagger)^2_{21}] = 0$, eq. (A.3) reduces to

$$\begin{aligned}\epsilon_1 + \epsilon_2 \;\approx\; & \frac{1}{8\pi(hh^\dagger)_{22}} \left(\mathrm{Im}[(hh^\dagger)^2_{13}] + \mathrm{Im}[(hh^\dagger)^2_{14}] + \mathrm{Im}[(hh^\dagger)^2_{23}] + \mathrm{Im}[(hh^\dagger)^2_{24}]\right) f_{13} \\ & -\frac{1}{8\pi}\frac{(y'y^\dagger)_{11} + (yy'^\dagger)_{11}}{(hh^\dagger)_{11}(hh^\dagger)_{22}} \left(\mathrm{Im}[(hh^\dagger)^2_{13}] + \mathrm{Im}[(hh^\dagger)^2_{14}]\right) f_{13}. \end{aligned} \tag{A.5}$$

It is worth mentioning that, if we only consider one generation of singlets, meaning only two degenerate Majorana states $\tilde{\Psi}_{1,2}$ left, $\epsilon_1 + \epsilon_2$ will vanish due to the absence of the CP phase.

Furthermore, according to eq. (A.2), we can find that

$$\begin{aligned}(hh^\dagger)^2_{13} &= \frac{1}{4}\left[(yy^\dagger)_{12} + (y'y^\dagger)_{12} + (yy'^\dagger)_{12} + (y'y'^\dagger)_{12}\right]^2 \\ (hh^\dagger)^2_{14} &= -\frac{1}{4}\left[(yy^\dagger)_{12} + (y'y^\dagger)_{12} - (yy'^\dagger)_{12} - (y'y'^\dagger)_{12}\right]^2 \\ (hh^\dagger)^2_{23} &= -\frac{1}{4}\left[(yy^\dagger)_{12} - (y'y^\dagger)_{12} + (yy'^\dagger)_{12} - (y'y'^\dagger)_{12}\right]^2 \\ (hh^\dagger)^2_{24} &= \frac{1}{4}\left[(yy^\dagger)_{12} - (y'y^\dagger)_{12} - (yy'^\dagger)_{12} + (y'y'^\dagger)_{12}\right]^2, \end{aligned} \tag{A.6}$$

and the sum

$$\begin{aligned}(hh^\dagger)^2_{13} + (hh^\dagger)^2_{14} &= (yy^\dagger)_{12}(yy'^\dagger)_{12} + \mathcal{O}(y'^2) \\ (hh^\dagger)^2_{13} + (hh^\dagger)^2_{14} + (hh^\dagger)^2_{23} + (hh^\dagger)^2_{24} &= 2\left[(yy^\dagger)_{12}(y'y'^\dagger)_{12} + (y'y^\dagger)_{12}(yy'^\dagger)_{12}\right]. \end{aligned} \tag{A.7}$$

Plugging eq. (A.7) into eq. (A.5), one could obtain

$$\epsilon_1 + \epsilon_2 \approx \frac{\mathrm{Im}\left[(yy^\dagger)_{12}(y'y'^\dagger)_{12} + (y'y^\dagger)_{12}(yy'^\dagger)_{12} - 2(yy^\dagger)_{12}(yy'^\dagger)_{12}|yy'^\dagger|_{11}/(yy^\dagger)_{11}\right]}{2\pi(yy^\dagger)_{11}} f_{13}, \tag{A.8}$$

to the second order in y'. Assuming no hierarchy among $y_{a\alpha}(y'_{a\alpha})$ and m_{Ψ_a} are not degenerate, namely f_{13} is $O(1)$ factor, the CP asymmetry can be schematically written as

$$\epsilon \equiv \epsilon_1 + \epsilon_2 \sim \frac{\mathrm{Im}[(y'y'^\dagger)(yy^\dagger)]}{(yy^\dagger)} \sim \frac{\Gamma}{m_\Psi}\varepsilon'^2 \quad (\varepsilon' \ll 1), \tag{A.9}$$

where ε' is the schematic notation for $\varepsilon'_{a\alpha}$.

According to eq. (3.19), one can also find that

$$\epsilon_1 \approx -\epsilon_2 \sim \frac{\Gamma}{m_\Psi}\varepsilon', \tag{A.10}$$

which is first order in ε', while the sum ϵ is second order in ε' [see eq. (A.9)]. As argued in appendix D, we shall use the sum ϵ instead of ϵ_1 or ϵ_2 in the estimation of final asymmetry.

Washouts and baryon asymmetry

Now we want to evaluate the effective washouts in linear seesaw. Follow the

method in ref. [74], one can calculate

$$K^{\text{eff}} \sim \frac{\Gamma}{H}\varepsilon'^2. \tag{A.11}$$

Using the formula for baryon asymmetry [eq. (3.29)] and the efficiency factor $\eta \lesssim 1/K^{\text{eff}}$, the baryon asymmetry in linear seesaw is

$$Y_{\Delta B} \lesssim 10^{-3}\frac{\epsilon}{K^{\text{eff}}} \lesssim 10^{-3}\sqrt{g_*}\frac{m_\Psi}{M_{\text{Pl}}}, \tag{A.12}$$

which is remarkably the same as the result in inverse seesaw [eq. (3.33)]. Leptogenesis in linear seesaw is also summarized in table 3.2.

Appendix B: Boltzmann equations and analytical approximate solutions

We start with a brief review of the general BEs in section B.1 before proceeding to derive analytical approximate solutions in section B.2. The results of our hybrid genesis presented in sections 3.5 and 3.6 are based on these analytical approximate solutions to the BEs.

B.1 Generalities

A general BE describing the evolution of n_X in time t can be written as [128]

$$\frac{dn_X}{dt} + 3Hn_X = -\sum_{b,\ldots,i,j,\ldots} [Xb\ldots \leftrightarrow ij\ldots] \tag{B.1}$$

where the Hubble rate is $H = 1.66\sqrt{g_\star}\frac{T^2}{M_{\rm Pl}}$ with $g_\star$ the total number of relativistic degrees of freedom (of the Universe) and $M_{\rm Pl} = 1.22 \times 10^{19}$ GeV the Planck mass and

$$\begin{aligned}[Xb\ldots \leftrightarrow \ldots] &= \Lambda^{ij\ldots}_{Xb\ldots}\left[|\mathcal{A}(Xb\ldots \to ij\ldots)|^2 f_X f_b\ldots(1+\eta_i f_i)(1+\eta_j f_j)\ldots\right. \\ &\quad \left. -|\mathcal{A}(ij\ldots \to Xb\ldots)|^2 f_i f_j\ldots(1+\eta_X f_X)(1+\eta_b f_b)\ldots\right], \end{aligned} \tag{B.2}$$

where

$$\begin{aligned}\Lambda^{ij\ldots}_{Xb\ldots} &\equiv \int d\Pi_X d\Pi_b\ldots d\Pi_i d\Pi_j\ldots(2\pi)^4\delta^{(4)}(p_X + p_b + \ldots - p_i - p_j - \ldots) \\ d\Pi_x &\equiv \frac{d^3p_x}{(2\pi)^3 2E_x}. \end{aligned} \tag{B.3}$$

In the above, f_x is general phase space distribution with $\eta_x = 1(-1)$ if x is a boson (fermion) and $|\mathcal{A}(ab\ldots \to ij\ldots)|^2$ is the squared amplitude summed over initial and final spin states and gauge multiplicities.

In our study, we will consider X as the only massive particle with mass M_X while all other particles are massless. In this scenario, it is convenient to trade t for

$z \equiv \frac{M_X}{T}$ and number density n_x for *abundance* $Y_x = \frac{n_x}{s}$ where $s = \frac{2\pi^2}{45} g_\star T^3$ is the entropic density. In this case, eq. (B.1) can be written, during radiation-dominated epoch, as

$$sHz\frac{dY_X}{dz} = -\sum_{b,\ldots,i,j,\ldots} [Xb\ldots \leftrightarrow ij\ldots]. \tag{B.4}$$

For massless particles, we assume kinetic equilibrium with phase space distribution $f_x = (e^{\frac{E_x-\mu_x}{T}} - \eta_x)^{-1}$ where μ_x is the chemical potential for x. For real scalar, we have $\mu_x = 0$; otherwise, we assume the chemical potential of the antiparticle x^* is given by $\mu_{x^*} = -\mu_x$. Given that $n_x = \int \frac{d^3p}{(2\pi)^3} f_x$, at leading order in μ_x/T, we have the relation

$$\frac{2\mu_x}{T} = \frac{Y_{\Delta x}}{\zeta_x g_x Y^{\rm eq}}, \tag{B.5}$$

where $Y_{\Delta x} \equiv \frac{n_x - n_{\bar{x}}}{s}$, g_x is the number of degrees of freedom of x and $\zeta_x = 1(2)$ for relativistic fermion (boson) and

$$Y^{\rm eq} = \frac{15}{8\pi^2 g_\star}. \tag{B.6}$$

For the massive particle X, we approximate $f_X \approx \frac{Y_X}{Y_X^{\rm eq}} f_X^{\rm eq}$ where $f_x^{\rm eq} = (e^{E_x/T} - \eta_x)^{-1}$ is the equilibrium phase space distribution and $Y_x^{\rm eq} = n_x^{\rm eq}/s$ denote the equilibrium abundance of x.

As shown in detail in appendix A of refs. [129], with the above approximations and expanding the right-hand side of eq. (B.4) up to first order in μ_x/T, the BEs can

be written in terms of Y_X, $Y_X^{\rm eq}$, $Y_{\Delta x}$, $\zeta_x g_x Y^{\rm eq}$ and (equilibrium) thermal averaged reaction densities

$$\gamma(ab... \leftrightarrow ij...) \equiv \Lambda^{ij...}_{ab...} \left[|\mathcal{A}(ab... \leftrightarrow ij...)|^2 f_a^{\rm eq} f_b^{\rm eq} ... (1+\eta_i f_i^{\rm eq})(1+\eta_j f_j^{\rm eq})...\right] \tag{B.7}$$

Notice that for the time reversal process, the only difference is in the squared amplitude while the phase space distribution combination remains the same i.e. $f_i^{\rm eq} f_j^{\rm eq} ... (1+\eta_a f_a^{\rm eq})(1+\eta_b f_b^{\rm eq})... = f_a^{\rm eq} f_b^{\rm eq} ... (1+\eta_i f_i^{\rm eq})(1+\eta_j f_j^{\rm eq})...$ due to energy conservation. Finally, as discussed in section 3.5.1, once the approximate $U(1)$ charges are identified, all particle asymmetries $Y_{\Delta x}$ can be expressed in term of these charges as in eq. (3.56).

Assuming Maxwell-Boltzmann distribution and ignoring the Fermi-Dirac/Bose-Einstein factor $1+\eta_x f_x^{\rm eq}$, the (inverse) decay process $X \leftrightarrow ij$ can be written as

$$\gamma(X \leftrightarrow ij) = n_X^{\rm eq} \Gamma(X \leftrightarrow ij) \frac{\mathcal{K}_1(z)}{\mathcal{K}_2(z)}, \tag{B.8}$$

where $\Gamma(X \to ij)$ is the decay width for $X \to ij$, $\Gamma(ij \to X) = \Gamma(X^* \to i^* j^*)$ should be interpreted as the CP conjugate process, and $\frac{\mathcal{K}_1(z)}{\mathcal{K}_2(z)}$ is the thermal averaged time dilation factor with $K_n(z)$ the modified Bessel function of second kind of n-th order. The equilibrium number density of X is

$$n_X^{\rm eq} = \frac{g_X}{2\pi^2} T_X^3 z^2 \mathcal{K}_2(z), \tag{B.9}$$

where g_X is the number degrees of freedom of X.

Under the same approximations as above, for the scatterings $ij \leftrightarrow kl$, we have

$$\gamma(ij \leftrightarrow kl) = n_i^{\rm eq} n_j^{\rm eq} \langle \sigma(ij \leftrightarrow kl) \rangle = n_i^{\rm eq} \Gamma(ij \leftrightarrow kl), \tag{B.10}$$

where $\langle \sigma(ij \leftrightarrow kl) \rangle$ is the thermal averaged cross section, $n_i^{\rm eq} = n_j^{\rm eq} = \frac{T^3}{\pi^2}$ and we have defined the scattering rate as[1]

$$\Gamma(ij \leftrightarrow kl) \equiv n_j^{\rm eq} \langle \sigma(ij \leftrightarrow kl) \rangle = \frac{\gamma(ij \to kl)}{n_i^{\rm eq}}. \tag{B.11}$$

Finally, one can define the CP parameter for the decay $X \to ij$ as

$$\epsilon(X \to ij) = \frac{\gamma(X \to ij) - \gamma(X^* \to i^* j^*)}{\gamma_X}, \tag{B.12}$$

where we have defined the total decay reaction density as

$$\gamma_X \equiv \sum_{ij} \left[\gamma(X \to ij) + \gamma(X^* \to i^* j^*) \right]. \tag{B.13}$$

With the Maxwell-Boltzmann approximation, eq. (B.12) can be written only in term of decay widths $\Gamma(X \to ij)$ and $\Gamma(X^* \to i^* j^*)$.

B.2 Analytical approximate solutions

One can construct the BEs according to the procedure discussed in the previous section. In this section, we will derive analytical approximate solutions to the set

[1] The number of degrees of freedom for initial and final states have been absorbed into the cross section $\sigma(ij \leftrightarrow kl)$.

of BEs used in sections 3.5 and 3.6. The BEs we consider involves only decays and inverse decays of a heavy particle X of mass M_X, which captures the dominant generation and washout of the asymmetry in Δ:

$$\frac{dY_X}{dz} = -D(z)\left(\frac{Y_X}{Y_X^{\rm eq}} - 1\right), \tag{B.14}$$

$$\frac{dY_\Delta}{dz} = \epsilon D(z)\left(\frac{Y_X}{Y_X^{\rm eq}} - 1\right) - \frac{1}{2}cD(z)\frac{Y_\Delta}{Y^{\rm eq}}, \tag{B.15}$$

where $z = \frac{M_X}{T}$, ϵ is the CP parameter[2] from decay of X defined in eq. (B.12), $Y^{\rm eq} = \frac{15}{8\pi^2 g_\star}$ [see eq. (B.6)] and $Y_X^{\rm eq} = \frac{45 g_X}{4\pi^4 g_\star} z^2 \mathcal{K}_2(z)$ [see eq. (B.9)]. In the (inverse decay) washout term [the second term of eq. (B.15)], the coefficient c can account for the following two effects. Firstly, it can capture the relevant spectator effects [130, 131]. In hybrid-genesis discussed in section 3.5, the spectator effects are captured by $c = c_{W_1}$ defined in eq. (3.82) or $c = c_{W_2}$ defined in eq. (3.86) with their values given in appendix C. Moreover, choosing $c = K^{\rm eff}/K \ll 1$ can also represent the reduced washout due to approximate symmetry in small lepton number violating models. For example, one can set $c \sim (\mu/\Gamma)^2$ in ISS (section 3.3) or $c \sim (y'/y)^2$ in LSS (appendix A) to study the BEs for leptogenesis in these models. The total decay reaction density eq. (B.13) compared to the Hubble expansion rate H is denoted as

$$D(z) \equiv \frac{\gamma_X}{sHz} = Kz\frac{\mathcal{K}_1(z)}{\mathcal{K}_2(z)}Y_X^{\rm eq} = \frac{1}{2}KY_X^{\rm eq}(0)z^3\mathcal{K}_1(z), \tag{B.16}$$

[2] In eq. (B.15) one may notice that there is overall sign difference for the term $\propto \epsilon$ compared to equations appearing in section 3.5.3. This sign depends on the precise definition of the aymmetry parameter Δ and equations with one sign ϵ are related to equations with opposite sign ϵ by a simple change $\epsilon \to -\epsilon$. Physically, $\epsilon \to -\epsilon$ just changes the notion of particle $\leftrightarrow$ anti-particle.

where the *washout parameter* is defined as

$$K \equiv \frac{\Gamma_X}{H(T = M_X)}, \tag{B.17}$$

with Γ_X the total decay width of X.

Let's first study the Boltzmann equation for Y_X as in eq. (B.14). Assuming $Y_X(z_i) = 0$, we can define $z_{\rm eq}$ as the temperature in which

$$Y_X(z_{\rm eq}) = Y_X^{\rm eq}(z_{\rm eq}). \tag{B.18}$$

For $z < z_{\rm eq}$, we can approximate $\frac{dY_X}{dz} \approx D(z)$ and obtain

$$Y_X(z) \approx \int_{z_i}^{z} dz' D(z') = \frac{1}{2} Y_X^{\rm eq}(0) K f(z_i, z), \tag{B.19}$$

where we have set $Y_X(z_i) = 0$ and defined

$$f(z_i, z) \equiv \int_{z_i}^{z} dz' z'^3 \mathcal{K}_1(z'). \tag{B.20}$$

Taking high initial temperature $z_i \to 0$, let us consider the following two cases. For $K \ll 1$, X reaches its equilibrium abundance at late time $z_{\rm eq} \gg 1$ and we can approximate[3]

$$Y_X(z_{\rm eq}) \approx \frac{3\pi}{4} Y_X^{\rm eq}(0) K \equiv Y_a. \tag{B.21}$$

[3]We approximate the result with the identity $f(0, \infty) = \frac{3\pi}{2}$.

On the other hand, for $K \gg 1$, X reaches its equilibrium abundance at early time $z_{\rm eq} \ll 1$ and we can approximate[4]

$$Y_X\left(z_{\rm eq}\right) \approx \frac{1}{6} Y_X^{\rm eq}(0) K z_{\rm eq}^3 \equiv Y_b. \tag{B.22}$$

According to the definition of $Y_X\left(z_{\rm eq}\right) = Y_X^{\rm eq}\left(z_{\rm eq}\right) \approx Y_X^{\rm eq}\left(0\right)$, we have $z_{\rm eq} \approx (6/K)^{1/3}$.

Next, we will look at the Boltzmann equation for Y_Δ as in eq. (B.15). It is convenient to parametrize the asymmetry generated in Y_Δ by

$$Y_\Delta(z) \equiv \epsilon\, \eta(z) Y_X^{\rm eq}(0), \tag{B.23}$$

where $\eta \equiv \eta(\infty)$ is known as the *efficiency* factor, which shows the effect from washout. $\eta \leq 1$ by definition and we will get $\eta = 1$ when there is thermal initial abundance of Y_X and no washout. Substituting eq. (B.23) into eq. (B.15), we have

$$\frac{d\eta(z)}{dz} = \frac{D\left(z\right)}{Y_X^{\rm eq}(0)} \left(\frac{Y_X}{Y_X^{\rm eq}} - 1 \right) - \frac{1}{2} c \frac{D\left(z\right)}{Y^{\rm eq}} \eta. \tag{B.24}$$

Notice that the equation above is independent of ϵ. This simplification arises because we have considered zero temperature CP parameter which is independent of temperature and the problem boils down to solving for $\eta(z)$. The formal solution

[4] We approximate the result with $f\left(0, z \ll 1\right) = \frac{z^3}{3}$.

for the equation above is

$$\begin{aligned}\eta(z) &= \eta(z_i)\, e^{-\frac{c}{2Y^{\rm eq}}\int_{z_i}^{z} dz' D(z')} + \frac{1}{Y_X^{\rm eq}(0)}\int_{z_i}^{z} dz' D(z') \left(\frac{Y_X}{Y_X^{\rm eq}} - 1\right) e^{-\frac{c}{2Y^{\rm eq}}\int_{z'}^{z} dz'' D(z'')} \\ &= \eta(z_i)\, e^{-\frac{c}{2Y^{\rm eq}}\int_{z_i}^{z} dz' D(z')} - \frac{1}{Y_X^{\rm eq}(0)}\int_{z_i}^{z} dz' \frac{dY_X}{dz'} e^{-\frac{c}{2Y^{\rm eq}}\int_{z'}^{z} dz'' D(z'')}. \end{aligned} \tag{B.25}$$

In the following, we will assume no initial asymmetry and set $\eta(z_i) = 0$. (After all, our aim is to generate an asymmetry dynamically.)

For $z \leq z_{\rm eq}$, we define $\eta^-(z)$:

$$\begin{aligned}\eta^-(z) \equiv \eta(z) &\approx -\frac{1}{Y_X^{\rm eq}(0)}\int_{z_i}^{z} dz' D(z')\, e^{-\frac{c}{2Y^{\rm eq}}\int_{z'}^{z} dz'' D(z'')} \\ &= -\frac{2Y^{\rm eq}}{cY_X^{\rm eq}(0)}\left[1 - e^{-\frac{c}{2Y^{\rm eq}}\int_{z_i}^{z} dz' D(z')}\right] \\ &= -\frac{2}{R\,c}\left[1 - e^{-\frac{c}{2Y^{\rm eq}}Y_X(z)}\right], \end{aligned} \tag{B.26}$$

where we use the approximation: $\frac{dY_X}{dz} \approx D(z)$ and define

$$R \equiv \frac{Y_X^{\rm eq}(0)}{Y^{\rm eq}}. \tag{B.27}$$

For $z > z_{\rm eq}$, we have

$$\eta(z) = \eta^-(z_{\rm eq})\, e^{-\frac{c}{2Y^{\rm eq}}\int_{z_{\rm eq}}^{z} dz' D(z')} + \eta^+(z), \tag{B.28}$$

where

$$\eta^+(z) = -\frac{1}{Y_X^{\rm eq}(0)}\int_{z_{\rm eq}}^{z} dz' \frac{dY_X}{dz'} e^{-\frac{c}{2Y^{\rm eq}}\int_{z'}^{z} dz'' D(z'')}. \tag{B.29}$$

The first term of eq. (B.28) is the contribution when X is being populated while the the second is the contribution when X decays. Next we will discuss the solutions in the following regimes.

B.2.1 Weak washout regime ($cK \ll 1$) with $Y_X(z_i) = 0$

As shown in eq. (B.15), the washout of the asymmetry is controlled by cK while the generation is controlled by K. In the weak washout regime: $cK \ll 1$, there is still freedom to choose $K \ll 1$ or $K \gg 1$ because $c \ll 1$ in ISS or LSS models. The region $cK \ll 1$ and $K \gg 1$ is not possible in the standard leptogenesis with type I seesaw due to c being order unity. Now we shall discuss these two cases in the weak washout regime.

Case I: $cK \ll 1$ **and** $K \ll 1$

Since $z_{\rm eq} \gg 1$ when $K \ll 1$, we can neglect the washout for $z > z_{\rm eq}$ in eq. (B.28). Hence, we have

$$\begin{aligned} \eta\left(z\right) &\approx \eta^{-}\left(z_{\rm eq}\right) - \frac{1}{Y_X^{\rm eq}(0)} \int_{z_{\rm eq}}^{z} dz' \frac{dY_X}{dz'}, \\ &= -\frac{2}{R\, c}\left[1 - e^{-\frac{c}{2Y^{\rm eq}} Y_a}\right] + \frac{1}{Y_X^{\rm eq}(0)}\left[Y_a - Y_X\left(z\right)\right], \end{aligned} \tag{B.30}$$

where we have used eq. (B.21).

For the final efficiency, we take $z \to \infty$ where $Y_X(\infty) = 0$ and obtain

$$\begin{aligned}
\eta^w_{K\ll 1}(K,c) &\approx -\frac{2}{R\,c}\left[1 - e^{-\frac{c}{2Y^{\rm eq}}Y_a}\right] + \frac{1}{Y_X^{\rm eq}(0)}Y_a \\
&\approx -\frac{2}{R\,c}\left[\frac{c}{2Y^{\rm eq}}Y_a - \frac{1}{2}\left(\frac{c}{2Y^{\rm eq}}Y_a\right)^2\right] + \frac{1}{Y_X^{\rm eq}(0)}Y_a \\
&= \frac{1}{Y_X^{\rm eq}(0)}\frac{c}{4Y^{\rm eq}}Y_a^2 \\
&= \frac{9\pi^2}{64}R\,c\,K^2. \qquad \text{(B.31)}
\end{aligned}$$

In the above, we have expanded the exponent in $cK \ll 1$ up to second order. If we choose $c \sim 1$, this gives the standard result $\eta^w_{K\ll 1} \sim K^2$ in the weak washout regime. While in the models with small lepton number breaking ($c = K^{\rm eff}/K \ll 1$), we would have $\eta^w_{K\ll 1} \sim K^{\rm eff}K$.

Case II: $cK \ll 1$ **and** $K \gg 1$

Since $z_{\rm eq} \ll 1$ when $K \gg 1$, we cannot neglect the washout for $z > z_{\rm eq}$ in eq. (B.28). In this case, we have

$$\begin{aligned}
\eta^-(z_{\rm eq})\, e^{-\frac{c}{2Y^{\rm eq}}\int_{z_{\rm eq}}^{z} dz' D(z')} &\approx -\frac{2}{R\,c}\left[1 - e^{-\frac{c}{2Y^{\rm eq}}Y_b}\right] e^{-\frac{c}{2Y^{\rm eq}}\int_{z_{\rm eq}}^{z} dz' D(z')} \\
&\approx -\frac{2}{R\,c}\left[1 - e^{-\frac{1}{2}R\,c}\right] e^{-\frac{c}{2Y^{\rm eq}}\int_{z_{\rm eq}}^{z} dz' D(z')}, \qquad \text{(B.32)}
\end{aligned}$$

and

$$\begin{aligned}
\eta^+(z) &\approx -\frac{1}{Y_X^{\rm eq}(0)}\int_{z_{\rm eq}}^{z} dz' \frac{dY_X^{\rm eq}}{dz'} e^{-\frac{c}{2Y^{\rm eq}}\int_{z'}^{z} dz'' D(z'')} \\
&= \frac{1}{Y_X^{\rm eq}(0)K}\int_{z_{\rm eq}}^{z} dz' \frac{1}{z'} D(z')\, e^{-\frac{c}{2Y^{\rm eq}}\int_{z'}^{z} dz'' D(z'')}, \qquad \text{(B.33)}
\end{aligned}$$

where we have used the following approximation:

$$\frac{dY_X}{dz'} \approx \frac{dY_X^{\rm eq}}{dz'} = -Y_X^{\rm eq}\frac{\mathcal{K}_1(z)}{\mathcal{K}_2(z)} = -\frac{1}{Kz}D(z)\,. \tag{B.34}$$

Writing the integrand as $e^{-g(z',z)}$, the dominant contribution for $\eta^+(z)$ comes from a region around z_B where $g(z',z)$ has a minimum. Following the approximation of ref. [39] by replacing the exponent of the integrand $D(z)$ by $\overline{D}(z) = \frac{\bar{z}}{z}D(z)$ with $\bar{z} = \min(z, z_B)$, we have

$$\begin{aligned}\eta^+(z) &\approx \frac{1}{Y_X^{\rm eq}(0)K\bar{z}}\int_{z_{\rm eq}}^{z} dz'\overline{D}(z')\,e^{-\frac{c}{2Y^{\rm eq}}\int_{z'}^{z}dz''\overline{D}(z'')} \\ &= \frac{2}{\bar{z}RcK}\left[1-e^{-\frac{c}{2Y^{\rm eq}}\int_{z_{\rm eq}}^{z}dz'\overline{D}(z')}\right].\end{aligned} \tag{B.35}$$

In the above, z_B is well approximated by [39] to be

$$z_B(K,c) \approx 1+\frac{1}{2}\ln\left[1+\frac{\pi K^2R^2c^2}{1024}\left(\ln\frac{3125\pi K^2R^2c^2}{1024}\right)^5\right], \tag{B.36}$$

for all K. For $K \gg 1$, we can approximate $z_{\rm eq} \approx 0$ and integrate eq. (B.35)[5]

$$\begin{aligned}\eta^+(\infty) &\approx \frac{2}{z_BRcK}\left[1-e^{-\frac{1}{4}z_BKRc\int_0^\infty dz'z'^2\mathcal{K}_1(z')}\right] \\ &= \frac{2}{z_BRcK}\left[1-e^{-\frac{1}{2}z_BRcK}\right].\end{aligned} \tag{B.37}$$

[5]We use the identity $\int_0^\infty dzz^2\mathcal{K}_1(z) = 2$.

Plugging eqs. (B.32) and (B.32) into eq. (B.28), the final efficiency ($z \to \infty$) is

$$\begin{aligned}\eta^{w}_{K\gg 1}\left(K,c\right) &\approx -\frac{2}{R\,c}\left[1-e^{-\frac{1}{2}R\,c}\right]e^{-\frac{c}{2Y^{\rm eq}}Y_a}+\frac{2}{z_B R\,cK}\left[1-e^{-\frac{1}{2}z_B R\,cK}\right]\\ &\approx \frac{1}{4}R\,cK\left(\frac{3\pi}{2}-z_B\right), \end{aligned} \tag{B.38}$$

where we have kept only the leading term in $cK \ll 1$. Notice that the result above depends on cK instead of K^2 as in the usual weak washout regime. To our knowledge, this is a *novel* which has not been presented elsewhere.

B.2.2 Strong washout regime ($cK \gg 1$)

In the strong washout regime $cK \gg 1$, we will also have $K \gg 1$ due to c being at most order unity. In this case, the term involving $\eta^{-}(z_{\rm eq})$ in eq. (B.28) is negligible because it suffers a strong exponential washout $e^{-\frac{c}{2Y^{\rm eq}}\int_{z_{\rm eq}}^{z}dz' D(z')}$. For $\eta^{+}\left(\infty\right)$, we can make use of eq. (B.37) which is valid for $K \gg 1$. According to eq. (B.28), the final efficiency is simply[6]

$$\eta^{s}\left(K,c\right) \approx \eta^{+}\left(\infty\right) \approx \frac{2}{z_B R\,cK}\left[1-e^{-\frac{1}{2}z_B R\,cK}\right]. \tag{B.39}$$

B.2.3 Regimes with thermal initial abundance of X

Now we move on to study the regimes with thermal initial abundance of X, i.e. $Y_X\left(z_i\right) = Y_X^{\rm eq}\left(z_i\right)$. According to the definition in eq. (B.18), we have $z_{\rm eq} = z_i$. This

[6]For improved approximation, we can also include contribution from η which gives $-\frac{2}{R\,c}\left[1-e^{-\frac{1}{2}R\,c}\right]e^{-\frac{3\pi}{8}R\,cK}$.

means $\eta(z) = \eta^+(z)$ in eq. (B.28). Hence for the case of thermal initial abundance of X, a approximate solution good for all K is

$$\eta^{\rm th}\left(K, c\right) = \eta^+\left(\infty\right) \approx \frac{2}{z_B R\, cK}\left[1 - e^{-\frac{1}{2} z_B R\, cK}\right]. \tag{B.40}$$

We can check several limits:

$$\eta^{\rm th}\left(K, c\right) \approx \begin{cases} 1 - \frac{1}{4} z_B R\, cK & (cK \ll 1) \\ \frac{2}{z_B R\, cK} & (cK \gg 1) \end{cases}. \tag{B.41}$$

In the weak washout regime $cK \ll 1$, $\eta^{\rm th}\left(K, c\right) \approx 1$, meaning there is almost no washout effect as expected. While in the strong washout regime, it coincides with eq. (B.39) because the efficiency factor is not sensitive to the initial condition in this region.

B.2.4 For all regimes

For the case of thermal initial abundance of X, we can use eq. (B.40) for all K and c. For the case of zero initial abundance of X, following ref. [39], we can interpolate η for all K and c wtih

$$\eta\left(K, c\right) \approx \eta^-\left(K, c\right) + \eta^+\left(K, c\right), \tag{B.42}$$

where

$$\eta^{-}(K,c) = -\frac{2}{Rc}e^{-\frac{3\pi}{8}RcK}\left\{\exp\left[\frac{\frac{3\pi}{8}K}{\left(1+\sqrt{\frac{3\pi}{4}K}\right)^{2}}Rc\right]-1\right\}, \quad \text{(B.43)}$$

$$\eta^{+}(K,c) = \frac{2}{z_B RcK}\left\{1-\exp\left[-\frac{\frac{3\pi}{8}K}{\left(1+\sqrt{\frac{3\pi}{4}K}\right)^{2}}z_B RcK\right]\right\}. \quad \text{(B.44)}$$

The equations above reproduce the approximate solutions eqs. (B.31), (B.38) and (B.39) in their respective regimes.

Appendix C: Spectator effects

Here we shall discuss the relevant spectator effects in analyzing BEs at different temperature regimes in section 3.5.

In the thermal bath, through fast scatterings, asymmetries will also be induced in other particles not directly involved in asymmetry generation (they are known as spectators). Although the effects remain generally less than order of one [130, 131], they are included for completeness. Such effects from spectators are encoded in c_Ψ, c_{Φ_λ} in BEs [see eq. (3.81)], which are defined as the ratio of Y_{Δ_Ψ}/Y_Δ or $Y_{\Phi_\lambda}/Y_\Delta$ respectively. c_Ψ, c_{Φ_λ} can be calculated using the charge matrix in eq. (3.56), which depends on the effective $U(1)$ symmetries [see section 3.5.1] present at the relevant temperature regime. In the following, we will briefly discuss the interactions

which are in or out of thermal equilibrium and the conserved charges in different temperature regimes.

In our hybrid seesaw model, we always assume singlet particles $(\Psi, \Psi^c, \Phi_\lambda, \Phi_\kappa)$ are in equilibrium when the genesis happens due to large couplings within the sector [see section 3.5.2.5]. Whether the SM particles are in equilibrium or not depends on the temperature. For $T \gtrsim 10^{15}$ GeV, as discussed in section 3.5.2.5, the SM particles cannot be in equilibrium via the SM interactions. Since we have $y\Psi^c H\ell$ interaction in our hybrid seesaw model [see eq. (3.49)] with unsuppressed coupling y, we assume the SM lepton doublets and Higgs are in equilibrium but not other SM particles in this temperature regime. For $T \lesssim 10^{15}$ GeV, the SM gauge interactions are in equilibrium. For $T \gtrsim 10^{12}$ GeV, EW sphaleron processes as well as all charged lepton Yukawa interactions are out of thermal equilibrium. In addition, the first and second family quark Yukawa interactions are out of thermal equilibrium while the third family quark Yukawa interactions are in thermal equilibrium.[1] For $T \lesssim 10^{12}$ GeV , the EW sphalerons get into thermal equilibrium. For $T \lesssim 10^{11}$ GeV, the τ and charm Yukawa interactions get into thermal equilibrium. For $T \lesssim 10^{9}$ GeV, μ Yukawa interactions are in thermal equilibrium. For $T \lesssim 10^{7}$ GeV, down Yukawa interactions are in thermal equilibrium and finally for $T \lesssim 10^{4}$ GeV, electron Yukawa interactions get into thermal equilibrium as well.

Knowing the relevant interactions at a given temperature regime, we can figure out the conservation of the charges. Since EW sphalerons are not in equilibrium for

[1] For $T \gtrsim 10^{13}$ GeV, QCD sphaleron processes and bottom Yukawa interactions are also out of thermal equilibrium.

Temperature regimes	Fully-symmetric model			Non-symmetric model
	c_Ψ	c_{Φ_λ}	c_{W1}	c_{W1}
$10^{15}\,\text{GeV} \lesssim T$	$\frac{5}{7}$	1	$\frac{31}{42}$	$\frac{1}{6}$
$10^{13}\,\text{GeV} \lesssim T \lesssim 10^{15}$ GeV	$\frac{2}{3}$	1	$\frac{13}{18}$	$\frac{1}{9}$
$10^{12}\,\text{GeV} \lesssim T \lesssim 10^{13}$ GeV	$\frac{35}{53}$	1	$\frac{229}{318}$	$\frac{4}{39}$
$10^{11}\,\text{GeV} \lesssim T \lesssim 10^{12}$ GeV	$\frac{15}{23}$	1	$\frac{33}{46}$	$\frac{1}{11}$
$10^{9}\,\text{GeV} \lesssim T \lesssim 10^{11}$ GeV	$\frac{42}{65}$	1	$\frac{93}{130}$	$\frac{5}{61}$
$10^{7}\,\text{GeV} \lesssim T \lesssim 10^{9}$ GeV	$\frac{573}{887}$	1	$\frac{1269}{1774}$	$\frac{17}{208}$
$10^{4}\,\text{GeV} \lesssim T \lesssim 10^{7}$ GeV	$\frac{363}{565}$	1	$\frac{807}{1130}$	$\frac{10}{131}$

Table C.1: We list the values of c_Ψ, c_{Φ_λ} and $c_{W1} = \frac{1}{3}c_\Psi + \frac{1}{2}c_{\Phi_\lambda}$ in different temperature regimes in the **fully-symmetric model**, as well as the values of $c_{W1} = \frac{1}{3}c_\Psi$ in the **non-symmetric model.** For simplicity, in our numerical estimations, we will fix $c_{W1} = 0.7(0.1)$ for all temperature regimes in the **fully-symmetric (non-symmetric) model** .

$T \gtrsim 10^{12}$ GeV, the baryon number B is an effective symmetry. Therefore, we impose baryon number conservation, i.e., $Y_{\Delta B} = 0$. We do not impose such conservation for $T \lesssim 10^{12}$ GeV because EW sphalerons processes break baryon number symmetry. Notice that our definition of Y_Δ changes from $-Y_{\Delta L'}$ for $T \gtrsim 10^{12}$ GeV to $Y_{\Delta(B-L')}$ for $T \lesssim 10^{12}$ GeV [see eq. (3.60)], which will lead to small changes in the spectator effects. Since we have two realizations of the hybrid seesaw model, namely **fully-symmetric model** and **non-symmetric model** (defined in section 3.5.2.1), we will discuss them separately here:

- **Fully-symmetric model**

  In this type of model, on top of hypercharge conservation, we also impose $U(1)_{B-L}$ and $U(1)_{\lambda-B}$ conservation in all temperature regimes. In table C.1, we list the values of c_Ψ, c_{Φ_λ} and $c_{W1} = \frac{1}{3}c_\Psi + \frac{1}{2}c_{\Phi_\lambda}$ [introduced in eq. (3.82)]

in different temperature regimes.

- **Non-symmetric model**

  In this type of model, we only impose hypercharge conservation due to the absence other global symmetries. Moreover, since the scalar Φ_λ in this model does not carry any charge, so $c_{\Phi_\lambda} = 0$ and we will get $c_{W1} = \frac{1}{3}c_\Psi$ according to eq. (3.82). In table C.1, we list the values of $c_{W1} = \frac{1}{3}c_\Psi$ in different temperature regimes.

As can be seen in table C.1, although the exact values varies at different temperatures, we can find that in all temperature regimes $c_{W1} \approx 0.7$ in the **fully-symmetric model** and $c_{W1} \approx 0.1$ in the **non-symmetric model**. Therefore, we will fix $c_{W1} = 0.7(0.1)$ in the estimation of BEs in the **fully-symmetric (non-symmetric) model** for simplicity.

Appendix D: Comments on Boltzmann equations for ISS and LSS

When we study leptogenesis in ISS and LSS models in section 3.3, we have used the sum of CP parameter of each particle within the pseudo-Dirac pair to estimate the size of total CP asymmetry as well as the final lepton or baryon asymmetry. In this section, we will justify this argument using a general parametric estimation.

Consider Boltzmann equation for the asymmetry in $\Delta(B-L)$ in inverse or linear seesaw,

$$\frac{dY_{\Delta(B-L)}}{dz} = \sum_i \epsilon_i \frac{dY_{\tilde{\Psi}_i}}{dz} - \frac{1}{2} W(z) Y_{\Delta(B-L)}, \tag{D.1}$$

where $\tilde{\Psi}_i$ are the mass eigenstates of the singlet fermions with $m_i \leq m_{i+1}$, ϵ_i is the CP asymmetry parameter for $\tilde{\Psi}_i$ decays and $z = \frac{m_1}{T}$. For simplicity let's focus on the asymmetry generated from decays of the lightest pseudo-Dirac pair only, i.e. consider the sum in eq. (D.1) to be only over $i = 1, 2$. The qualitative conclusion will not change when we include more generations of $\tilde{\Psi}_i$. The washout is controlled by $W(z)$ and we assume the dominant washout comes from the inverse decay (on-shell part of $\Delta(B-L) = 2$ scattering process). Correctly including the interference among $\tilde{\Psi}_{1,2}$, one would get (see ref. [74])

$$W(z) \approx \frac{1}{2} K^{\text{eff}} \frac{Y^{\text{eq}}_{\tilde{\Psi}}(0)}{Y^{\text{eq}}} z^3 \mathcal{K}_1(z), \tag{D.2}$$

where $K^{\text{eff}} = K_1 \delta_1^2$ for ISS and $K^{\text{eff}} = K_1 \varepsilon_1'^2$ for with $\delta \sim \mu/\Gamma$, $\varepsilon' \sim y'/y$ and K_i defined in eq. (3.30). This is the same washout factor in eq. (B.15) with $c = K^{\text{eff}}/K_1$. The formal solution to the differential equation eq. (D.1) is

$$Y_{\Delta(B-L)}(z) = \int_0^z dz' \sum_i \epsilon_i \frac{dY_{\tilde{\Psi}_i}}{dz'} e^{-\frac{1}{2}\int_{z'}^z dz'' W(z'')}, \tag{D.3}$$

assuming $Y_{\Delta(B-L)}(0) = 0$, meaning no initial asymmetry. Since $W(z)$ is the same

for all $\tilde{\Psi}_i$, we can simply put the sum out of the integration:

$$\begin{aligned} Y_{\Delta(B-L)}(\infty) &= \sum_i \int_0^\infty dz' \epsilon_i \frac{dY_{\tilde{\Psi}_i}}{dz'} e^{-\frac{1}{2}\int_{z'}^\infty dz'' W(z'')} \\ &= \sum_i \epsilon_i \eta_i Y^{\rm eq}_{\tilde{\Psi}}(0), \end{aligned} \tag{D.4}$$

where $\eta_i \equiv \eta_i(\infty)$ and $\eta(z)$ is defined in eq. (B.24) with $c = K^{\rm eff}/K_1$. This means we could treat the generation of asymmetry and washout separately for each $\tilde{\Psi}_i$ and the total effect is the sum of the result of each one. Now eq. (D.4) can be rewritten as

$$\frac{Y_{\Delta(B-L)}(\infty)}{Y^{\rm eq}_{\tilde{\Psi}}(0)} = \left[(\epsilon_1+\epsilon_2)\eta_1 + \epsilon_2(\eta_2-\eta_1)\right]. \tag{D.5}$$

As discussed in section 3.3 and appendix A, we have $\epsilon_1 \approx -\epsilon_2 = \mathcal{O}(\varepsilon y^2)$, where $\varepsilon \sim \mu/m_\Psi$ and we assume $y^2 \gg \mu/\Gamma$, in ISS and $\epsilon_1 \approx -\epsilon_2 = \mathcal{O}(\varepsilon' y^2)$ in LSS. The sum $\epsilon_1+\epsilon_2$, however, is second order in $\varepsilon(\varepsilon')$: $\epsilon_1+\epsilon_2 = \mathcal{O}(\varepsilon^2/y^2)$ in ISS and $\epsilon_1+\epsilon_2 = \mathcal{O}(\varepsilon'^2 y^2)$ in LSS. Since the mass splitting and the difference in Yukawa couplings within the pseudo-Dirac pair are controlled by ε or ε', the difference of the η_i should go to zero as ε or $\varepsilon' \to 0$. Taking $\eta_1 - \eta_2 \propto \varepsilon(\varepsilon')\eta_1$ as an conservative estimation, we would find the first term in eq. (D.5) is $\mathcal{O}(\varepsilon^2/y^2)\eta_1$ in ISS or $\mathcal{O}(\varepsilon'^2 y^2)\eta_1$ in LSS. Whereas the second term is at most $O(\varepsilon^2 y^2)\eta_1$ in ISS or $\mathcal{O}(\varepsilon'^2 y^2)\eta_1$ in LSS. This means the second term in eq. (D.5) is parametrically smaller or at most the same order as the first term. Since our estimation here is only order of magnitude, it is

appropriate to keep only the term with $\epsilon_1 + \epsilon_2$, meaning eq. (D.5) approximates to

$$\frac{Y_{\Delta(B-L)}(\infty)}{Y^{\rm eq}_{\tilde{\Psi}}(0)} \sim (\epsilon_1 + \epsilon_2)\eta_1. \tag{D.6}$$

This allows us to simply treat the contribution to the $Y_{\Delta(B-L)}$ from a pseudo-Dirac pair as if only one of the particle (say $\tilde{\Psi}_1$) decays with the effective CP asymmetry parameter being $\epsilon_1 + \epsilon_2$.

We shall justify the above argument with analytic approximations of $\eta_2 - \eta_1$ in both ISS and LSS models. We first consider the LSS case where $m_2 = m_1$. There is a unified definition of z for each $\tilde{\Psi}_i$ because $z \equiv \frac{m_1}{T} = \frac{m_2}{T}$. Therefore we could simply use the results for η_i derived in appendix B:

$$\eta_i \sim \begin{cases} 1/(K^{\rm eff} z_B) & (K^{\rm eff} \gg 1) \\ K^{\rm eff} & (K^{\rm eff} \ll 1 \& K_i \gg 1 \text{with zero initial } \tilde{\Psi}_i) \\ K^{\rm eff} K_i & (K_i \ll 1 \text{with zero initial } \tilde{\Psi}_i) \\ 1 & (K^{\rm eff} \ll 1 \text{with thermal initial } \tilde{\Psi}_i) \end{cases}, \tag{D.7}$$

where z_B is defined in eq. (B.36) and it only depends on $K^{\rm eff}$. Since only in $K_i \ll 1$ region (with zero initial $\tilde{\Psi}_i$) η_i depends on K_i and knowing that $K_2 \approx K_1(1 - 4\varepsilon_1')$ [derived using eq. (A.2)] to the first order in ε_1', we can conclude that

$$\frac{Y_{\Delta(B-L)}(\infty)}{Y^{\rm eq}_{\tilde{\Psi}}(0)} \approx \begin{cases} [(\epsilon_1 + \epsilon_2)\eta_1 - 4\epsilon_2 \varepsilon_1' \eta_1] & (K_i \ll 1) \\ (\epsilon_1 + \epsilon_2)\eta_1 & (\text{others}) \end{cases}. \tag{D.8}$$

Since $(\epsilon_1 + \epsilon_2) = O(\varepsilon'^2 y^2) \sim \epsilon_2 \varepsilon_1' = O(\varepsilon'^2 y^2)$, it matches our estimation in eq. (D.6).

Now we move on to study the case of ISS, which is bit subtler due to mass difference $m_2 = m_1(1+\varepsilon_1)$. We can not simply use the same expression in appendix B to get η_2. Instead, we should consider

$$\eta_2 = \frac{1}{Y^{\rm eq}_{\tilde{\Psi}}(0)} \int_0^\infty dz' \frac{dY_{\tilde{\Psi}_2}(z'_2)}{dz'_2} e^{-\frac{1}{2}\int_{z'}^\infty dz'' W(z'')}, \tag{D.9}$$

where $z'_2 = z'(1+\varepsilon_1)$. In the strong washout region ($K^{\rm eff} \gg 1$), as discussed in appendix B.2.2, we can treat $Y_{\tilde{\Psi}_2} \approx Y^{\rm eq}_{\tilde{\Psi}}$ in all relevant regions. Therefore the part involving z'_2 in eq. (D.9) can be approximated to be

$$\begin{aligned} \frac{dY_{\tilde{\Psi}_2}(z'_2)}{dz'_2} &\approx \frac{dY^{\rm eq}_{\tilde{\Psi}}(z'_2)}{dz'_2} \\ &\approx \frac{dY^{\rm eq}_{\tilde{\Psi}}(z')}{dz'} + \varepsilon_1 z' \frac{d^2 Y^{\rm eq}_{\tilde{\Psi}}(z')}{dz'^2}, \end{aligned} \tag{D.10}$$

to the first order in ε_1. Plugging the first part of the second line of eq. (D.10) to eq. (D.9) will simply get η_1 and thus we can write $\eta_2 \approx \eta_1 + \delta\eta$ with

$$\delta\eta = \frac{\varepsilon_1}{Y^{\rm eq}_{\tilde{\Psi}}(0)} \int_0^\infty dz' z' \frac{d^2 Y^{\rm eq}_{\tilde{\Psi}}(z')}{dz'^2} e^{-\frac{1}{2}\int_{z'}^\infty dz'' W(z'')}. \tag{D.11}$$

For $K^{\rm eff} \gg 1$, due to the exponential washout controlled by $W(z)$, the integration in the region $z \gtrsim z_B \gg 1$ dominates. This allows us to keep only $z' \gg 1$ region of the integrand:

$$\frac{1}{Y^{\rm eq}_{\tilde{\Psi}}(0)} z' \frac{d^2 Y^{\rm eq}_{\tilde{\Psi}}(z')}{dz'^2} \overset{z'\gg 1}{\approx} -\frac{1}{K^{\rm eff} R} W(z'), \tag{D.12}$$

where $R \equiv \frac{Y^{\rm eq}_{\tilde{\Psi}}(0)}{Y^{\rm eq}}$ and we have used the properties of $\mathcal{K}_1(z')$ function:

$$z' \frac{d(z'^2 \mathcal{K}_1(z'))}{dz'} \overset{z' \gg 1}{\approx} -z'^3 \mathcal{K}_1(z'). \tag{D.13}$$

Combining eq. (D.11) and eq. (D.12), one will find

$$\begin{aligned} \delta\eta &\approx -\frac{\varepsilon_1}{K^{\rm eff} R} \int_0^\infty dz' W(z') e^{-\frac{1}{2}\int_{z'}^\infty dz'' W(z'')} \\ &= \frac{2\varepsilon_1}{K^{\rm eff} R} \left(1 - e^{-\frac{1}{2}\int_0^z dz'' W(z'')}\right) \\ &= \frac{2\varepsilon_1}{K^{\rm eff} R} \left(1 - e^{-\frac{3\pi}{8} K^{\rm eff} R}\right). \end{aligned} \tag{D.14}$$

Using the expression for η_1 in eq. (B.39) and $K^{\rm eff} \gg 1$, we can get

$$\delta\eta \approx z_B \varepsilon_1 \eta_1. \tag{D.15}$$

Therefore, the asymmetry in ISS in the strong washout region can be summarized as

$$\frac{Y_{\Delta(B-L)}(\infty)}{Y^{\rm eq}_{\tilde{\Psi}}(z=0)} \approx [(\epsilon_1 + \epsilon_2)\eta_1 + \epsilon_2 \varepsilon_1 z_B \eta_1] \qquad (K^{\rm eff} \gg 1). \tag{D.16}$$

Since $(\epsilon_1 + \epsilon_2) = O(\varepsilon^2/y^2) \gg \epsilon_2 \varepsilon_1 z_B = O(\varepsilon^2 y^2 \ln K^{\rm eff})$, this will reduce to eq. (D.6). We also checked numerically that the results for weak washout regions are consistent

with eq. (D.6).

Appendix E: Gauge model

The structure of the hybrid seesaw introduced in eq. (3.49) can be obtained introducing appropriate gauge symmetries and additional fields. In this appendix we present a minimal model that reduces to our hybrid scenario after the additional fields (χ, S in table E.1) have been integrated out or decoupled. In this model, $U(1)_{B-L}$ global symmetry in table 3.3 is promoted to be a gauge symmetry while $U(1)_{\lambda-B}$ arises as an accidental global symmetry.

We assume the full model has gauge group $G_{\rm SM} \times U(1)_{B-L} \times U(1)_X$, where $G_{\rm SM} \equiv SU(3)_c \times SU(2)_L \times U(1)_Y$. While the new gauge symmetry $U(1)_{B-L}$ is different from the usual $(B-L)$ symmetry of the SM, we decided to use this name since SM particles are charged as baryon (B) minus lepton (L) number symmetry. The fields beyond the SM are singlets under $G_{\rm SM}$. Their charges under the two new $U(1)$ gauge groups are specified in table E.1. It is easy to check that the gauge symmetry is anomaly-free [132]. Notice that in our case we have two N_i and, as a result, the lightest SM neutrino will be massless. Scenarios with three N_i (or more) can be constructed, but at the cost of introducing new fermions.

Other than the kinetic terms, the only renormalizable couplings allowed by

	$U(1)_{B-L}$	$U(1)_X$	spin
$\Psi^c_{a=1,2,3}$	$+1$	0	$1/2$
$\Psi_{a=1,2,3}$	0	α	$1/2$
$N_{i=1,2}$	0	-4α	$1/2$
Φ_κ	-1	$-\alpha$	0
Φ_λ	0	3α	0
χ	0	5α	$1/2$
S	0	8α	0

Table E.1: Beyond the SM fields and their charges under new gauge symmetries $U(1)_{B-L} \times U(1)_X$. Here α is some arbitrary real number.

the symmetries are

$$-\mathcal{L}_{\text{Yukawa}} \;=\; y_{a\alpha}\Psi^c_a H \ell_\alpha + \kappa_{ab}\Psi^c_a \Phi_\kappa \Psi_b + \lambda_{ai}\Psi_a \Phi_\lambda N_i + c_{ij} S N_i N_j + \text{h.c.} \quad \text{(E.1)}$$

In addition to the fields of the hybrid seesaw [eq.(3.49)] we have added a Weyl fermion χ and one complex scalar S. As mentioned earlier, the former is necessary to obtain a gauge anomaly-free $U(1)_X$. The scalar S is assumed to acquire large VEV, thus generating the large Majorana masses for N_i. The hybrid model is effectively recovered once S gets a VEV $M_N \propto \langle S \rangle$ and its radial mode gets integrated out. In particular, note that no number-changing interaction between $\Phi_{\lambda,\kappa}, S$ is allowed by gauge invariance at the renormalizable level. The lowest dimensional operator in the scalar potential that breaks the $U(1)_{\lambda-B}$ symmetries in table 3.3 (after S gets a VEV) arises at dimension 11, $\sim \frac{\Phi^8_\lambda (S^*)^3}{M^7_{\text{Pl}}}$, and as a result, its effect is negligible at low energies. Further number changing operators may exist, e.g. $\frac{\Phi^8_\lambda (S^*)^3}{M^7_{\text{Pl}}} \left(\frac{\Phi^\dagger_\kappa \Phi_\kappa}{M^2_{\text{Pl}}}\right) \to \frac{\langle S \rangle^3}{M^3_{\text{Pl}}} \frac{\Phi^8_\lambda \Phi^\dagger_\kappa \Phi_\kappa}{M^6_{\text{Pl}}}$. Unlike previous dimension 11 operator, this operator can generate number changing processes among Φ_λ's and Φ_κ's within the EFT of hy-

brid model, and in principle can washout asymmetry as discussed in section 3.5.2.3. However, being dimension 13 or higher, those effects can safely be ignored.

The global symmetry $U(1)_{\lambda-B}$ is spontaneously broken by $\langle\Phi_\lambda\rangle \sim$ TeV, generating Nambu-Goldstone boson (NGB). Due to explicit breakings by higher-dimensional operators, this NGB will acquire mass. This fact, together with resulting phenomenological implications were discussed in [54].

The additional fermion χ is very light and stable on cosmological scales. Its mass dominantly arises from $\chi\chi(S^*\Phi_\lambda)^2/M_{\rm Pl}^3$[1], and is thus of order

$$m_\chi \sim (M_N/M_{\rm Pl})^2(\mathrm{TeV}^2/M_{\rm Pl}) \ll 10^{-3}\,\mathrm{eV}.$$

However, because it is also very weakly-coupled, its presence is still allowed by all experimental data. After the gauge boson associated with $U(1)_X$ becomes massive, the dominant interaction involving χ is $\bar{\chi}\chi\bar{\Psi}\Psi/\langle S\rangle^2$. This decouples around $T \sim (\langle S\rangle^4/M_{\rm Pl})^{1/3} \sim (M_N^4/M_{\rm Pl})^{1/3}$, which is always much higher than the QCD phase transition in our model. This ensures that χ behaves like dark radiation and contributes negligibly to $\Delta N_{\rm eff}$ at BBN and CMB [133]. Other constraints on the hybrid seesaw model are discussed in [54].

[1]This operator also breaks $U(1)_{\lambda-B}$ and induces $U(1)_{\lambda-B}$-violating decay of Φ_λ. However, such decay is not harmful for the genesis if either (i) corresponding decay rate is slow (and it is: at any temperature $T \lesssim M_{\rm Pl}$ the decay is inactive) or (ii) (even if Φ_λ decay were rapid) χ does not interact with SM sector strongly that it does not transfer asymmetry (from Φ_λ decay) to the SM.

Bibliography

[1] G. Aad *et al.* [ATLAS Collaboration], Phys. Lett. B **716**, 1 (2012) doi:10.1016/j.physletb.2012.08.020 [arXiv:1207.7214 [hep-ex]].

[2] S. Chatrchyan *et al.* [CMS Collaboration], Phys. Lett. B **716**, 30 (2012) doi:10.1016/j.physletb.2012.08.021 [arXiv:1207.7235 [hep-ex]].

[3] M. K. Gaillard, P. D. Grannis and F. J. Sciulli, Rev. Mod. Phys. **71**, S96 (1999) doi:10.1103/RevModPhys.71.S96 [hep-ph/9812285].

[4] Y. Fukuda *et al.* [Super-Kamiokande Collaboration], Phys. Rev. Lett. **81**, 1562 (1998) doi:10.1103/PhysRevLett.81.1562 [hep-ex/9807003].

[5] Q. R. Ahmad *et al.* [SNO Collaboration], Phys. Rev. Lett. **87**, 071301 (2001) doi:10.1103/PhysRevLett.87.071301 [nucl-ex/0106015].

[6] T. Araki *et al.* [KamLAND Collaboration], Phys. Rev. Lett. **94**, 081801 (2005) doi:10.1103/PhysRevLett.94.081801 [hep-ex/0406035].

[7] M. Tanabashi *et al.* [Particle Data Group], Phys. Rev. D **98**, no. 3, 030001 (2018). doi:10.1103/PhysRevD.98.030001

[8] S. Scherer, Adv. Nucl. Phys. **27**, 277 (2003) [hep-ph/0210398].

[9] D. B. Kaplan and H. Georgi, Phys. Lett. **136B**, 183 (1984). doi:10.1016/0370-2693(84)91177-8

[10] D. B. Kaplan, H. Georgi and S. Dimopoulos, Phys. Lett. **136B**, 187 (1984). doi:10.1016/0370-2693(84)91178-X

[11] M. J. Dugan, H. Georgi and D. B. Kaplan, Nucl. Phys. B **254**, 299 (1985). doi:10.1016/0550-3213(85)90221-4

[12] R. Contino, Y. Nomura and A. Pomarol, Nucl. Phys. B **671**, 148 (2003) doi:10.1016/j.nuclphysb.2003.08.027 [hep-ph/0306259].

[13] K. Agashe, R. Contino and A. Pomarol, Nucl. Phys. B **719**, 165 (2005) doi:10.1016/j.nuclphysb.2005.04.035 [hep-ph/0412089].

[14] G. Panico and A. Wulzer, Lect. Notes Phys. **913**, pp.1 (2016) doi:10.1007/978-3-319-22617-0 [arXiv:1506.01961 [hep-ph]].

[15] W. D. Goldberger and M. B. Wise, Phys. Rev. Lett. **83**, 4922 (1999) [arXiv:hep-ph/9907447].

[16] J. M. Maldacena, Int. J. Theor. Phys. **38**, 1113 (1999) [Adv. Theor. Math. Phys. **2**, 231 (1998)] doi:10.1023/A:1026654312961, 10.4310/ATMP.1998.v2.n2.a1 [hep-th/9711200].

[17] E. Witten, Adv. Theor. Math. Phys. **2**, 253 (1998) doi:10.4310/ATMP.1998.v2.n2.a2 [hep-th/9802150].

[18] O. Aharony, S. S. Gubser, J. M. Maldacena, H. Ooguri and Y. Oz, Phys. Rept. **323**, 183 (2000) [hep-th/9905111].

[19] L. Randall and R. Sundrum, Phys. Rev. Lett. **83**, 3370 (1999) [arXiv:hep-ph/9905221]

[20] and Phys. Rev. Lett. **83**, 4690 (1999) doi:10.1103/PhysRevLett.83.4690 [hep-th/9906064].

[21] N. Arkani-Hamed, M. Porrati and L. Randall, JHEP **0108**, 017 (2001) [hep-th/0012148]

[22] R. Rattazzi and A. Zaffaroni, JHEP **0104**, 021 (2001) doi:10.1088/1126-6708/2001/04/021 [hep-th/0012248].

[23] K. Agashe *et al.*, arXiv:1309.7847 [hep-ph].

[24] P. Minkowski, *Phys. Lett.* **B67** (1977) 421;

[25] T. Yanagida in *Workshop on Unified Theories, KEK Report 79-18*, p. 95, 1979.

[26] M. Gell-Mann, P. Ramond and R. Slansky, *Supergravity*, p. 315. Amsterdam: North Holland, 1979;

[27] S. L. Glashow, *1979 Cargese Summer Institute on Quarks and Leptons*, p. 687. New York: Plenum, 1980;

[28] R. N. Mohapatra and G. Senjanovic, *Phys. Rev. Lett.* **44**, 912 (1980).

[29] S. Weinberg, Phys. Rev. Lett. **43**, 1566 (1979). doi:10.1103/PhysRevLett.43.1566

[30] K. S. Babu and R. N. Mohapatra, Phys. Rev. Lett. **70**, 2845 (1993) doi:10.1103/PhysRevLett.70.2845 [hep-ph/9209215].

[31] P. L. Cho, Phys. Rev. D **48**, 5331 (1993) doi:10.1103/PhysRevD.48.5331 [hep-ph/9304223].

[32] F. T. Avignone, III, S. R. Elliott and J. Engel, Rev. Mod. Phys. **80**, 481 (2008) doi:10.1103/RevModPhys.80.481 [arXiv:0708.1033 [nucl-ex]].

[33] A. D. Sakharov, Pisma Zh. Eksp. Teor. Fiz. **5**, 32 (1967) [JETP Lett. **5**, 24 (1967)] [Sov. Phys. Usp. **34**, no. 5, 392 (1991)] [Usp. Fiz. Nauk **161**, no. 5, 61 (1991)]. doi:10.1070/PU1991v034n05ABEH002497

[34] V. A. Rubakov and M. E. Shaposhnikov, Usp. Fiz. Nauk **166**, 493 (1996) [Phys. Usp. **39**, 461 (1996)] doi:10.1070/PU1996v039n05ABEH000145 [hep-ph/9603208].

[35] M. Trodden, Rev. Mod. Phys. **71**, 1463 (1999) doi:10.1103/RevModPhys.71.1463 [hep-ph/9803479].

[36] M. Dine, R. G. Leigh, P. Huet, A. D. Linde and D. A. Linde, Phys. Lett. B **283**, 319 (1992) doi:10.1016/0370-2693(92)90026-Z [hep-ph/9203201].

[37] K. Kajantie, M. Laine, K. Rummukainen and M. E. Shaposhnikov, Nucl. Phys. B **466**, 189 (1996) doi:10.1016/0550-3213(96)00052-1 [hep-lat/9510020].

[38] M. Fukugita and T. Yanagida, Phys. Lett. B **174**, 45 (1986). doi:10.1016/0370-2693(86)91126-3

[39] W. Buchmuller, P. Di Bari and M. Plumacher, Annals Phys. **315**, 305 (2005) doi:10.1016/j.aop.2004.02.003 [hep-ph/0401240].

[40] For a review, see, for example, S. Davidson, E. Nardi and Y. Nir, Phys. Rept. **466**, 105 (2008) doi:10.1016/j.physrep.2008.06.002 [arXiv:0802.2962 [hep-ph]].

[41] I. M. Oldengott and D. J. Schwarz, EPL **119**, no. 2, 29001 (2017) doi:10.1209/0295-5075/119/29001 [arXiv:1706.01705 [astro-ph.CO]].

[42] D. B. Kaplan, Nucl. Phys. B **365**, 259 (1991). doi:10.1016/S0550-3213(05)80021-5.

[43] R. N. Mohapatra, Phys. Rev. Lett. **56**, 561 (1986);

[44] R. N. Mohapatra and J. W. F. Valle, Phys. Rev. D **34**, 1642 (1986).

[45] S. J. Huber, Q. Shafi, Phys. Lett. **B583**, 293-303 (2004). [hep-ph/0309252];

[46] K. Agashe, S. Hong and L. Vecchi, Phys. Rev. D **94**, no. 1, 013001 (2016) doi:10.1103/PhysRevD.94.013001 [arXiv:1512.06742 [hep-ph]].

[47] K. Agashe, P. Du and S. Hong, Phys. Rev. D **97**, no. 7, 075032 (2018) doi:10.1103/PhysRevD.97.075032 [arXiv:1612.04810 [hep-ph]].

[48] K. Agashe, P. Du and S. Hong, Phys. Rev. D **97**, no. 7, 075033 (2018) doi:10.1103/PhysRevD.97.075033 [arXiv:1703.07763 [hep-ph]].

[49] C. Csaki, C. Grojean, J. Hubisz, Y. Shirman and J. Terning, Phys. Rev. D **70**, 015012 (2004) [hep-ph/0310355].

[50] G. Perez and L. Randall, JHEP **0901**, 077 (2009) [arXiv:0805.4652 [hep-ph]];

[51] C. Csaki, C. Delaunay, C. Grojean and Y. Grossman, JHEP **0810**, 055 (2008) [arXiv:0806.0356 [hep-ph]];

[52] M. Carena, A. D. Medina, N. R. Shah and C. E. M. Wagner, Phys. Rev. D **79**, 096010 (2009) [arXiv:0901.0609 [hep-ph]].

[53] M. Malinsky, J. C. Romao and J. W. F. Valle, Phys. Rev. Lett. **95**, 161801 (2005) doi:10.1103/PhysRevLett.95.161801 [hep-ph/0506296].

[54] K. Agashe, P. Du, M. Ekhterachian, C. S. Fong, S. Hong and L. Vecchi, Phys. Lett. B **785**, 489 (2018) doi:10.1016/j.physletb.2018.09.006 [arXiv:1804.06847 [hep-ph]].

[55] K. Agashe, P. Du, M. Ekhterachian, C. S. Fong, S. Hong and L. Vecchi, JHEP **1904**, 029 (2019) doi:10.1007/JHEP04(2019)029 [arXiv:1812.08204 [hep-ph]].

[56] C. H. Lee, P. S. Bhupal Dev and R. N. Mohapatra, Phys. Rev. D **88**, no. 9, 093010 (2013) doi:10.1103/PhysRevD.88.093010 [arXiv:1309.0774 [hep-ph]].

[57] R. N. Mohapatra, Nucl. Phys. B **908**, 423 (2016). doi:10.1016/j.nuclphysb.2016.03.006

[58] A. Pilaftsis, J. Phys. Conf. Ser. **171**, 012017 (2009) doi:10.1088/1742-6596/171/1/012017 [arXiv:0904.1182 [hep-ph]].

[59] F. F. Deppisch, P. S. Bhupal Dev and A. Pilaftsis, New J. Phys. **17**, no. 7, 075019 (2015) doi:10.1088/1367-2630/17/7/075019 [arXiv:1502.06541 [hep-ph]].

[60] F. F. Deppisch and A. Pilaftsis, Phys. Rev. D **83**, 076007 (2011) doi:10.1103/PhysRevD.83.076007 [arXiv:1012.1834 [hep-ph]].

[61] P. S. Bhupal Dev, P. Millington, A. Pilaftsis and D. Teresi, Nucl. Phys. B **886**, 569 (2014) doi:10.1016/j.nuclphysb.2014.06.020 [arXiv:1404.1003 [hep-ph]].

[62] M. J. Dolan, T. P. Dutka and R. R. Volkas, arXiv:1802.08373 [hep-ph].

[63] P. H. Gu and U. Sarkar, Phys. Lett. B **694**, 226 (2011) doi:10.1016/j.physletb.2010.09.062 [arXiv:1007.2323 [hep-ph]].

[64] M. Aoki, N. Haba and R. Takahashi, PTEP **2015**, no. 11, 113B03 (2015) doi:10.1093/ptep/ptv149 [arXiv:1506.06946 [hep-ph]].

[65] K. N. Abazajian *et al.* [Topical Conveners: K.N. Abazajian, J.E. Carlstrom, A.T. Lee Collaboration], Astropart. Phys. **63**, 66 (2015) doi:10.1016/j.astropartphys.2014.05.014 [arXiv:1309.5383 [astro-ph.CO]].

[66] T. P. Cheng and L. F. Li, Phys. Rev. Lett. **45**, 1908 (1980). doi:10.1103/PhysRevLett.45.1908

[67] A. M. Baldini *et al.* [MEG Collaboration], Eur. Phys. J. C **76**, no. 8, 434 (2016) doi:10.1140/epjc/s10052-016-4271-x [arXiv:1605.05081 [hep-ex]].

[68] M. Frigerio, M. Nardecchia, J. Serra and L. Vecchi, arXiv:1807.04279 [hep-ph].

[69] S. Blanchet, P. S. B. Dev and R. N. Mohapatra, Phys. Rev. D **82**, 115025 (2010) doi:10.1103/PhysRevD.82.115025 [arXiv:1010.1471 [hep-ph]].

[70] E. Nardi, Y. Nir, E. Roulet and J. Racker, JHEP **0601**, 164 (2006) doi:10.1088/1126-6708/2006/01/164 [hep-ph/0601084];

[71] A. Abada, S. Davidson, F. X. Josse-Michaux, M. Losada and A. Riotto, JCAP **0604**, 004 (2006) doi:10.1088/1475-7516/2006/04/004 [hep-ph/0601083];

[72] A. Abada, S. Davidson, A. Ibarra, F.-X. Josse-Michaux, M. Losada and A. Riotto, JHEP **0609**, 010 (2006) doi:10.1088/1126-6708/2006/09/010 [hep-ph/0605281].

[73] L. Covi, E. Roulet and F. Vissani, Phys. Lett. B **384**, 169 (1996) doi:10.1016/0370-2693(96)00817-9 [hep-ph/9605319].

[74] S. Blanchet, T. Hambye and F. X. Josse-Michaux, JHEP **1004**, 023 (2010) doi:10.1007/JHEP04(2010)023 [arXiv:0912.3153 [hep-ph]];

[75] P. A. R. Ade *et al.* [Planck Collaboration], Astron. Astrophys. **594**, A13 (2016) doi:10.1051/0004-6361/201525830 [arXiv:1502.01589 [astro-ph.CO]].

[76] D. V. Nanopoulos and S. Weinberg, Phys. Rev. D **20**, 2484 (1979). doi:10.1103/PhysRevD.20.2484

[77] R. Adhikari and R. Rangarajan, Phys. Rev. D **65**, 083504 (2002) doi:10.1103/PhysRevD.65.083504 [hep-ph/0110387].

[78] A. Bhattacharya, R. Gandhi and S. Mukhopadhyay, Phys. Rev. D **89**, no. 11, 116014 (2014) doi:10.1103/PhysRevD.89.116014 [arXiv:1109.1832 [hep-ph]].

[79] A. Pilaftsis and T. E. J. Underwood, Nucl. Phys. B **692**, 303 (2004) doi:10.1016/j.nuclphysb.2004.05.029 [hep-ph/0309342];

[80] A. Pilaftsis, Phys. Rev. Lett. **95**, 081602 (2005) doi:10.1103/PhysRevLett.95.081602 [hep-ph/0408103];

[81] A. Pilaftsis and T. E. J. Underwood, Phys. Rev. D **72**, 113001 (2005) doi:10.1103/PhysRevD.72.113001 [hep-ph/0506107].

[82] M. J. Dolan, T. P. Dutka and R. R. Volkas, arXiv:1812.11964 [hep-ph].

[83] M. C. Gonzalez-Garcia, J. Racker and N. Rius, JHEP **0911**, 079 (2009) doi:10.1088/1126-6708/2009/11/079 [arXiv:0909.3518 [hep-ph]].

[84] E. K. Akhmedov, V. A. Rubakov and A. Y. Smirnov, Phys. Rev. Lett. **81**, 1359 (1998) doi:10.1103/PhysRevLett.81.1359 [hep-ph/9803255].

[85] A. Abada, G. Arcadi, V. Domcke and M. Lucente, JCAP **1511**, no. 11, 041 (2015) doi:10.1088/1475-7516/2015/11/041 [arXiv:1507.06215 [hep-ph]];

[86] A. Abada, G. Arcadi, V. Domcke and M. Lucente, JCAP **1712**, no. 12, 024 (2017) doi:10.1088/1475-7516/2017/12/024 [arXiv:1709.00415 [hep-ph]].

[87] A. Antaramian, L. J. Hall and A. Rasin, Phys. Rev. D **49**, 3881 (1994) doi:10.1103/PhysRevD.49.3881 [hep-ph/9311279].

[88] C. S. Fong, Phys. Lett. B **752**, 247 (2016) doi:10.1016/j.physletb.2015.11.055 [arXiv:1508.03648 [hep-ph]].

[89] G. 't Hooft, Phys. Rev. Lett. **37**, 8 (1976). doi:10.1103/PhysRevLett.37.8; G. 't Hooft, Phys. Rev. D **14**, 3432 (1976) Erratum: [Phys. Rev. D **18**, 2199 (1978)]. doi:10.1103/PhysRevD.18.2199.3, 10.1103/PhysRevD.14.3432.

[90] S. Y. Khlebnikov and M. E. Shaposhnikov, Nucl. Phys. B **308**, 885 (1988). doi:10.1016/0550-3213(88)90133-2

[91] M. D'Onofrio, K. Rummukainen and A. Tranberg, Phys. Rev. Lett. **113**, no. 14, 141602 (2014) doi:10.1103/PhysRevLett.113.141602 [arXiv:1404.3565 [hep-ph]].

[92] B. Garbrecht, F. Glowna and P. Schwaller, Nucl. Phys. B **877**, 1 (2013) doi:10.1016/j.nuclphysb.2013.08.020 [arXiv:1303.5498 [hep-ph]];

[93] B. Garbrecht and P. Schwaller, JCAP **1410**, no. 10, 012 (2014) doi:10.1088/1475-7516/2014/10/012 [arXiv:1404.2915 [hep-ph]].

[94] J. A. Harvey and M. S. Turner, Phys. Rev. D **42**, 3344 (1990). doi:10.1103/PhysRevD.42.3344

[95] T. Inui, T. Ichihara, Y. Mimura and N. Sakai, Phys. Lett. B **325**, 392 (1994) doi:10.1016/0370-2693(94)90031-0 [hep-ph/9310268].

[96] K. Enqvist and J. Sirkka, Phys. Lett. B **314**, 298 (1993) doi:10.1016/0370-2693(93)91239-J [hep-ph/9304273].

[97] J. Racker, JCAP **1403**, 025 (2014) doi:10.1088/1475-7516/2014/03/025 [arXiv:1308.1840 [hep-ph]];

[98] D. Aristizabal Sierra, C. S. Fong, E. Nardi and E. Peinado, JCAP **1402**, 013 (2014) doi:10.1088/1475-7516/2014/02/013 [arXiv:1309.4770 [hep-ph]].

[99] P. A. R. Ade *et al.* [BICEP2 and Planck Collaborations], Phys. Rev. Lett. **114**, 101301 (2015) doi:10.1103/PhysRevLett.114.101301 [arXiv:1502.00612 [astro-ph.CO]].

[100] H. Pagels and J. R. Primack, Phys. Rev. Lett. **48**, 223 (1982). doi:10.1103/PhysRevLett.48.223;

[101] S. Weinberg, Phys. Rev. Lett. **48**, 1303 (1982). doi:10.1103/PhysRevLett.48.1303;

[102] M. Y. Khlopov and A. D. Linde, Phys. Lett. **138B**, 265 (1984). doi:10.1016/0370-2693(84)91656-3;

[103] J. R. Ellis, J. E. Kim and D. V. Nanopoulos, Phys. Lett. **145B**, 181 (1984). doi:10.1016/0370-2693(84)90334-4;

[104] J. R. Ellis, D. V. Nanopoulos and S. Sarkar, Nucl. Phys. B **259**, 175 (1985). doi:10.1016/0550-3213(85)90306-2.

[105] T. Moroi, H. Murayama and M. Yamaguchi, Phys. Lett. B **303**, 289 (1993). doi:10.1016/0370-2693(93)91434-O;

[106] M. Kawasaki, K. Kohri, T. Moroi and A. Yotsuyanagi, Phys. Rev. D **78**, 065011 (2008) doi:10.1103/PhysRevD.78.065011 [arXiv:0804.3745 [hep-ph]].

[107] Y. Aoki, G. Endrodi, Z. Fodor, S. D. Katz and K. K. Szabo, Nature **443**, 675 (2006) doi:10.1038/nature05120 [hep-lat/0611014].

[108] S. Borsanyi *et al.* [Wuppertal-Budapest Collaboration], JHEP **1009**, 073 (2010) doi:10.1007/JHEP09(2010)073 [arXiv:1005.3508 [hep-lat]].

[109] A. Bazavov *et al.*, Phys. Rev. D **85**, 054503 (2012) doi:10.1103/PhysRevD.85.054503 [arXiv:1111.1710 [hep-lat]].

[110] T. Bhattacharya *et al.*, Phys. Rev. Lett. **113**, no. 8, 082001 (2014) doi:10.1103/PhysRevLett.113.082001 [arXiv:1402.5175 [hep-lat]].

[111] E. Witten, Adv. Theor. Math. Phys. **2**, 505 (1998) doi:10.4310/ATMP.1998.v2.n3.a3 [hep-th/9803131].

[112] P. Creminelli, A. Nicolis and R. Rattazzi, JHEP **0203**, 051 (2002) doi:10.1088/1126-6708/2002/03/051 [hep-th/0107141].

[113] L. Randall and G. Servant, JHEP **0705**, 054 (2007) doi:10.1088/1126-6708/2007/05/054 [hep-ph/0607158].

[114] J. Kaplan, P. C. Schuster and N. Toro, hep-ph/0609012.

[115] G. Nardini, M. Quiros and A. Wulzer, JHEP **0709**, 077 (2007) doi:10.1088/1126-6708/2007/09/077 [arXiv:0706.3388 [hep-ph]].

[116] T. Konstandin and G. Servant, JCAP **1112**, 009 (2011) doi:10.1088/1475-7516/2011/12/009 [arXiv:1104.4791 [hep-ph]].

[117] B. von Harling and G. Servant, JHEP **1801**, 159 (2018) doi:10.1007/JHEP01(2018)159 [arXiv:1711.11554 [hep-ph]].

[118] P. Baratella, A. Pomarol and F. Rompineve, JHEP **1903**, 100 (2019) doi:10.1007/JHEP03(2019)100 [arXiv:1812.06996 [hep-ph]].

[119] E. Megas, G. Nardini and M. Quirs, JHEP **1809**, 095 (2018) doi:10.1007/JHEP09(2018)095 [arXiv:1806.04877 [hep-ph]].

[120] B. Hassanain, J. March-Russell and M. Schvellinger, JHEP **0710**, 089 (2007) doi:10.1088/1126-6708/2007/10/089 [arXiv:0708.2060 [hep-th]].

[121] T. Konstandin, G. Nardini and M. Quiros, Phys. Rev. D **82**, 083513 (2010) doi:10.1103/PhysRevD.82.083513 [arXiv:1007.1468 [hep-ph]].

[122] D. Bunk, J. Hubisz and B. Jain, Eur. Phys. J. C **78**, no. 1, 78 (2018) doi:10.1140/epjc/s10052-018-5529-2 [arXiv:1705.00001 [hep-ph]].

[123] B. M. Dillon, B. K. El-Menoufi, S. J. Huber and J. P. Manuel, Phys. Rev. D **98**, no. 8, 086005 (2018) doi:10.1103/PhysRevD.98.086005 [arXiv:1708.02953 [hep-th]].

[124] P. Amaro-Seoane, *et al.*, [arXiv:1702.00786 [astro-ph.IM]].

[125] Z. Chacko and R. K. Mishra, Phys. Rev. D **87**, no. 11, 115006 (2013) doi:10.1103/PhysRevD.87.115006 [arXiv:1209.3022 [hep-ph]].

[126] Z. Chacko, R. K. Mishra and D. Stolarski, JHEP **1309**, 121 (2013) doi:10.1007/JHEP09(2013)121 [arXiv:1304.1795 [hep-ph]].

[127] A. D. Linde, Nucl. Phys. B **216**, 421 (1983) Erratum: [Nucl. Phys. B **223**, 544 (1983)]. doi:10.1016/0550-3213(83)90293-6, 10.1016/0550-3213(83)90072-X

[128] E. W. Kolb and S. Wolfram, Nucl. Phys. B **172**, 224 (1980) Erratum: [Nucl. Phys. B **195**, 542 (1982)]. doi:10.1016/0550-3213(80)90167-4, 10.1016/0550-3213(82)90012-8

[129] C. S. Fong, M. C. Gonzalez-Garcia and E. Nardi, Int. J. Mod. Phys. A **26**, 3491 (2011) doi:10.1142/S0217751X1105405X [arXiv:1107.5312 [hep-ph]].

[130] W. Buchmuller and M. Plumacher, Phys. Lett. B **511**, 74 (2001) doi:10.1016/S0370-2693(01)00614-1 [hep-ph/0104189].

[131] E. Nardi, Y. Nir, J. Racker and E. Roulet, JHEP **0601**, 068 (2006) doi:10.1088/1126-6708/2006/01/068 [hep-ph/0512052].

[132] P. Batra, B. A. Dobrescu and D. Spivak, J. Math. Phys. **47**, 082301 (2006) doi:10.1063/1.2222081 [hep-ph/0510181].

[133] C. Brust, D. E. Kaplan and M. T. Walters, JHEP **1312**, 058 (2013) doi:10.1007/JHEP12(2013)058 [arXiv:1303.5379 [hep-ph]].